COMPUTATIONAL INVESTIGATIONS OF BIOPOLYMER TRANSLOCATION THROUGH NANOPORE DEVICES

A Dissertation
Presented to
The Academic Faculty

by

Christopher M. Edmonds

In Partial Fulfillment
of the Requirements for the Degree
Doctor of Philosophy in the
School of Electrical and Computer Engineering

Georgia Institute of Technology

December 2013

COMPUTATIONAL INVESTIGATIONS OF BIOPOLYMER TRANSLOCATION THROUGH NANOPORE DEVICES

Approved by:

Dr. Peter J. Hesketh, Advisor
G.W. Woodruff School of Mechanical Engineering
Georgia Institute of Technology

Dr. Hang Lu
School of Chemical & Biomolecular Engineering
Georgia Institute of Technology

Dr. Sankar Nair, Co-Advisor
School of Chemical & Biomolecular Engineering
Georgia Institute of Technology

Dr. Peter J. Ludovice
School of Chemical & Biomolecular Engineering
Georgia Institute of Technology

Dr. David Sholl
School of Chemical & Biomolecular Engineering
Georgia Institute of Technology

Date Approved: August 8, 2013

ACKNOWLEDGEMENTS

First, I would like to thank my advisors Dr. Peter Hesketh and Dr. Sankar Nair for their time and support while working on my PhD. I would also like to thank Dr. David Sholl whom assisted me with the many questions I have had related to my research. He gave me wonderful advice both academically and professionally. I am very grateful for his support and was blessed to have him on my committee as well as a professor during my PhD studies. I also would like to thank Dr. Hang Lu and Dr. Peter Ludovice for taking time out of their busy schedules to serve on my committee. I am very fortunate to have such a wonderful PhD committee.

I would also like to thank Dr. Andrew Peterson for his assistance with the electrostatics portion of my research. Dr. Peterson always had time to answer my questions for which I am grateful. I would also like to thank Dr. Whit Smith for all of his support, guidance, and friendship not only while working on my PhD, but during my entire scholastic career. In addition, I would like to thank Dr. Micah Coleman and Dr. Mick West at GTRI for their support in helping me complete this PhD.

I would also like to thank my parents for their love and support. I would also like to thank Mr. Chris Ruffin from the Bioengineering department. He was a great friend and a wonderful person whom I will miss very much. I could not have completed this PhD without his kindness and support.

Finally, I would like to dedicate this thesis to my wife Rebekah and my son José, who has brought me great joy and inspiration since the day we adopted him. Using the immortal words of José when he has finished his homework – "Ahh Bah" (All Done).

TABLE OF CONTENTS

LIST OF TABLES

LIST OF FIGURES

LIST OF ABBREVIATIONS

GC	Gouy-Chapman Equation
RPY	Rotne-Prager-Yamakawa Tensor
SOR	Successive Over-Relaxation Method
PNP	Poisson-Nernst-Planck Equations
DNA	Deoxyribonucleic Acid
ds-DNA	Double-Stranded DNA
ss-DNA	Single-Stranded DNA
HI	Hydrodynamic Interactions
MMC	Metropolis Monte Carlo Procedure
ME	Minimum Energy
MD	Molecular Dynamics
SRD	Stochastic Rotation Dynamics
DPD	Dissipative Particle Dynamics
α-HL	α-hemolysin pore
SNR	Signal-to-Noise Ratio
BDTP	Brownian Dynamics Tension Propagation theory
NHGRI	National Human Genome Research Institute
FENE	Finitely Extendable Nonlinear Elastic
WCA	Weeks-Chandler-Anderson Potential
TEA	Truncated Expansion Ansatz
BD	Brownian Dynamics
NVE	Constant particle Number (N) Constant Volume (V) Constant Energy (E)
PECVD	Plasma-enhanced chemical vapor deposition

LD	Langevin dynamics
M	Mole (unit of concentration)
KCl	Potassium Chloride
K+	Potassium
Cl-	Chlorine
pH	Measure of solutions acidity

SUMMARY

Nanopores (1 – 10 nm diameter) constructed in solid-state membranes, have shown promise as next-generation biopolymer analysis devices offering both high resolution and high throughput. One promising application of nanopores is in the analysis of nucleic acids, such as DNA. This involves translocation experiments in which DNA is placed in an ionic solution and is forced through a nanopore with the aid of an applied electric field. The modulation of ionic current through the pore during DNA translocation can then be correlated to various properties of the biopolymer such as the length. This method of measuring DNA length is potentially orders of magnitude faster than conventional gel electrophoresis, and does not require any staining or labeling of the DNA.

To optimally design and operate nanopore devices, it would be advantageous to develop an accurate computer simulation methodology to predict the physics of the translocation process. Hence, I have developed a physically accurate, computationally efficient simulation methodology to predict and analyze the physics of biopolymer translocation through solid-state (silicon nitride) nanopores. The overall theme of this thesis is to use this simulation methodology to thoroughly investigate important issues in the physics underlying translocation experiments and thereby determine the effects of key structural and operation parameters, such as the nanopore dimensions, applied voltage, solvent viscosity, and the polymer chain length.

The first chapter in this thesis presents an overview of nanopores and how they can be used to analyze biopolymers such as DNA. I also discuss potential challenges in using nanopore devices and why it is important to have an accurate computational simulation methodology to predict the underlying physics involved in a translocation time experiment. One primary issue that has yet to be completely resolved is the scaling law behavior of translocation time versus chain length ($\tau \sim N^{\alpha}$) [1]. If the scaling exponent α were known, one could easily determine the length of the polymer simply from the time required for the polymer to translocate through the pore. As I thoroughly discuss in this introduction chapter, there are many hypotheses to what this scaling law should be for both forced and unforced (i.e. applied voltage = 0) translocation. In fact, as will be shown in later chapters, the scaling exponent is heavily dependent upon many parameters such as applied force, pore length and diameter, and initial polymer configuration. One of the main objectives in this work is to determine under what conditions are the theoretical values for this scaling exponent obtained and what leads to deviations from theory. Developing a computational model that agrees with theoretical predictions, and comparing those results to experimental findings, can lead to a better understanding of which physical mechanisms are important when modeling polymer translocation through nanopore devices.

Chapter 2 discusses the simulation methodology and models used to investigate biopolymer translocation through solid-state nanopores. To perform realistic simulations much faster than traditional molecular dynamics (MD) calculations, I use either Brownian or Langevin Dynamics simulations to model the solute-solvent interactions for both Rouse and Zimm polymer models. This allows larger integration time steps,

permitting simulations to be performed for larger durations of time and longer polymer chains. I also incorporate atomistically detailed nanopore models constructed from the crystal structure of β-Si_3N_4 in my simulation methodology to achieve higher simulation accuracy. In order to understand the effects due to the electrolytic ions, nanopore surface charge, and a charged polymer, I compute the coupled Poisson-Nernst-Planck equations to determine the potential and ionic concentration distribution inside the nanopore for both situations of when the polymer is present or absent from the nanopore. In this chapter, I thoroughly test my simulation methodology and demonstrate all fundamental theoretical laws are obeyed.

As previously discussed, one of the main objectives is to determine the translocation time scaling exponent α. In Chapter 3, I study how this scaling exponent varies with applied force, pore length and diameter, and viscosity using Rouse polymers (no hydrodynamic interactions). Whereas most polymers behave as Zimm polymers (with hydrodynamic interactions) in bulk solution, hydrodynamic interactions can be screened for polymers moving near a wall or inside a channel, which indicate the importance of Rouse polymer studies when investigating polymer translocation through small structures such as nanopores. My first studies involved polymers much longer than the pore length, which is often the case in translocation measurements. I found that during forced translocation, the polymer "crowds" at the exit of the nanopore, causing the scaling exponent to be much smaller than the theoretical value of $\alpha = 1 + \upsilon$, where υ is the 3 dimensional Flory exponent ($\upsilon = 0.588$). This crowding is due to the translocation time being much faster than the Rouse polymer relaxation time. When the applied voltage is decreased, the translocation time is increased, which permits the polymer to relax longer,

resulting in an increase in the scaling exponent. In my next Rouse polymer studies, I found that when the polymer length is shorter or on the same order as the length of the nanopore, a continuous scaling law does not exist, but the scaling exponent (α) increases as the length of the polymer increases, converging to the same value obtained when the polymer length is much longer than the pore length. These findings indicate the scaling exponent α is dependent not only on the applied voltage, but also the relationship between the length of the polymer chain and the pore length. One disadvantage to using nanopores in DNA investigations is the high rate at which the translocation takes place, often putting very strenuous demands on measurement equipment used to measure the modulated ionic current. One method that has been used to slow down the translocation process is to increase the solvent viscosity by adding glycerol. Hence, I studied the effects of increasing the solvent viscosity and found that, while the translocation time is increased as the solvent viscosity is increased, the polymer relaxation time is also increased, and thus there was no effect on the scaling exponent α. Finally, I studied the relationship between the translocation time and the applied voltage for different polymer lengths and obtained the theoretical scaling of $\tau \sim V^{-1}$ at low to moderate voltages, which has also been observed in experimental results as well. At high applied voltages, once again the polymer crowds at the exit of the nanopore resulting in scaling exponents larger than -1. These findings indicate the translocation physics are heavily dependent upon applied voltage.

Whereas Rouse polymers that do not include hydrodynamic interactions (HI) diffuse as $D \sim N^{-1}$, Zimm polymers that include HI diffuse as $D \sim N^{-0.6}$, which more resembles biopolymers such as double stranded DNA (ds-DNA). Because of this, in

Chapter 4, I study the effects of hydrodynamic interactions on polymer translocation and obtain the theoretical scaling exponent of $\alpha = 2\upsilon$, which is vastly different from the theoretical scaling exponent obtained for Rouse polymers ($\alpha = 1 + \upsilon$). I also observed in my simulation studies that due to secondary polymer-solvent interactions, the Zimm polymer not only translocates through the nanopore faster, but also has a much shorter relaxation time. Interestingly, the Zimm polymer scaling exponent resembles those obtained in experiments for nanopores with large diameters (10 nm), whereas the Rouse scaling exponent ($\alpha = 1.44$) is more in agreement with experiments with smaller diameters (4 nm). These finding indicate that whereas hydrodynamic interactions are vital when modeling biopolymer translocation through large nanopores, polymer translocation through smaller nanopores more resemble Rouse polymer behavior, possibly due to larger polymer-pore interactions screening out HI affects. Also in this chapter, I continue my study for Rouse polymers and find the only way to obtain theoretical scaling exponent of $\alpha = 1 + \upsilon$ is if the polymer is in equilibrium throughout the translocation process. In other words, the radius of gyration of the polymer must scale as $R_g^2 \sim N^{2\upsilon}$, both on the *cis* (at the beginning of the simulation) and on the *trans* (at the end of the simulation) side of the nanopore (Figure 3 (b)), which only occurs with low applied voltages. This is an important finding because it indicates at what nanopore operating conditions one can obtain the theoretical scaling exponent. Similar to the Rouse polymer studies in chapter 3, in chapter 4 I also studied the effects of solvent viscosity and applied voltage on the Zimm polymers as well. Once again, I found that while the translocation time is increased as the solvent viscosity is increased, the polymer relaxation time is also increased, and thus there was no effect on the scaling exponent α. In addition, I obtained

the theoretical scaling of $\tau \sim V^{-1}$ at low to moderate voltages. At high applied voltages, once again the polymer crowds at the exit of the nanopore resulting in scaling exponents larger than -1. The importance of this finding is that this scaling relationship of $\tau \sim V^{-1}$ does not hold for all voltages, for both Rouse and Zimm polymers, further indicating that large applied voltages are responsible for extreme polymer crowding at the nanopore exit and deviations from theoretical derivations.

The final objective of Chapter 4 is the investigation of translocation scaling exponents for unforced (i.e. no applied voltage) translocation of both Rouse and Zimm polymers. Theoretically, the scaling law for a polymer that translocates through a nanopore without the aid of an applied force should be on the same order as the polymer relaxation time defined as the time required for a polymer to diffuse its radius of gyration, which is $\tau \sim N^{1+2\upsilon}$ for the Rouse polymer model and $\tau \sim N^{3\upsilon}$ for the Zimm polymer models. As will be shown in chapter 4, I obtain the scaling relationship of $\tau \sim N^{1+2\upsilon}$ in very narrow pores not only for the Rouse polymer model but also for the Zimm polymer model as well. This is in part due to the hydrodynamic interactions being screened close to the pore wall as well as the strong polymer-pore interactions slowing down the polymer translocation and, thus, reducing the hydrodynamic interactions. Thus, as discussed before, polymers that behave as Zimm polymers in bulk solution may translocate as Rouse polymers in narrow nanopores due to HI effects being screened. In other simulations, when the diameter of the pore is increased, the polymer-pore interactions are decreased, resulting in an increase in the scaling exponent α and a reduction in the translocation time. When the pore is removed from the simulation, the scaling exponent of both polymer models converge to their relaxation scaling behavior of

$\tau \sim N^{1+2\upsilon}$ for Rouse and $\tau \sim N^{3\upsilon}$ for Zimm models. These findings emphasize how polymer-pore interactions can greatly affect polymer translocation through nanopores.

The final objective of this work, as discussed in Chapter 5, is to determine the potential and ion distribution inside negatively charged silicon nitride nanopores in the presence of a 1 M electrolyte and a charged polymer in order to obtain a preliminary assessment of the effects of electrostatics on translocation processes. In order to find the potential and ion distribution, I solve the coupled Poisson-Nernst-Planck equations for nanopores of varying diameter. In these simulation results, due to the high electrolytic concentration (1 M) and, as a result very short Debye length (~ 3 Å), I find the potential as a result of the surface charge of both the nanopore and polymer is largely screened at very short distances. In addition, due to the charge on each monomer, a large buildup of ions occurs on the surface of each monomer. One could hypothesize, due to the large ion concentrations in close proximity to the polymer, that electro-osmotic forces along the backbone of the polymer would greatly affect the translocation dynamics in an experiment with a charged biopolymer such as ds-DNA. The importance of these findings indicates how important it is to include the electrolytic solution for not only electrostatic effects but possible electro-osmotic effects as well.

CHAPTER 1: INTRODUCTION

1.1 Introduction to Nanopores

One of the most significant advances in the single-molecule analysis of polymers is with the use of nanopore devices. Nanopores typically have diameters in the 1-10 nm range and have been fabricated using ion channel proteins [2–6] or solid-state materials such as silicon oxide [7–10] and silicon nitride [11–20]. Because the diameter of the nanopore is similar to the size of a macromolecule of interest[2] and due to the high rate at which macromolecules can potentially translocate through the pore, nanopores are seen as potential 'next-generation' single-molecule analysis devices possessing both very high resolution and throughput[21].

One potential application of nanopore devices is in the analysis of nucleic acids. Because of the significant role genetics play in biological systems and disease findings ways cheaper and faster methods of DNA sequencing has become a widely studied area of research [2]. The goal of the US National Human Genome Research Institute (NHGRI) is to create a system that can sequence an entire mammalian-scale genome for about $1,000 by 2014[22] (currently, the cost is around $4000 - $5000 and takes about 2 days to complete [23,24]). The use of biological nanopores, such as the α-hemolysin (α-HL) pore, and/or solid state nanopores constructed using Silicon Nitride or Silicon Dioxide, could possibly provide an even faster, less expensive sequencing method.

One example of the use of nanopore devices is in the determination of DNA chain lengths. Because DNA possesses an inherent negative charge, it can be driven through a nanopore with the aid of an applied voltage (Figure 1). When placed in an aqueous

electrolyte solution, a current flows through the nanopore. At the beginning of the experiment, when the DNA is on the '*cis*' side of the nanopore (corresponding to the electrode with negative voltage) and not blocking the pore, the current is at its maximum value. When the DNA chain begins to thread through the nanopore, a large fraction of the electrolyte ions will be blocked and hence the current decreases to a minimum value. Once the DNA has fully translocated and reaches the '*trans*' side of the nanopore, the ionic current returns to its original maximum value. Based upon the duration of current blockage, theoretically, the length of the DNA chain can be determined. This experiment, which is orders of magnitude faster than conventional gel electrophoresis [21] and doesn't require any staining or labeling of the DNA[25–27], is referred to as a translocation time measurement [4,21,22].

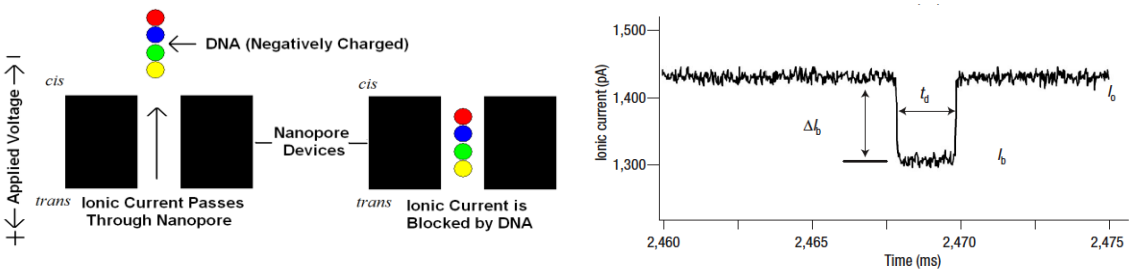

Figure 1: (Left) Simple illustration defining aspects of translocation process. (Right) Example ionic current measurement using 30 Å silicon nitride nanopore [11].

Due to the reduction in the number of configurations the DNA chain can take when entering the pore, there is an entropic free energy barrier that must be overcome in order for the DNA to flow through the nanopore[4]. In addition, an enthalpic barrier may also exist depending on the interactions between the nanopore wall and the DNA chain.

The free energy barrier that needs to be overcome is therefore dependent upon many characteristics of the system such as the length of the DNA chain, properties of the nanopore (size, attractive/repulsive forces, etc.), and properties of the solvent (such as temperature, pH). The applied potential helps overcome the free energy barrier and facilitates the translocation of the DNA through the nanopore device.

1.2 Types of Nanopores

1.2.1 Biological Nanopores

The first types of nanopores used in translocation time experiments were composed of biological materials. Not only can biological nanopores be genetically modified to meet the requirements for a specific end-user application [27,28], they are also created by cells with high reproducibility and precision [27]. One type of biological nanopore that has been used in translocation time experiments is made from the α-hemolysin (α-HL) protein reconstituted in a synthetic lipid bilayer[2,4,21] as shown in Figure 2 (a) [2,4]. The pore is comprised of a large opening, called the vestibule, located in the *cis* chamber and a cylinder-like region, called the β-barrel, in the *trans* chamber. Due to its small pore size, the α-HL pore has been primarily used in single-stranded DNA (ss-DNA) translocation experiments. Even though there have been promising results using α-HL nanopores, there are some major hindrances that could prohibit its use in sequencing applications. For instance, the α-HL pore is not very durable and, because they are constructed using biological materials, will only stay intact for about 36 hours[21,29]. Also, due to the large size of the vestibule, DNA chains can assume different forms before entering the β-barrel. This results in translocation time histograms having several peaks and long tails, indicating that it may be difficult to use this device

when trying to determine DNA chain lengths that differ by a small number of monomers[21]. Finally, due to the pore being a poor conductor of ionic current, experiments have to be performed at unphysiologically high salt concentrations to obtain a good signal-to-noise ratio (SNR) [21,29]. Another type of biological nanopore that has been used in DNA sequencing experiments is the Mycobacterium smegmatis porin A (MspA) [27,30–32]. As shown in Figure 2 (b), the MspA pore has more of a consistent funnel like shape, rather than the irregular shape of the α-HL pore. One of the main advantages of the MspA pore over the α-HL pore is at its most narrow point (diameter = 1.2 nm), it is only 0.6 nm long [31]. This is important because only about 3 nucleotides will occupy that space, and thus contribute to the modulating ionic current[27]. This makes it more ideal for single nucleotide sequencing rather than the α-HL pore which has a β-barrel that is 10 – 12 nucleotides long [27,30].

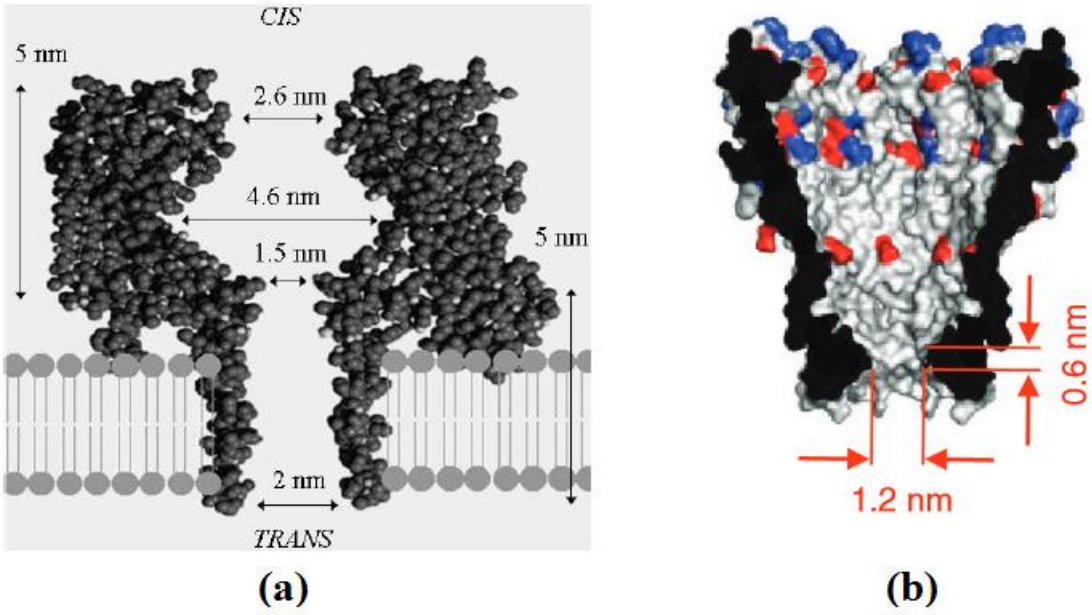

Figure 2: Cross section and approximate dimensions for a single (a) α-HL[2] and (b) MspA pores[31].

1.2.2 Solid State Nanopores

Due to the limitations of the α-HL pore, solid state nanopores, constructed from materials such as silicon oxide [7–10] and silicon nitride [11–20] are now being used in translocation experiments. Solid-state nanopores have many advantages over their biologically-derived counterparts, such as longer durability, wider range of operation, and controllable size[21,29]. A number of experimental studies have reported the fabrication and operation of solid-state nanopore devices produced by a variety of techniques such as milling or ablation of solid-state membranes by focused ion beams and electron beams generated by transmission electron microscopes [33–37]. Recent work has also addressed the development of wafer-scale processes for producing arrays of nanopores by combining electron-beam lithography and atomic layer deposition techniques[16].

Furthermore, the incorporation of electronic measurement devices (such as tunneling detectors) within solid state nanopores has also been recently reported[38]. Such a development may allow the direct reading of biopolymer sequence information during translocation.

1.3 The Need for Simulation Models

In order to realize the technological potential of nanopore devices, a detailed theoretical and experimental understanding of polymer translocation dynamics in the nanopore is necessary. Computational studies of polymer translocation though nanopore devices are expected to provide valuable insight regarding the physics of translocation, as well as guidelines for better nanopore device design and operation[39]. Previous studies have reported Molecular Dynamics (MD) simulations of events occurring during translocation of DNA through a solid-state nanopore[40–44]. Although MD simulations provide atomistically detailed information, they typically describe phenomena occurring on time scales shorter than ~100 ns. To obtain physical insight into full translocation processes occurring on much longer time scales, 'coarse-grained' simulation techniques are necessary. Such approaches, based upon Brownian or Langevin dynamics simulations, can address a number of important questions relating to the translocation process.

1.4 Translocation Time Scaling Exponents

Unfortunately, the underlying mechanisms of biopolymer translocation through a nanopore are far from well-understood. Several authors, including myself, have studied a number of aspects of biopolymer translocation with coarse-grained dynamical simulation

techniques [1,45–71]. One primary issue, that has yet to be completely resolved, is the relationship between the translocation time τ and the polymer chain length N [1], often expressed in the form of an exponential relationship $\tau \sim N^{\alpha}$. In fact, finding a universal scaling exponent, α, has been the subject of many simulation studies including the ones cited above. Knowing this scaling relationship in advance of a nanopore experiment would make the task of determining the polymer chain length trivial from a translocation time measurement. As I will discuss in this introduction and demonstrate throughout this thesis, the scaling exponent is heavily dependent upon many parameters such as applied force, pore length and diameter, and initial polymer configuration.

1.4.1 Unforced Translocation Time Studies

In the first studies involving unforced polymer translocation, Sung and Park [72] and Muthukumar [73], using a derived free energy equation involving polymer translocation through a narrow hole, found the translocation time scales as $\tau \sim N^2$ where N is the number of monomers in the chain. Chuang *et al.* [45] later found an inconsistency in this scaling law in relation to self-avoiding polymers, in which the radius of gyration scales as $R_g \sim N^{\upsilon}$, where υ (the Flory exponent) is 0.588 in three dimensions [74]. By estimating the distance a polymer travels during the translocation process as R_g and noting that the center-of-mass diffusivity of a Rouse polymer (*i.e.*, no hydrodynamic interactions) is D_o/N (where D_o is the diffusion coefficient of a single monomer), Chuang *et al.* [45] estimated the unforced translocation time scaling law as $\tau \sim (R_g)^2/(D_o/N) \sim N^{1+2\upsilon}$, which is the same scaling behavior of the Rouse relaxation time [74], estimated as the time required for a polymer to diffuse its radius of gyration [45,53]. Thus, for self-avoiding polymers, a scaling exponent of $\tau \sim N^2$ would indicate translocation being much

faster than the polymer relaxation time, which is not possible. Hence, $\tau \sim N^{1+2\upsilon}$ could be seen as a better estimate. Unfortunately, as Chuang *et al.* [45] points out, one would assume that a polymer would diffuse through a pore much slower than in the bulk. As a result, this scaling exponent could be seen as a lower bound. Panja *et al.* [46] modified the expression to $\tau \sim N^{\upsilon+2}$ to account for memory effects, due to a local change in monomer concentration on both sides of the pore during the translocation process, which was also observed by Dubbeldam *et al.* [70] and Gauthier *et al*.[75]. In addition, de Haan and Slater [66] found the scaling exponent is heavily dependent on the pore diameter varying from $\tau \sim N^{1+2\upsilon} \sim N^{2.2}$ for a diameter of σ up to a value of $\tau \sim N^{2.93}$ for a diameter of 10σ, where σ is the diameter of each monomer. This increase in scaling exponent is due to the fact that for pore diameters larger than 1.5σ, the monomers do not translocate in a single-file fashion but rather the polymer folds inside the nanopore during the translocation process.

1.4.2 Forced Translocation (Rouse Polymers)

When translocation is aided with an applied force, the scaling laws will change. For example, Kantor and Kardar [47] derived a scaling law expression for a long polymer chain traversing a short pore with an applied force F, *viz*. $\tau \sim R_g/(F/N) \sim N^{\upsilon+1}/F$. A limitation of this scaling law is the assumption that the polymer is in equilibrium throughout the translocation process. This may not always be correct, especially in the presence of high driving forces. Vocks *et al*. [48] derived a new scaling law, $\tau \sim N^{(1+2\upsilon)/(1+\upsilon)}/F$, including the memory affects due to local tension in the polymer chain when a monomer translocates from one side of the pore to the other. Another factor that greatly affects scaling law behavior is the applied force strength. In some previous

simulations it was found that the scaling exponent increased with increasing force [49–51], while in others the scaling exponent decreases with increasing force [52–54,76].

One proposed explanation for these differing observations is that during forced translocation, the polymer is driven out of equilibrium [52,53,55,56]. At first, as was demonstrated in previous simulation studies, extreme monomer crowding on the *trans* side of the nanopore [49–54,56], a clear indication that the polymer has not had ample time to equilibrate once it has passed through the nanopore, was thought to be responsible for scaling laws differing from the value predicted by Kantor and Kardar [47]. However, in more recent studies involving tension propagation theory [51,76–85], it has been proposed that non-equilibrium effects are solely based on changes to the polymer on the *cis* side of the nanopore rather than any *trans* side effects. As discussed by Lehtola *et al.* [50], in the presence of a moderate driving force, the translocation time process can be thought of as a force balance between the applied driving force and the drag force due to the monomers on the *cis* side moving towards the nanopore. When the force used to drive the polymer through the nanopore is applied to monomers inside the nanopore, a tension in the chain is created. This tension propagates along the backbone of the chain creating a "tension front" or boundary in which monomers influenced by the tension move towards the nanopore, and thus contribute to the overall drag force, while the other monomers beyond the front do not. This tension in the chain, depending upon the strength of the applied force, will alter the initial equilibrium shape of the polymer. Weak forces ($N^{-\upsilon} < F < 1$) will result in a "Trumpet" shape, moderate forces ($1 < F < N^{\upsilon}$) will result in a "Stem-Flower" (or "Stem-Trumpet") shape, whereas strong forces ($F > N^{\upsilon}$) will result in

"Strong stretching" (or "Stem") shape [51,79]. These changes in polymer shape are potential reasons for scaling law deviations.

One of the goals of tension propagation theory is to predict the movement of the tension front as a function of time during the translocation process. Using the conservation of mass relating the tension front and the number of monomers experiencing the chain backbone tension, Saito and Sakaue [78,79] and Dubbeldam *et al.* [51], predicted that the total translocation time is the sum of three individual time components with different scaling laws. The first component, τ_{ini}, is the time that it takes to create an initial blob state before monomer translocation. This term, in both the research of Dubbeldam *et al.* [51] and Saito and Sakaue [79], has been hypothesized to be force, not length dependent and, in recent Brownian Dynamics Tension propagation theory [76], has been questioned to even exist. Hence, I will omit it from the discussions here. The second component, τ_1, is the time required for the tension in the chain (generated by the pulling force) to propagate to the end of the polymer. This term dominates for longer chains. Once the tension reaches the end of the chain, the polymer then moves with a constant velocity for a time period τ_2, which is the dominant term in short chains. For moderate to strong forces, the range at which most simulations and experiments are performed at [79], Dubbeldam *et al.* [51] concluded the translocation time $\tau = \tau_1 + \tau_2$, where $\tau_1 \sim N^{1+\upsilon}/F$ and $\tau_2 \sim N^{2\upsilon}/F$. In addition, they also proposed a scaling law transition from $\tau \sim N^{2\upsilon}$ to $\tau \sim N^{1+\upsilon}$ as the applied force is increased, thereby indicating a lower bound exponent of $\alpha = 2\upsilon$, also proposed by Vocks *et al.* [48]. Slight differences were obtained for these scaling laws in the research of Saito and Sakaue [79]. For example, for moderately applied driving forces, the second translocation time component was found to

scale as $\tau_1 \sim N^{\alpha}/F$, where $\alpha = ((z-1)(1+\upsilon)-(1-\upsilon))/(z-1)$. For a Rouse polymer, $z = (1+2\upsilon)/\upsilon$, which results in $\tau_1 \sim N^{1.43}/F$, which is smaller than the values obtained by Kantor and Kardar [47] and Dubbeldam *et al.* [51]. On the other hand, for strong forces, Saito and Sakaue [79] obtained $\tau_1 \sim N^{1+\upsilon}/F$, agreeing with the previous results. Finally, for both moderate and strong forces, Saito and Sakaue [79] obtained the third time component to scale as $\tau_2 \sim N^{2\upsilon}/F$, which agrees with the results obtained from Dubbeldam *et al.* [51].

Most recently, using the same mechanisms described in the tension propagation theory discussed above, Ikonen and coworkers [76,82,83], beginning with the energy balance equations initially derived by Sung and Park [72] and Muthukumar [73], developed a method for computing the Brownian Dynamics motion of the translocation coordinate (length of the chain that has translocated to the *trans* side of the nanopore) in the high damping limit known as the Brownian Dynamics Tension Propagation (BDTP) theory. As shown in previous simulation results [50,62,86,87], the velocity of a polymer translocating through a nanopore is not constant, but rather varies with time. Using this observation, instead of assuming a constant drag coefficient throughout the translocation time simulation, Ikonen and coworkers [76,82,83] instead assumed a drag coefficient that varied in time. Interestingly, from their results, not only did they find good agreement between their predictions and results from MD simulations, but they also discovered that the translocation time scaling exponent is dependent upon length, only converting to the value predicted by Kantor and Kardar [47] ($\alpha = 1 + \upsilon$) in the limit of very long chain lengths. This important discovery implies that there is no universal scaling exponent and explains why there is such discrepancy in the literature. In addition, Lehtola *et al.* [50] investigated how the initial polymer configuration affects the scaling law behavior, by

simulating a polymer chain with an initial configuration of monomers in a straight line. They observed a scaling exponent of $\alpha = 2$, far different than the scaling exponent predicted by Kantor and Kardar [47]. These findings indicate that, not only the applied force and the length of the chain, but also the initial polymer configuration, affects the scaling exponents strongly.

1.4.3 Forced Translocation (Zimm polymer models)

As mentioned before, the formulations discussed above all assume polymer translocation in the absence of hydrodynamic interactions (HI) as modeled by a Rouse polymer. In other words, the diffusion of one monomer does not affect the diffusion of another and, as a result, the center-of-mass diffusion coefficient scales as $D \sim N^{-1}$ and the polymer relaxation time scales as $\tau_R \sim N^{1+2\upsilon}$ [74]. On the other hand, when hydrodynamic interactions are introduced - as modeled by a Zimm polymer - the diffusion of each monomer is affected by every other monomer in the chain through solvent interactions, resulting in a center-of-mass diffusion coefficient scaling law $D \sim R_g \sim N^{-\upsilon}$ and a Zimm polymer relaxation time scaling law of $\tau_Z \sim N^{3\upsilon}$ [74]. The assumption of Rouse behavior is likely valid inside a nanopore as long as minimal folding occurs during the translocation process or if very little water is present inside the pore as would be the case for a very narrow nanopore. However, because many polymers such as double-stranded DNA (ds-DNA) behave as Zimm polymers in bulk solution [88–90], it would seem that assuming Rouse behavior would underestimate the diffusivity of the polymer, especially in the case of studies involving unforced translocation through a nanopore. To complicate matters, hydrodynamic interactions are long ranged in bulk solution [91], but have shown to be screened for polymers moving near a wall or inside a channel [45,68,91]. Hence,

the effect of hydrodynamic interactions in translocation time simulation studies is not trivial and should not be omitted in any thorough investigation.

Under the assumption that, in the presence of hydrodynamic interactions, the translocation process is governed by a force balance between a drag force of a polymer 'blob' with size equal to its R_g on the *cis* side of the nanopore and the driving force to facilitate translocation of the polymer through the pore, Storm *et al.* [9] arrived at a translocation scaling law of $\tau \sim N^{2\upsilon}$, which was also obtained by Sakaue [78]. Fyta *et al.* [57] also investigated Zimm polymer translocation by writing an energy balance equation for the system equating the kinetic energy to the potential energy of the system where the potential energy consisted of the following terms: the change in energy due to the increase and/or decrease in size of the polymer 'blobs' on both sides of the nanopore, the change in energy due to the hydrodynamic drag caused by the fluid, and the energy provided by the applied force used to drive the polymer through the nanopore. Interestingly, Fyta *et al.* [57] also derived the same scaling relationship of $\tau \sim N^{2\upsilon}$. Unlike the derivation by Storm *et al.* [9], which only studied at the effects of the polymer on the *cis* side of the nanopore, the derivation by Fyta *et al.* [57] included effects on both sides of the nanopore, which could be viewed as a more accurate model. Just as was done with the Rouse polymer model, Vocks *et al*. [48] derived a new scaling law, which also includes memory affects due to local tension in the polymer chain, and found $\tau \sim N^{3\upsilon/(1+\upsilon)}$. Later, Saito and Sakaue [79] obtained a different scaling law for polymer translocation with hydrodynamic interactions using the tension propagation theory discussed above. As mentioned earlier, for very long chains, the τ_1 time component dominates with a scaling relationship given by: $\tau_1 \sim N^{\alpha}/F$, where $\alpha = ((z-1)(1+\upsilon)-(1-\upsilon))/(z-1)$, for moderate driving

forces. For a Zimm polymer, $z = 3$, which results in $\tau_1 \sim N^{1.38}/F$, which is different from the values given above. However, the scaling law for short chains obtained by Saito and Sakaue [79] was found to be $\tau_2 \sim N^{2\upsilon}/F$, which agrees very well with the results given above. Just as before with Rouse polymers, Ikonen et al.[83], using BDTP theory, also found the scaling exponent for Zimm polymers is also dependent upon chain length, and, interestingly, converges to approximately the same value of $\alpha = 1 + \upsilon$ [47] in the limit of large N, although much slower than for Rouse polymers. Hence, just as for Rouse polymers, a universal scaling law for Zimm polymers may not exist.

1.5 Objectives and Aims of this Thesis

The overall objective of this thesis is, to investigate the underlying physics involved in biopolymer translocation through solid-state nanopore devices, using the detailed simulation tool developed by myself. More specifically, I aim to define what factors, such as nanopore size, applied voltage, polymer model, etc. most influence the translocation time versus chain length scaling parameter, α. This work includes extensive simulation studies using a highly accurate computation tool, developed by myself using the Fortran programming language, in an attempt to predict the correct values of α under different conditions. The detailed research and objectives of this thesis are as follows:

A. Design and Implement Simulation Methodology

My first objective is to design and implement a physically accurate, computationally efficient, simulation methodology that accurately predicts the underlying physics involved in a translocation time experiment. I do this by modeling atomistically detailed nanopore models constructed from the crystal

structure of β-Si_3N_4, as opposed to many previous simulation studies that assume the nanopore is either a hole in a continuous solid or in a simple homogeneous lattice of atoms. Instead of using Molecular Dynamics (MD) simulations methods, I employ coarse-graining techniques which include Langevin and Brownian Dynamics integration methods to study both Rouse and Zimm polymer models. This allows the use of larger integration time steps, and, as result, I perform simulations for larger time durations using longer polymer chains than possible with MD methods. As will be shown in Chapter 2, I thoroughly test the simulation methodology to ensure all fundamental theoretical laws are obeyed.

B. Rouse polymer Investigation

I thoroughly investigate the translocation time versus chain length (N) scaling law, α, in the absence of hydrodynamic interactions (Rouse polymer model) under different simulation conditions. I perform simulations for different applied voltages, viscosity values, and pore length and diameters to determine how these quantities influence the scaling exponent α. I also investigate the translocation time versus applied voltage scaling behavior and show that, at small to intermediate forces, the scaling law agrees with theoretical predictions ($\tau \sim V^{-1}$). However, at very high applied voltages, extreme crowding at the exit of the nanopore exists, which results in deviations from this theoretical scaling behavior. I also compare this simulation data to measurement results to determine if exclusion of hydrodynamic interactions is

appropriate for modeling biopolymers, such as double stranded DNA (ds-DNA) or single stranded DNA (ss-DNA), used in translocation time experiments.

C. Hydrodynamic Interaction (Zimm Polymer) Studies

Biopolymers, such as ds-DNA and ss-DNA have been shown to behave as Zimm polymers rather than Rouse polymers in bulk solution. Hence, in order to perform a complete study on biopolymer translocation through nanopore devices, it is crucial to include hydrodynamic interactions in the simulation model. As a result, I thoroughly investigate the effects of hydrodynamic interactions on the scaling exponent α and determine whether or not the use of Zimm polymers are important when comparing simulation data to experimental results.

D. Forced vs. Unforced Polymer Translocation

Whereas most experiments involve biopolymer translocation through nanopores using the aid of an applied voltage, equally important are translocation time studies in the absence of an applied voltage (i.e. unforced).

I investigate unforced polymer translocation time studies, for both Rouse and Zimm polymer models, using differing pore sizes, to determine the effect of polymer-pore interactions on unforced translocation time studies. Hence, I sought to answer the question: How does the inclusion of a nanopore alter the diffusivity of a polymer from its characteristic behavior in bulk solution?

These studies are important because they tell us when diffusion greatly affects the translocation process, and when it does not (e.g. in simulations with high applied forces).

E. Inclusion of Electrostatics

In most coarse-grained simulation methodologies, electrostatic effects such as the presence of electrolytic ions and pore surface charge have a negligible impact on a translocation time experiment. However, I sought to investigate (using the coupled Poisson-Nernst-Planck equations) how the inclusion of electrostatic interactions affects the potential distribution inside nanopores of varying diameter and monomer charge distribution. The purpose of this study is to provide more details on the effects of the electrostatic interactions and how they may influence polymer translocation through nanopores.

1.5 Potential Impact of this Work

Nanopore devices, because of their ability to possess high resolution and throughput very high resolution and throughput[21], are seen as potential 'next-generation' single-molecule analysis devices. One very important area that nanopores could have an immediate impact in is the analysis of nucleic acids, more specifically DNA. As mentioned earlier, DNA sequencing has become a widely studied area of research with the goal of the US National Human Genome Research Institute (NHGRI) to create a system that can sequence an entire mammalian-scale genome for about $1,000 by 2014[22]. The use of solid state nanopores constructed in silicon nitride, similar to the

ones that I model in my simulation methodology, could possibly provide a faster, less expensive sequencing method.

Although the mechanisms of biopolymer translocation through a nanopore are far from well-understood, my work accurately predicts the theoretical values of the translocation time versus chain length scaling exponent α and provides example scenarios of when the simulated exponent deviates from theory. I also investigate biopolymer translocation using both Rouse and Zimm polymer models and show that hydrodynamic interactions have a large impact on the translocation time scaling exponent. Furthermore, I have thoroughly studied the effects of nanopore dimensions and applied voltages and their effects on the underlying physics involved in a translocation time experiment. Finally, I studied the effects of the electrolytic ions and nanopore surface charge using the coupled Poison-Nernst-Planck equation to determine the significance of electrostatic interactions. The results from my simulation studies can assist in not only proper nanopore design, but also help determine the proper experimental environments and operational parameters for nanopore operation.

CHAPTER 2: MODEL IMPLEMENTATION AND COMPUTATIONAL METHODS

2.1 Polymer Model

I model the polymer as a freely jointed chain [92] with each monomer represented by a single bead. Each bead has a mass of 312 atomic mass units (amu)[63] and a diameter of 4.3 Å [93], which are the corresponding values for single stranded DNA. Because of the phosphate backbone on the DNA, each monomer has an associated negative charge[94]. This value can vary greatly from 4*e* [95] to 0.094*e* [96] (where *e* is the charge of an electron) depending upon what pH level is used in the experiments. In my simulation results, I assigned a value of 1*e* for the charge on each monomer which has been used in other similar simulation studies [97,98].

Adjacent beads in the polymer model are connected by spring models using one of two different potential types: (1) the Fraenkel model (Equation (2-1))[99] or a combination of the (2) Warner model (often referred to as the "finitely extendable nonlinear elastic" or FENE model[99] and the (Equation (2-2)) Weeks-Chandler-Anderson potential (WCA) [100], which prevents the beads from overlapping (Equation (2-3)).

$$U_{Fran}(r) = \frac{1}{2} k_{Fran} (r - r_o)^2 \tag{2-1}$$

$$U_{FENE}(r) = -\frac{1}{2} k_{FENE} R_o^2 \ln\left(1 - \left(\frac{r}{R_o}\right)^2\right), r < R_o \tag{2-2}$$

$$U_{WCA}(r) = \begin{cases} 4\varepsilon\left[\left(\frac{\sigma}{r}\right)^{12} - \left(\frac{\sigma}{r}\right)^{6}\right] + \varepsilon, r \le 2^{1/6}\sigma \\ 0, r > 2^{1/6}\sigma \end{cases} \quad (2\text{-}3)$$

In my preliminary simulations, I used the Fraenkel model with an equilibrium bead-to-bead distance of r_o = 4.3 Å and an associated spring constant k_{Fran} of 171 kcal/molÅ^2 as used in similar simulation studies [98]. This spring constant value could be considered too high for a coarse-grained DNA model since it is on the same order as Carbon-Carbon bonds[101,102]. When I used this value for k_{Fran} (or other smaller values as well), there was a very sensitive relationship between the simulation time step and the model's ability to keep adjacent DNA beads connected together. If the time step was too high, the DNA chain of beads would break apart and the translocation simulation would fail. Because of the extreme sensitivity of the time step using the Fraenkel model, all of the simulations studies, unless otherwise specified, use the FENE-WCA spring model described in Equations (2-2) and (2-3), which models a more loosely connected spring, thus allow for a larger time step to be used.

Using the FENE-WCA bead-spring model, I assign the values for the spring constant $k_{FENE} = 7\ \varepsilon_{poly}/\sigma_{poly}^2$, the maximum allowed distance between beads R_o = 8.6 Å, the Lennard-Jones energy well-depth $\varepsilon = \varepsilon_{poly} = k_BT$ (where k_B is Boltzmann's constant), and $\sigma = \sigma_{poly}$ = 4.3 Å (where $2^{1/6}\sigma$ is the distance of the energy well depth). Using these values, the potential energy function is a minimum when the distance between beads is ~ 4.48 Å. The bead-to-bead energy for non-adjacent beads (excluded volume effect) is computed using the same Weeks-Chandler-Anderson potential in Equation (2-3) with ε =

ε_{poly} and $\sigma = \sigma_{poly}$. I provide more detail, including potential energy plots, about the differences between the Fraenkel and FENE-WCA bead-spring models in the Appendix section A.1.

The non-adjacent monomer model described in Equation (2-3) has been used in many previous simulation methodologies to mimic a polymer with high excluded volume interactions which cause the polymer to swell. However, I was also interested in how the polymer would behave in bulk conditions in which the excluded volume interactions were decreased ("poor" solvent conditions). To do this, I also implemented a polymer model using a full Lennard-Jones potential energy function, which includes both the repulsive and attractive terms, as shown in Equation (2-4), where r_c is the cutoff distance at which the energy is no longer computed. As will be shown later, I compute the radius of gyration and diffusion coefficient using both models from Equations (2-3) and (2-4) in order to understand the differences of each model.

$$U_{LJ}(r) = \begin{Bmatrix} 4\varepsilon\left[\left(\frac{\sigma}{r}\right)^{12} - \left(\frac{\sigma}{r}\right)^{6}\right], r \le r_c \\ 0, r > r_c \end{Bmatrix} \tag{2-4}$$

It should be noted that the persistence length of the polymer used in a majority of simulations discussed in this thesis can be thought of as being on the same order as the length of the nanopore. This is because, as described earlier, the bead-to-bead distance in the polymer, using the FENE-WCA potential energy function, will vary between and σ_{poly} = 4.3 Å and R_o = 8.6 Å. In most of the simulations performed in this thesis, the length of

the nanopore is 5 Å. These simulations are intended to model long polymer chains translocating through nanopores much shorter in length, which is often seen in experimental methods. In addition, due to the repulsive Weeks-Chandler-Anderson potential in Equation (2-3) used to compute the bead-to-bead energy for non-adjacent beads, the polymer will swell to a large radius of gyration as is the case in good solvent conditions. It should be noted, however, that I do perform simulations using longer pores of 50 Å and 100 Å. In those simulation studies, I intended to study how the translocation time scaling exponents change when the length of the polymer is much shorter or on the same order as than the length of the pore.

2.2 Nanopore Model

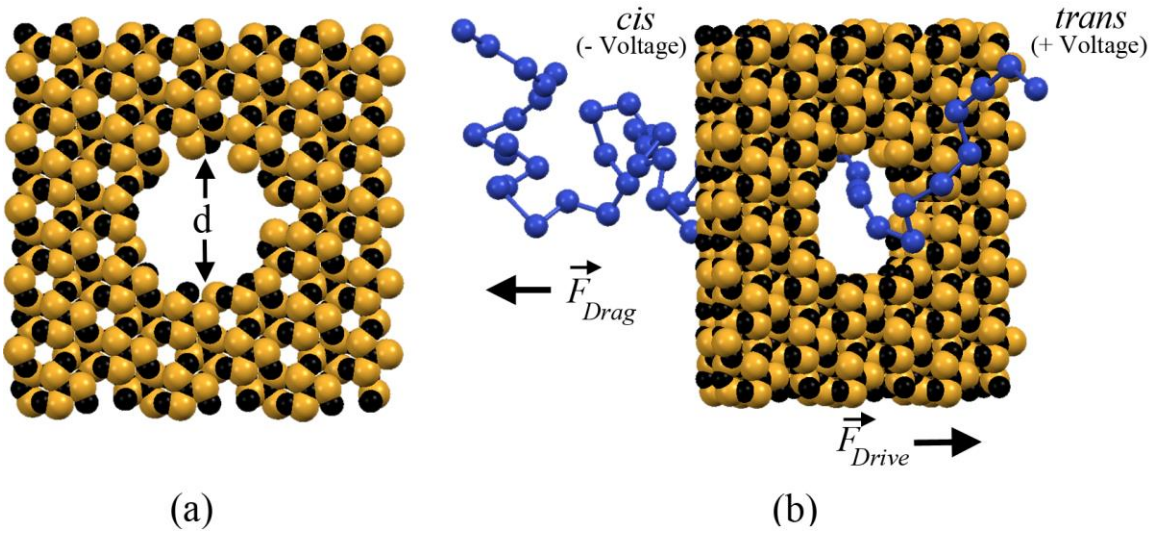

Figure 3: (a) Top view of silicon nitride (β-Si_3N_4) nanopore with diameter d. Orange: Si, Black: N. (b) Polymer chain translocating through nanopore from the *cis* side to the *trans* side with the aid of a driving force due to an applied voltage.

Unlike many previous coarse-graining simulation studies that assume the nanopore is either a hole in a continuous solid or in a simple homogeneous lattice of atoms, I employ atomistically detailed nanopore models. The crystal structure of β-Si_3N_4 is used to construct membranes of different thicknesses, and approximately circular pores of different diameters are constructed by removing atoms from the membrane. An example of a nanopore with a diameter of 1.5 nm (denoted by d) and length of 0.5 nm is shown in Figure 3(a). As will be discussed later, I perform studies in which I vary both the pore diameter and length. Figure 3(b) is an example snapshot of a 50-monomer polymer, each monomer represented by a blue sphere, translocating through a 1.5 nm nanopore with the aid of applied driving forced. As shown, the drag force is in the opposite direction of translocation. Included in the simulation volume is an implicit reservoir of water both to the left (*cis*) and right (*trans*) of the nanopore as well as inside

the nanopore. The length of the simulation box in the direction of translocation (which is the z direction) is 60 nm. Finally, periodic boundary conditions were employed in these simulations as well.

The energies and forces due to the interactions between the atoms in the nanopore and the monomers are computed using the same Weeks-Chandler-Anderson potential energy function given in Equation (2-3), with the exception of different parameters σ and ε, thus creating a very repulsive interaction between the polymer and the pore. The energy well depth for the interaction between a monomer and a nitrogen atom, $\varepsilon_{poly\text{-}N}$, is assigned a value of $0.1k_BT$. This value was determined empirically through extensive trial simulations. From previous measurements using silicon nitride[103], a ~ 63% increase was found between the van der Waals energy well depth parameter, ε, of silicon and nitrogen. Hence, in all of my simulations, I increase $\varepsilon_{poly\text{-}N}$ by 63% to determine the energy well depth for the interaction between a monomer and a silicon atom $\varepsilon_{poly\text{-}Si}$. To compute $\sigma_{poly\text{-}N}$ and $\sigma_{poly\text{-}Si}$ I use the measured values of σ for silicon and nitrogen[103], σ_{poly} = 4.3 Å, and the Lorentz-Berthelot mixing rules[100] given in Equations (2-5.1) and (2-5.2).

$$\sigma_{Si/N-Polymer} = \frac{\sigma_{Si/N} + \sigma_{DNA}}{2} \tag{2-5.1}$$

$$\varepsilon_{Si/N-Polymer} = \sqrt{\varepsilon_{Si/N}\varepsilon_{Polymer}} \tag{2-5.2}$$

2.3 Force Due to applied Voltage

Due to the high dielectric constant of the water that is present on the *cis* and *trans* side of the nanopore, it was first assumed, as was done in previous studies [49,51,52,55,58,59,62–64], that the electric field (and hence the force due to the applied voltage) is non-zero only inside the pore. The force due to the applied voltage in the direction of translocation is $F = qV/d$, where q and d are the charge and diameter of each monomer respectively and V is the voltage drop across the pore. Although the force due to the applied voltage varies as a function of ionic concentration, the force has been measured in previous experiments to be in the 10 - 30 pN range for voltages between 50 - 150 mV[19]. In the work presented here, I varied the applied force from ~ 11 pN to 279 pN, which corresponds to a voltage range of 30 - 750 mV (assuming a charge of 1e on each monomer [97,98]), which are consistent with previous measurements using silicon nitride nanopores and ds-DNA [19]. Later, as will be discussed in this chapter, I studied the effects of electrostatics in solid state nanopores.

2.4 Integration Methods

In this section, I describe the integration methods used to solve for the underlying physics involved in polymer translocation through nanopore devices. As described below, I first implemented the Velocity Verlet algorithm to perform NVE simulations to ensure energy was being conserved in the translocation time simulations. In addition, I implemented a Langevin Dynamics integrator [104] to study Rouse polymer translocation through nanopores. And finally, I implemented a Brownian Dynamics integrator [105] to include hydrodynamic interactions in my model to study Zimm polymer translocation through nanopores. Extensive tests were performed using each of these algorithms with the results given in this chapter.

2.4.1 Velocity Verlet (NVE) Simulations

In order to ensure energy conservation was met I implemented the Velocity Verlet integration algorithm [100] to perform molecular dynamic simulations of biopolymer translocation through nanopore devices. The Velocity Verlet algorithm consists of two equations:

$$\vec{v}(t+\Delta t) = \vec{v}(t) + \frac{\vec{F}(t+\Delta t) + \vec{F}(t)}{2m}\Delta t \tag{2-6}$$

$$\vec{r}(t+\Delta t) = \vec{v}(t)\Delta t + \frac{\vec{F}(t)}{2m}(\Delta t)^2 \tag{2-7}$$

where r is the position of each monomer, v is the monomer velocity, $\vec{F}$ is the sum of all forces, m is the monomer mass, and Δt is the integration time step.

To ensure these algorithms were working properly and the forces and energies were being computed correctly, several simulations involving different chain lengths, applied potentials, integration time steps, and pore sizes were conducted in which the total energy was plotted versus time. One example, shown in Figure 4, demonstrates that the sum of the kinetic energy and the potential energy is constant for the duration of the translocation process for both the Fraenkel and FENE models, each consisting of 10 monomers, using a linear potential of -1 V through a nanopore of length 50 Å with a diameter of 30 Å. The integration time step, Δt, used in the simulation was 0.1 psec. A thorough discussion about how the integration time step was chosen for all simulations is provided in Appendix section A.3 of this thesis.

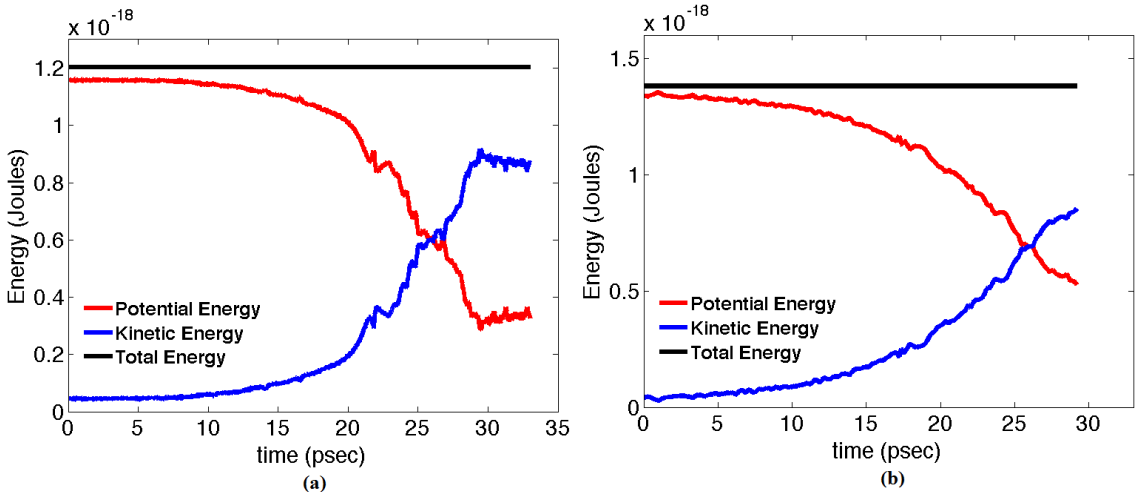

Figure 4: Energy vs. time for a 10 monomer length chain using the (a) Fraenkel and (b) FENE-WCA polymer models. As seen in both cases, the total energy is constant for the duration of the translocation process.

2.4.2 Langevin Dynamics Simulations for Rouse polymers

In order to study Rouse polymer (no hydrodynamic interactions) translocation through nanopores, I selected an algorithm that integrates the Langevin equation of motion (1) in three dimensions[104]:

$$m\frac{d^2\vec{r}}{dt^2} = -\zeta\frac{d\vec{r}}{dt} + \vec{F} + \vec{R} \tag{2-8}$$

where *m* is the monomer mass, *r* is the monomer position, ζ is the friction coefficient, $\vec{F}$ is the sum of the total forces, and $\vec{R}$ is a random thermal force. Unlike molecular dynamics (MD) simulations, which directly solve Newton's equations of motion by explicitly modeling the interactions between monomers and solvent molecules, the stochastic Langevin equation of motion models the solute-solvent interactions by a random thermal force, which is defined by a Gaussian distribution, $\vec{R}$, and viscous drag

force ($-\zeta \vec{dr}/dt$) . The integration method used to solve Equation (2-8) updates each velocity using the following equations:

$$\vec{v}(t+\Delta t) = \vec{v}(t)e^{-\beta\Delta t} + \frac{\vec{F}}{m\beta}\left(1-e^{-\beta\Delta t}\right) + B_1 \tag{2-9}$$

$$\left\langle B_1 \right\rangle^2 = \left(\frac{3k_BT}{m}\right)\left(1-e^{-2\beta t}\right) \tag{2-10}$$

where k_B is the Boltzmann constant, v is the velocity, t is the current time, Δt is the integration time step, the collision frequency, $\beta = \zeta/m$, and B_1 is Gaussian random number with mean 0 and variance given in Equation (2-10). In addition, the positions of each monomer are updated with the following equations:

$$\vec{r}(t+\Delta t) = \vec{r}(t) + \frac{1}{\beta}\left(\vec{v}(t) + \vec{v}(t+\Delta t) - \frac{2\vec{F}}{m\beta}\right)\frac{\left(1-e^{-\beta\Delta t}\right)}{\left(1+e^{-\beta\Delta t}\right)} + \frac{\vec{F}}{m\beta}\Delta t + B_2 \tag{2-11}$$

$$\left\langle B_2^2 \right\rangle = \frac{6k_BT}{m\beta^2}\left[\beta\Delta t - 2\frac{\left(1-e^{-\beta\Delta t}\right)}{1+e^{-\beta\Delta t}}\right] \tag{2-12}$$

where B_2 is a random Gaussian value with mean 0 and variance given by Equation (2-12).

The interaction between the polymer and the solvent, or the drag force, is determined by the friction coefficient ζ in Equation (2-8). The friction coefficient is computed to be $\zeta = 40(m/t_{LJ})$, where m is the mass of each monomer and $t_{LJ} = (m\sigma^2/\varepsilon)^{1/2}$ is the Lennard-Jones time step. Setting $\varepsilon = k_BT$ and $\sigma = 4.3$ Å, I obtain $\zeta = 4.2 \times 10^{-12}$ kg/sec, which is approximately the same value found from Stokes law[106,107] using a sphere

with hydrodynamic radius of 2.15 Å[93]. The integration time step in these simulations was 0.1 psec.

In order to test the functionality of the Langevin dynamics (LD) simulations, I performed an ensemble of 1000 simulations for 5000 psec using a single bead (diameter of 3.4 Å) in the absence of an applied voltage and nanopore, with an initial velocity v_0 = 0, and compared these results to the theoretical average squared velocity (v) (Equation (2-13))[108] and the theoretical average squared displacement (Equation (2-14))[108]. As shown in Figure 5, the simulation results match the values obtained from the equations very well.

$$\left\langle v^2 \right\rangle = \frac{3k_B T}{m} + \left(v_o - \frac{3k_B T}{m} \right) e^{-2\beta t} \tag{2-13}$$

$$\left\langle \left| r - r_o \right|^2 \right\rangle = \frac{6k_B T}{m\beta} t \tag{2-14}$$

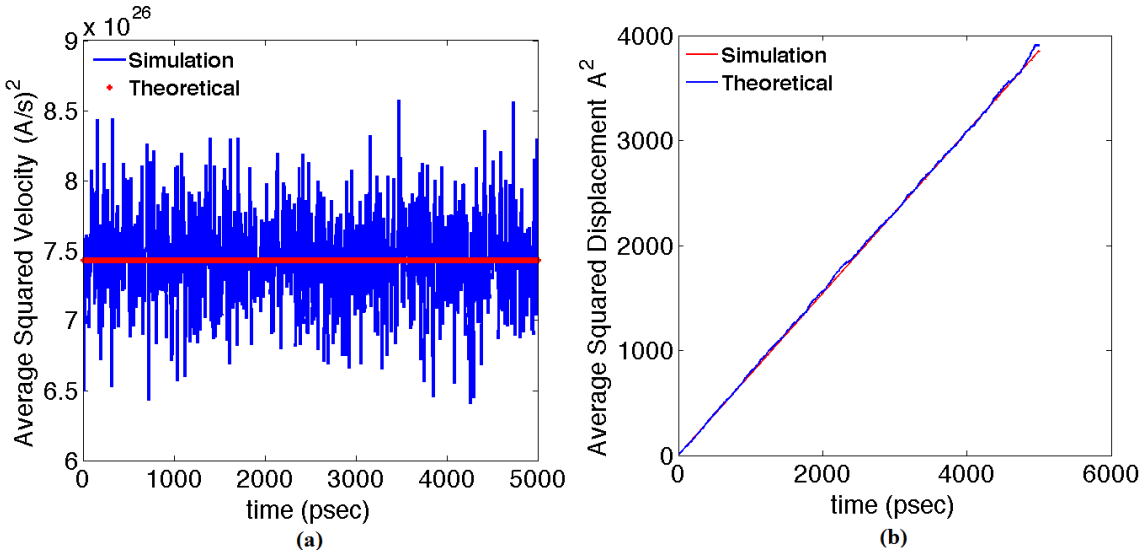

Figure 5: Ensemble of 1000 simulations using a single bead in the absence of an applied potential and nanopore for (a) Average squared velocity $(Å/s)^2$ and (b) Average squared displacement $(Å)^2$ vs. time.

In the next set of simulation tests, I placed the polymer in bulk solution, in the absence of a nanopore and applied voltage, and recorded the radius of gyration and the diffusion coefficient for polymer models implemented with the FENE-WCA (Equation (2-3) and the full Lennard-Jones (Equation (2-4)) potential energy functions in which I implemented a cutoff radius (r_c) of 9 Å because, using the polymer model parameters described in section 2.1, the potential energy is very small beyond this distance.

As shown in Figure 6(a), the radius of gyration for the polymer described by the FENE-WCA potential energy function scales as $\langle R_g^2 \rangle \sim N^{1.18}$, which agrees with the theoretical prediction of $\langle R_g^2 \rangle \sim N^{2\nu}$, where $\nu = 0.588$[74]. In addition, when the excluded volume interaction is removed, the radius of gyration decreases significantly as indicated by the much smaller slope. As shown in Figure 6(b), however, the diffusion coefficient, which scales as $D \sim 1/N$, does not change between polymer models. In fact, it is seen that both polymers diffuse as a Rouse polymer[74] due to the absence of

hydrodynamic interactions between the polymer and the solvent. From previous measurements for very long strands, ss-DNA[93] diffuses as $D \sim 1/N^{0.49}$ and ds-DNA[88–90] diffuses as $D \sim 1/N^{0.6}$ in bulk solution, indicating that hydrodynamic interactions are significant when describing the interactions between DNA and the solvent. It may be argued that hydrodynamic interactions between DNA monomers inside a narrow pore are negligible [52,63,109]. On the other hand, hydrodynamic interactions between DNA monomers outside the nanopore will change the diffusivity of the polymer during the translocation process which, in turn, could alter scaling laws such as translocation time versus chain length. In my initial studies as described in Chapter 3, I focused on simulations involving Rouse polymers, as was done in previous investigations[52,53,62–65,71,86,109]. Later, in Chapter 4, I include hydrodynamic interactions into my simulation models as well.

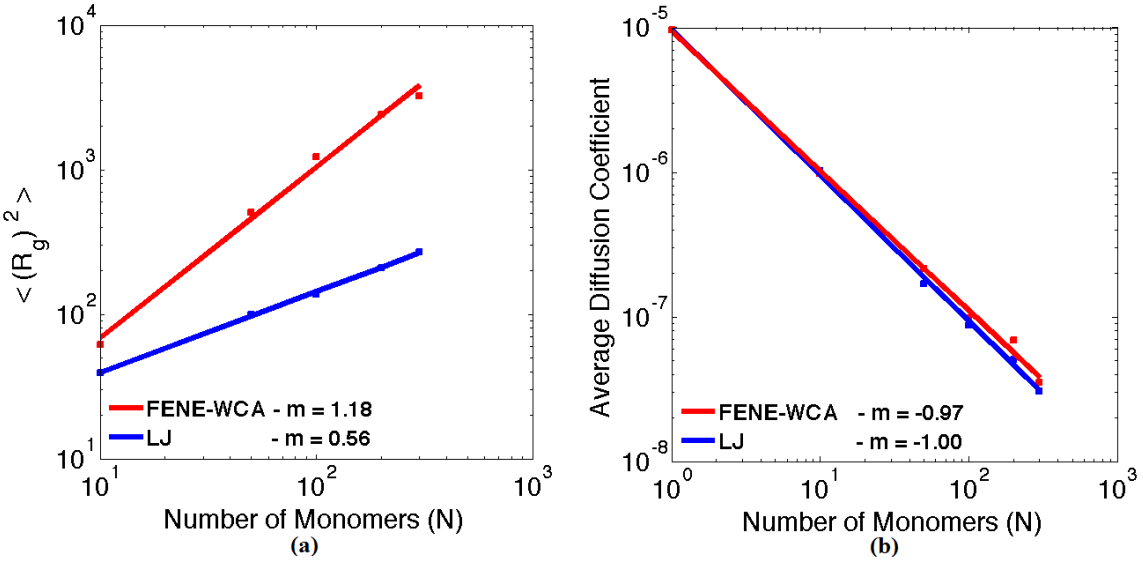

Figure 6: (a) Average radius of gyration and (b) center of mass diffusion coefficient versus number of monomers for two different polymer models, where m is the slope of each line.

2.4.3 Brownian Dynamics Simulations with Hydrodynamic Interactions

The next studies involved investigating the effects of hydrodynamic interactions on polymer translocation through nanopores using a recently developed method - referred to as a truncated expansion ansatz (TEA)[105] - in three dimensions. The development of the TEA algorithm begins with the equation derived by Ermak and McCammon [110] used to study Brownian Dynamics (BD) with hydrodynamic interactions:

$$\Delta r_i(\Delta t) = \sum_j \frac{D_{ij} F_j}{k_B T} \Delta t + \sum_j \frac{\partial D_{ij}}{\partial r_j} \Delta t + R_i(\Delta t) \tag{2-15}$$

where $\Delta r_i(\Delta t)$ is the monomer displacement over coordinate i, D_{ij} are the components of the $3N$ x $3N$ diffusion tensor, F_j is the sum of all forces acting on each monomer, k_B is Boltzmann's constant, T is the system temperature, and $R_i(\Delta t)$ is the random thermal displacement with mean and covariance given by:

$$\langle R_i(\Delta t) \rangle = 0, \quad \langle R_i(\Delta t) R_j(\Delta t) \rangle = 2 D_{ij} \Delta t \tag{2-16}$$

The hydrodynamic interactions are described by the Rotne-Prager-Yamakawa (RPY) tensor [111]:

$$\mathbf{D}_{ii} = \frac{k_B T}{6\pi\eta a} \mathbf{I} \tag{2-17}$$

$$\mathbf{D}_{ij} = \frac{k_B T}{8\pi\eta r_{ij}}\left[\left(\mathbf{I} + \hat{r}_{ij} \otimes \hat{r}_{ij}\right) + \frac{2a^2}{3r_{ij}^2}\left(\mathbf{I} - 3\hat{r}_{ij} \otimes \hat{r}_{ij}\right)\right] \quad \text{for } i \neq j \quad \text{and} \quad r_{ij} \geq 2a \qquad (2\text{-}18)$$

$$\mathbf{D}_{ij} = \frac{k_B T}{6\pi\eta a}\left[\left(1 - \frac{9}{32}\frac{r_{ij}}{a}\right)\mathbf{I} + \frac{3}{32}\frac{r_{ij}}{a}\hat{r}_{ij} \otimes \hat{r}_{ij}\right] \quad \text{for } i \neq j \quad \text{and} \quad r_{ij} < 2a. \qquad (2\text{-}19)$$

where i and j are the indices of two monomers, a is the hydrodynamic radius of each monomer, η is the solvent viscosity and **I** is the identity matrix. Using the above tensor, the second term in Equation (2-15) vanishes. As stated in the fluctuation-dissipation theorem [112], there is a relationship between the viscous drag and random thermal collisions. The viscous drag force is dictated by the $3N$ x $3N$ diffusion tensor **D** in Equations (2-17 – 2-19). The terms in the random thermal displacement $R_i(\Delta t)$, can be expressed as the product of a $3N$ x $3N$ tensor, **B**, and a Gaussian random variable with zero mean and variance Δt [105,113]. To satisfy the fluctuation dissipation theorem, the following relationship must hold:

$$\mathbf{D} = \mathbf{B}\mathbf{B}^{\mathbf{T}} \qquad (2\text{-}20)$$

One issue that limits the application of hydrodynamic interactions is the enormous computational expense in obtaining **B** from **D**. Two widely used methods are Cholesky factorization [110] and Chebyshev polynomial approximation [114], which are both expensive and scale as $O(N^3)$and $O(N^{2.25})$ respectively. The TEA algorithm, on the other hand, scales as $O(N^2)$, has been shown to have high accuracy [113], and is being used in

other simulation studies [61,115] as well as included in recently released Brownian dynamics simulation packages [116,117].

The TEA algorithm updates the positions of each monomer by decomposing Equation (2-15) into a sum of two terms [105,113,117]. The first term is simply Equation (2-15) with the random displacement term, $R_i(\Delta t)$, removed and can be written as follows:

$$\Delta r_i^{Term\,1}(\Delta t) = \sum_j \frac{D_{ij} F_j}{k_B T} \Delta t = \frac{D_{ii} \Delta t}{k_B T} F_i^{eff} \tag{2-21}$$

where:

$$F_i^{eff} = \sum_j \frac{D_{ij}}{D_{ii}} F_j \tag{2-22}$$

Intuitively, this first term can be thought of as the displacement of each monomer due to the applied force terms, F_j, that are corrected for hydrodynamic interactions resulting in F_i^{eff}. The second term accounts for the displacements due to the random forces and is written as:

$$\Delta r_i^{Term\,2}(\Delta t) = \frac{D_{ii} \Delta t}{k_B T} C_i \sum_j \beta_{ij} \frac{D_{ij}}{D_{ii}} f_j = \frac{D_{ii} \Delta t}{k_B T} f_i^{eff} \tag{2-23}$$

where f_j is a random force, in the absence of hydrodynamic interactions, with the following characteristics:

$$\langle f_i \rangle = 0, \quad \langle f_i f_j \rangle = \frac{2(k_B T)^2}{D_{ii} \Delta t} \delta_{ij} \tag{2-24}$$

Similar to the first displacement term, f_j is also corrected for hydrodynamic interactions resulting in f_i^{eff}:

$$f_i^{eff} = C_i \sum_j \beta_{ij} \frac{D_{ij}}{D_{ii}} f_j \tag{2-25}$$

In order to compute this displacement term, two coefficients, C_i and β_{ij}, need to be determined. The C_i values are normalization constants which ensure that for each coordinate i, the diffusion coefficient for no hydrodynamic interactions, D_{ii} (i=j in Equation (2-16)), is kept. To understand the purpose of the β_{ij} coefficients, recall from Equation (2-20) that the random thermal displacements are determined by the contents of the **B** matrix. The β_{ij} coefficients are weighting values that effectively assign a diffusion tensor of $\sqrt{\mathbf{D}}$ in the $\Delta r_i^{Term\ 2}$ displacement value as opposed to the **D** tensor in the $\Delta r_i^{Term\ 1}$ term. One of the assumptions of the TEA algorithm that allow for efficient computation of the C_i and β_{ij} coefficients is that the hydrodynamic interactions are weak, i.e. $D_{ij} << D_{ii}$. This assumption is valid for my simulation studies because, as explained in the polymer model section in this chapter, it is assumed the polymer is in good solvent and, thus, will experience high excluded volume interactions which results in minimal overlapping thus decreasing the effect of hydrodynamic interactions. Based on these assumptions and assigning $\beta_{ii} = 1$ and $\beta_{ij} = \beta'$ is computed by:

$$\beta_{ij} = \beta' = \frac{1-\sqrt{1-[(3N-1)\varepsilon^2-(3N-2)\varepsilon]}}{(3N-1)\varepsilon^2-(3N-2)\varepsilon} \tag{2-26}$$

where ε is computed using the following equation:

$$\varepsilon = \frac{\sum\sum_{i<j} D_{ij}}{(3N-1)3N/2} \tag{2-27}$$

The normalization coefficients are computed by:

$$C_i = \sqrt{\frac{1}{1+\beta'^2 \sum_{i\neq j} \frac{D_{ij}^{\ 2}}{D_{ii}D_{jj}}}} \tag{2-28}$$

In order to perform simulations without hydrodynamic interactions, which directly compare to the cases that include hydrodynamic interactions, the β' value is simply assigned to 1/2 and the normalization coefficients, C_i , all converge to 1.

It should be noted that, whereas in these simulations water is included inside the nanopore, the model does not include hydrodynamic coupling between the polymer and the nanopore. However, as will be shown later, the simulation results agree very well with theoretical predictions and experimental results, which could be an indication that hydrodynamic coupling effects are negligible for the studies that I am interested in. In addition, the hydrodynamic radius and the solvent viscosity are assigned to be 2.15 Å and 1 centipoise respectively in Equations (2-17), (2-18), and (2-19). The integration time

step for these simulations was 0.05 psec. A thorough discussion about the integration time step is given in section A.3 in the appendix of this thesis.

Just as I did in the previous section for the algorithm defined by Equations (2-9 – 2-12), I first performed simulations in bulk water, *i.e*. in the absence of a nanopore and driving force, for polymer models with and without hydrodynamic interactions. I measured the radius of gyration, diffusion coefficient, and time required for the polymer to reach its steady-state radius of gyration starting from the minimum energy configuration. Theoretically, for a polymer in a good solvent (high excluded volume) one should obtain $\langle R_g^2 \rangle \sim N^{2\upsilon} \sim N^{1.18}$ where the Flory exponent $\upsilon = 0.588$ in 3-D [74]. As shown in Figure 7(a), the calculations give scaling exponents for the steady state radius of gyration only slightly higher than this theoretical value for both Rouse (~6.5%) and Zimm (~8%) polymers, and are in good agreement with previous work using the TEA algorithm and a similar polymer model [113]. In addition, Figure 8 (a) shows how the average squared displacement for a single monomer with a diameter of 4.3 Å agrees very well with the theoretical result given by Equation (2-14). In addition, the center of mass diffusion coefficient scaling exponent obtained for the Rouse model agrees very well with the theoretical scaling of $D \sim N^{-1}$ as shown in Figure 8(b) [74]. A Zimm polymer, using the RPY tensor, should have a diffusion coefficient scale as $D \sim N^{-\upsilon} \sim N^{-0.588}$, which is in good agreement with my simulation results, other simulation results using the TEA algorithm [105] and also measurements of ds-DNA [88–90]. Finally as shown in Figure 7 (b), the time required for the polymer to reach its steady state radius of gyration was measured for both the Rouse polymer ($\tau_R \sim N^{2.19}$) and the Zimm model ($\tau_Z \sim N^{1.84}$) and found to agree very well with the theoretical relaxation scaling [74] of $\tau_R \sim N^{1+2\upsilon} \sim N^{2.18}$

and $\tau_Z \sim N^{3\upsilon} \sim N^{1.76}$ and with other simulations using the TEA algorithm for HI interactions [105].

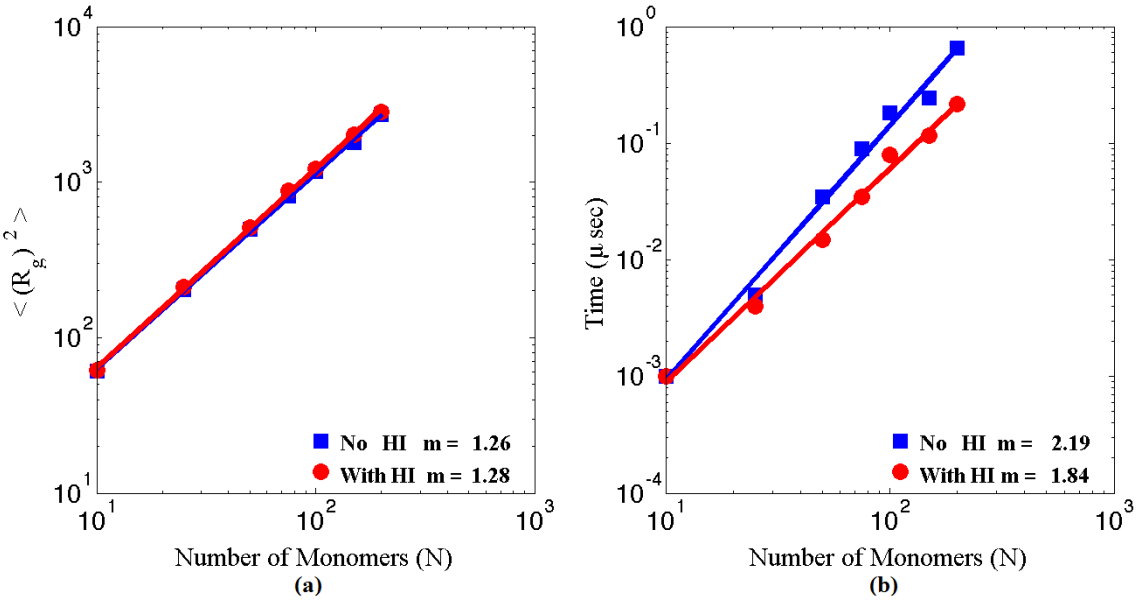

Figure 7: Scaling of the (a) average radius of gyration squared and (b) time required for polymer to reach its steady-state radius of gyration with number of monomers (N), for two different polymer models where m is the slope of each line.

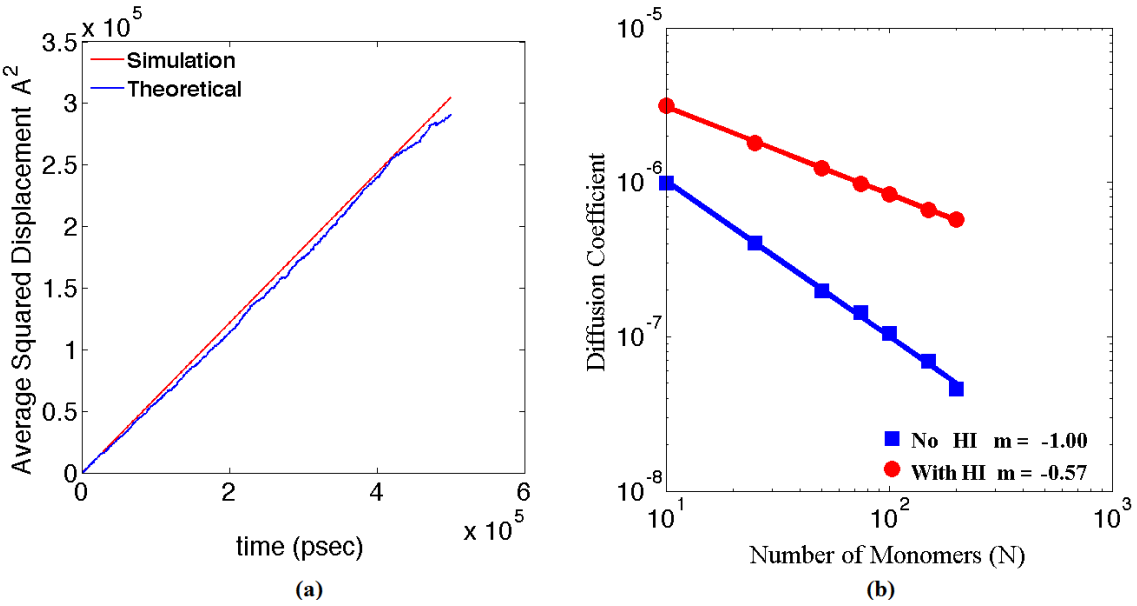

Figure 8: (a) Average squared displacement vs. time for single monomer of 4.3 Å in diameter (b) Center of mass diffusion coefficient for both Rouse and Zimm polymer models**.**

2.5 Equilibration Methods

As will be discussed in Chapter 4, I sought out to investigate how the initial polymer configuration (i.e. radius of gyration on the *cis* side of the nanopore at time t = 0) affects the translocation time scaling law. To do this, I began the translocation process with the polymer in one of the two different starting configurations. In configuration (1), the first monomer is placed inside pore and the remaining monomers are placed with random orientations in the *cis* reservoir with center-to-center spacing of σ_{poly} (0.43 nm). Next, I perform a Metropolis Monte Carlo (MMC) [118] procedure with 50,000 trials to place the polymer in its minimum energy configuration. The translocation timer then begins and the monomers are permitted to move through the pore. In configuration (2), after the MMC procedure, the monomers in the *cis* reservoir are allowed to relax to a 'steady-state' radius of gyration for a certain time period (based upon Figure 7 (b)) before

translocation is allowed. In either configuration, the translocation time is defined as the time required for all monomers to translocate from the *cis* reservoir to the *trans* reservoir. Interestingly, because of the polymer model defined by the FENE-WCA potentials, the 'minimum energy' configuration of the polymer is not the same as the 'steady-state' configuration (which is commonly referred to as the 'equilibrium' configuration). I discuss this difference in more detail in Chapter 4. In this section I discuss the details of the MMC procedure. It should be noted that the 'minimum energy' configuration of the polymer does not involve any interaction with the pore. In other words, during the MMC procedure, the computed energy only consists of terms between the polymer and itself and no terms between the polymer and pore. As will be demonstrated later, this leads to a much smaller radius of gyration than the 'steady-state' configuration (2).

Essentially, at each trial of the MMC procedure, a monomer is moved to a random position and the new energy, μ_{Trial} is compared to the energy as if the monomer had not moved, $\mu_{Current}$. If the new energy is smaller than the current energy ($\mu_{Trial} < \mu_{Current}$) then the move is accepted and the monomer is placed at its new position. If the new energy is larger than the current energy, then the move is accepted with probability:

$$P(Accept) = e^{-\frac{(\mu_{Trial} - \mu_{Current})}{kT}} \tag{2-29}$$

The MMC procedure tests every possible microstate of the system and it is possible for a trial move that results in a higher energy be accepted. However, trial moves that result in higher energy are accepted with a much lower probability than trials that result in lower energy which are always accepted.

In order to verify the functionality of the MMC code, from statistical mechanics, in a microcanonical ensemble (constant particle number, N, constant volume, V, and constant energy, E), the probability of a particular particle being at energy state, *r*, can be found by Equation (2-30) [119,120]:

$$\frac{P(r)}{P\left(r=r_o\right)}=\frac{e^{-\frac{\mu(r)}{k_BT}}}{e^{-\frac{\mu(r_o)}{k_BT}}} \tag{2-30}$$

where r_o is the position of lowest potential energy.

Using a simple two bead simulation, as shown in Figure 9, a MMC trial move that results in a distance in which the bead to bead energy is a minimum is always accepted (probability = 1). In addition, the statistics obtained from the simulation, shown in blue discrete staffs, follow the theoretical equation drawn in red. One can also observe the curves are much broader for the FENE spring model than the Fraenkel model indicating large displacement distances away from the minimum distance of 4.48 Å still result in small energy values and, thus, are accepted with high probability. This is also seen in the potential energy curves for the FENE spring model shown in Figure 61 in section A.1 of the appendix of this thesis.

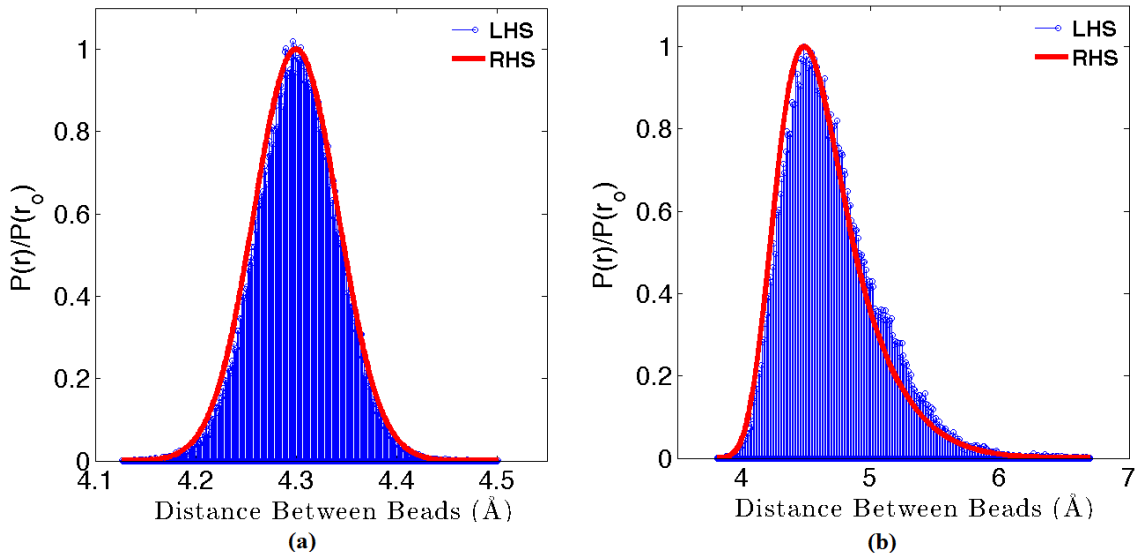

Figure 9: Two bead simulation results for: (a) Fraenkel and (b) FENE-WCA spring models. Blue staffs are probability ratio from left side of equation 2-30, red curve represents points obtained from exponential ratio on right side of equation 2-30.

To understand how the overall energy changes as a function of MMC iteration, I performed a simulation using two polymer chains, each with 10 monomers, in which the distance between each monomer was initially set to a value different from the equilibrium distance. For one polymer chain, composed of beads using the Fraenkel spring model, I initially set the monomer distance to be 5 Å (equilibrium distance = 4.3 Å). For another polymer chain with the same number of monomers, I used the FENE model and changed the monomer distance to 3 Å (equilibrium distance = 4.48 Å). As shown in Figure 10, for both examples, the energy is minimized as a function of MMC trial.

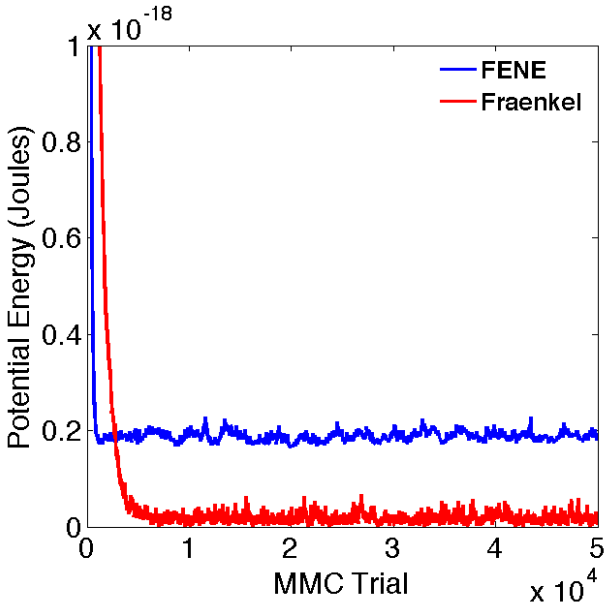

Figure 10: Energy as a function of MMC trial using a 10 bead polymer chain for Fraenkel and FENE spring models.

Tables 1 and 2 in section A.2 in the appendix of this thesis provide a list of the initial and final monomer distances for both simulation results. In addition, further details of the MMC procedure as well as a descriptive flow chart are also provided in section A.2.

In all of the simulation studies presented in this thesis, the first monomer is always placed inside the nanopore before the translocation time simulation begins. This may not always be the case in experimental findings because the polymer will not always overcome the entropic boundary required for translocation nor will the first monomer in the chain always enter the pore first (i.e. the polymer could enter the pore in a folded fashion). However, because one of the main goals of this research was to compare derived theoretical results to successful experimental translocation events in which the polymer was not folded, I assumed the first monomer in the chain would be the first

monomer to enter the pore. Furthermore, because the time required for the polymer to diffuse to the pore was not of interest, each simulation began with the first monomer placed inside the pore.

2.6 Electrostatics

2.6.1 Simulation Description

As mentioned previously, most coarse-grained simulation methodologies assume electrostatic effects such as the presence of electrolytic ions and pore surface charge have a negligible impact on a translocation time experiment. However, in this thesis, I sought to investigate, using the coupled Poisson-Nernst-Planck equations, how the inclusion of electrostatic interactions affects the potential distribution inside nanopores of varying diameter and monomer charge distribution. The purpose of this study is to provide more details on the effects of the electrostatic interactions and how they may influence polymer translocation through nanopores.

2.6.2 Poisson-Nernst-Planck Equations

To calculate the potential throughout the simulation volume due to the surface charge and ionic electrolyte, I treat the ionic solution as a continuum and solve the coupled Poisson-Nernst-Planck (PNP) equations using a finite difference approach described in [121]. The coupled PNP equations can be found by first noting the relationship between the time dependence of the ion concentration, *C*, and the total ion flux J_{Total} can be found using Equation (2-31):

$$\frac{\partial C\left(\vec{R},t\right)}{\partial t} = -\nabla \bullet J_{Total}\left(\vec{R},t\right) \tag{2-31}$$

The total ion flux in the system J_{Total} can be found by summing the individual flux terms, $J_{diffusion}$ and J_{drift}, which are a result of concentration and electrical gradients respectively [122].

$$J_{Total} = J_{diffusion} + J_{drift} \tag{2-32}$$

The first term, $J_{diffusion}$, is found using Fick's first law for diffusion, whereas the second term, J_{drift}, is computed using Ohm's law for ion drift [122], where the sum is given in Equation (2-33) [121]:

$$J_{Total}\left(\vec{R},t\right) = -D\left[\nabla C\left(\vec{R},t\right) + \frac{\nabla \Phi C\left(\vec{R},t\right)}{k_B T}\right] \tag{2-33}$$

where D is the diffusion coefficient and Φ is the potential. Under steady state conditions the left side of Equation (2-31) is set to zero resulting in Equation (2-34) which describes how to compute the change in ion concentration:

$$\nabla \bullet \left[\nabla C\left(\vec{R},t\right) + \frac{\nabla \Phi C\left(\vec{R},t\right)}{k_B T}\right] = 0 \tag{2-34}$$

In order to solve the Equation (2-34), Poisson's equation, given by Equation (2-35) is used to solve for the potential Φ:

$$\varepsilon_o \nabla \bullet \left(\varepsilon\left(\vec{R}\right)\nabla\Phi\left(\vec{R}\right)\right) = -\rho_{pore}\left(\vec{R}\right) - \rho_{polymer}\left(\vec{R}\right) - \sum_i z_i C_i\left(\vec{R}\right) \tag{2-35}$$

where ε is the dielectric constant, ε_o is the permittivity of free space, ρ_{pore} is the charge density on the surface of the nanopore, $\rho_{polymer}$ is the charge density associated with the individual monomers of the polymer, and C_i is the concentration density of ion i with valence z_i. Hence, Equations (2-34) and (2-35) are the coupled Poisson-Nernst-Planck (PNP) equations used to compute the electrostatic effects due to the electrolytic ions, charged biopolymer, and nanopore surface charge.

In order to solve the coupled PNP equations above, I implement a finite difference algorithm, derived in reference [121], using Equations (2-36) and Equations (2-37)

$$\phi_i = \frac{\sum_j \frac{\varepsilon_j \phi_j}{h_j^2} + \sum_\nu \frac{z_\nu e c_{\nu i}}{\varepsilon_o} + \frac{q_i}{\varepsilon_o V}}{\sum_j \frac{\varepsilon_j}{h_j^2}} \tag{2-36}$$

$$c_i = \frac{\sum_{j=1}^{6}\left[\frac{1}{h_j} + \left(\frac{ez}{2k_BT}\right)\left(\frac{\phi_j - \phi_i}{h_j}\right)\right]c_j}{\sum_{j=1}^{6}\left[\frac{1}{h_j} - \left(\frac{ez}{2k_BT}\right)\left(\frac{\phi_j - \phi_i}{h_j}\right)\right]} \tag{2-37}$$

where z is the valence of each ion, h is the grid size in the x, y, and z directions, e is the charge on an electron, q is the charge at a particular grid point, and V is the volume of each box defined by the spacing given by h.

My simulations employ a 100 Å x 100 Å x 600 Å simulation box (for x, y, and z respectively) divided onto a 1 Å x 1 Å x 1 Å grid. To find the potential and concentration, Equations (2-36) and (2-37) are solved in an iterative fashion by the Successive Over-Relaxation (SOR) method[123,124] using the six point "nearest neighbors" summation at each grid point in a checkerboard pattern[125]. The SOR approach consists of solving Equations (2-36) and (2-37) at each grid point i in the simulation volume and "adjusting" the solution using an over-relaxation parameter, ω, until the assigned number of iterations has been reached or the iteration-to-iteration error for both the potential and ion concentration at each grid point has dropped below a certain threshold. Equations (2-38) and (2-39) describe how the potential and concentration at each grid point i for iteration j are solved for.

$$\phi_{i,j} = \phi_{i,j-1} + \omega\left(\phi_i - \phi_{i,j-1}\right) \tag{2-38}$$

$$c_{i,j} = c_{i,j-1} + \omega\left(c_i - c_{i,j-1}\right) \tag{2-39}$$

Although there are many different methods for computing ω [123–125], I performed several trial experiments and found the value that results in the smallest error was ω = 1.35 using 200,000 trials. The final iteration-to-iteration error for each grid point was approximately 10^{-7} V for the potential and 10^{-10} 1/Å^3 for the concentration. Finally, I employ Dirichlet boundary conditions, both at the top (z = 0) and bottom (z = 600 Å) of the simulation volume and periodic boundary conditions in x and y.

Once the potential has been obtained from the PNP solver, the electric field and the resultant force need to be computed. The electric field in the x direction at grid point (I,J,K) (the y and z directions are computed identically) is found by using a center-difference approximation as shown in Equation (2-40)[124]. Since periodic boundary conditions only exist in the x and y directions, finding the electric field at both the minimum and maximum z values are found using either a forward or backward-biased Taylor series difference formula given in Equations (A-8) and (A-9) in section A.5 of the appendix [124]. The force then is found as the product of the electric field and the charge on the DNA monomer, which was determined to be -1*e* [97,98], where *e* is the charge on an electron.

$$\vec{E}_{x,IJK} = \frac{\phi_{I+1JK} - \phi_{I-1JK}}{2\Delta x} \tag{2-40}$$

Since my computational methodology permits monomers to flow anywhere in the simulation volume, the potential and electric field are often needed at positions other than at grid points. In order to do this, I implement a Trilinear interpolation method [126], discussed thoroughly in appendix section A.6, to find the exact value of the electric field and force on each monomer anywhere in the simulation volume.

In each simulation, the nanopore is centered in the simulation volume, with a reservoir of water both above and below the pore. Before the PNP calculations begin, the simulation tool assigns a dielectric value for each grid point in the simulation volume. If a grid point lies in the water portion of the simulation volume, the dielectric constant is assigned a value of 80 [121,127–131], whereas if a grid point lies in the solid portion of the pore, the dielectric constant is assigned a value of 7, which is the dielectric constant of silicon nitride developed by Plasma-enhanced chemical vapor deposition (PECVD) methods [132]. Figure 11 (a) provides an example of how the dielectric constant is assigned for a pore with diameter of 30 Å and length 50 Å at the Z = 302 Å plane. Each green marker represents the location of the silicon nitride membrane, whereas every blue marker represents water.

In addition, the simulation tool also assigns charge values to the nanopore as well. In solutions commonly used in translocation time measurements, the pH level ranges between pH 7-8 [9–11,13–15,41]. Under these conditions, silicon nitride has a negative surface charge density of σ_{Si3N4} = -0.02 C/m^2 [41]. By using the computed surface area of the nanopore structure and σ_{Si3N4}, the simulation tool will assign a surface charge value to each grid point represented by the surface of the pore. Figure 11 (b) provides an example

of how the charge is assigned for a pore with diameter of 30 Å and length 50 Å. Each red marker indicates where the charge is labeled.

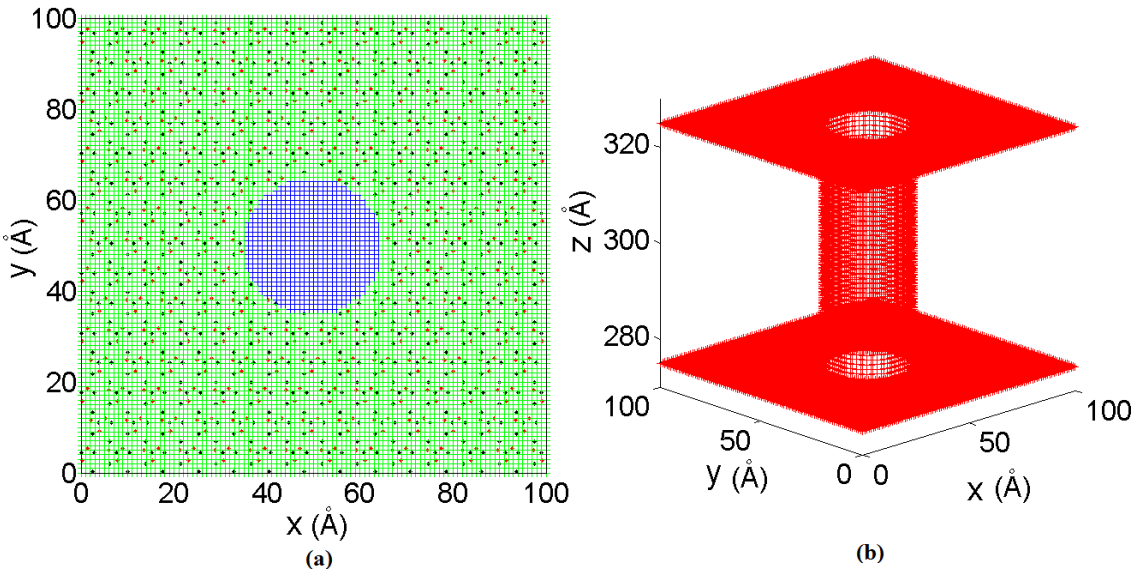

Figure 11: Charge and Dielectric labels for 30 Å nanopore. (a) Example dielectric constant labeling for Z = 302 Å plane. Blue (water) – ε = 80, Green (Si_3N_4) – ε = 7. (b) Example charge assignment. Red labels indicate where charges are located in nanopore.

Finally, in all of my simulations, I employ an electrolyte solution with a concentration of 1 M which is the same amount commonly used in translocation time experiments [9–11,13–15,18,41].

2.6.2 Simulation Testing and Validation

To validate my PNP simulation methodology, I first performed tests using simple dielectric slabs with length of 5 Å and 50 Å in the z direction, with sheets of charge located on top and bottom of each slab. A drawing of these structures is shown in Figure 12 with the face of slab on the x axis removed for ease of visualization of the bottom

sheet of charge. As stated earlier, there is a reservoir of water both above (*cis*) and below (*trans*) the structures resulting in an overall simulation length of 600 Å in the z direction.

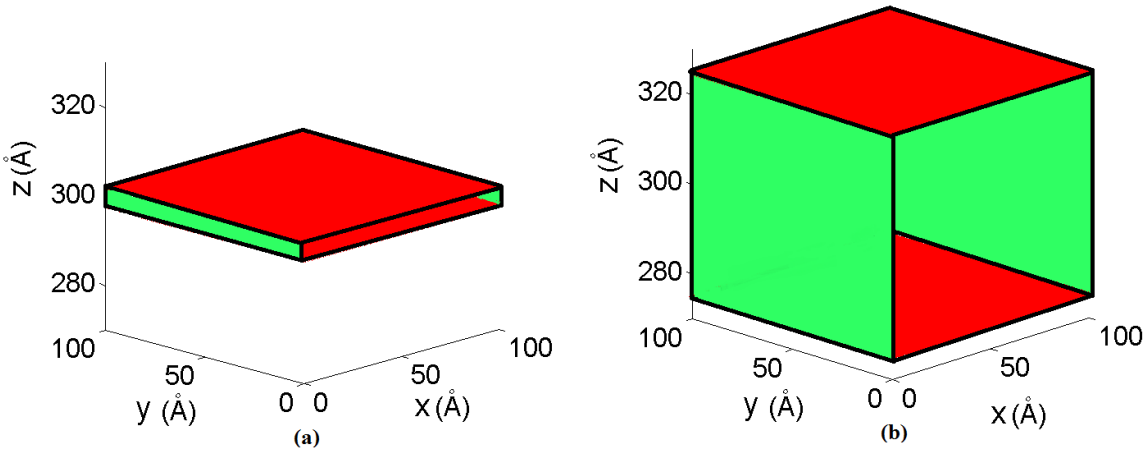

Figure 12: Dielectric slabs of length (a) 5 Å and (b) 50 Å with sheets of charge (shown in red) on top and bottom of each slab. The green area indicates material with dielectric constant of ε = 7. X plane is removed from figure to show bottom sheet of charge**.**

In my first simulations using the simplified structures above, I computed the potential, in the absence of an electrolyte solution (by setting the ionic concentrations to zero), for both the 5 Å and 50 Å slab. In these simulations, I employ Dirichlet Boundary conditions, both at the top and bottom of the simulation volume in which the voltage is assigned to 0, and, just as stated before, periodic boundary conditions in x and y. Figure 13 provides the potential as a function of z, with both x and y set to 50 Å. Since the structure in Figure 12 is symmetric, the potential as a function of z will be the same for any x and y value.

As shown, the potential is linear with a negative slope from the z = 0 Å boundary to the beginning of the slab and is linear with a positive slope from the end of the slab to the end of the simulation volume (z = 600 Å). Since the electric field is the negative gradient of the potential, the z component of the electric field component in the *cis* reservoir points in the positive z direction, whereas in the electric field in the *trans* reservoir points in the negative z direction. The direction of the electric field components agree with basic electrostatic theory that states the electric field will point towards an infinite negative charged plane.

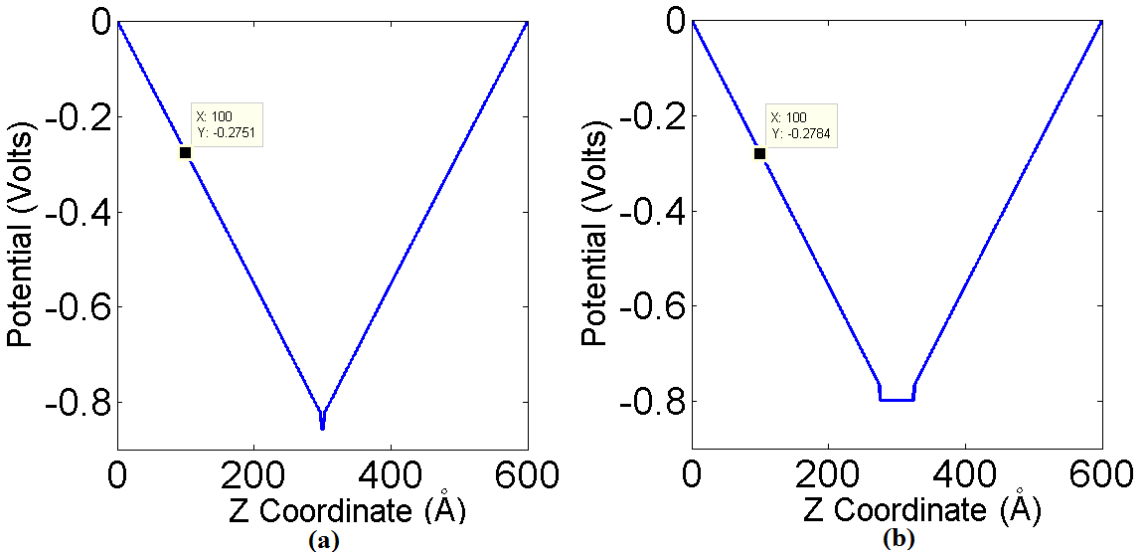

Figure 13: Potential results using dielectric slabs of length (a) 5 Å and (b) 50 Å with sheets of charge on top and bottom of each slab. The markers indicate the potential at z = 100 Å.

If it is assumed the charged planes above are infinite, Equation (2-41) can be used to obtain an estimate as to what the theoretical result should be for an electric field as a result of two infinite negative charged planes[133].

$$E = 2\left[\frac{\sigma_{Si_3N_4}}{2\varepsilon_r\varepsilon_o}\right] \tag{2-41}$$

Setting of σ_{Si3N4} = -0.02 C/m^2 , ε_r = 80, and ε_o = 8.854 x 10^{-12} F/m, I obtain an electric field of 2.82 x 10^7 V/m or 2.82 x 10^{-3} V/Å. Looking at Figure 13 (a), and noting that the electric field is the negative of the slope of the potential, E = 0.2751 V / 100 Å = 2.751 x 10^{-3} V/Å. Similarly, for the 50 Å slab E = 2.784 x 10^{-3} V/Å. Both of these results are within a few percent of the theoretical value computed from Equation (2-41).

As a next test, I added an electrolytic solution with a 1 M (6.022 x 10^{-4} Å^{-3}) concentration and performed a PNP simulation on the 50 Å dielectric slab structure given in Figure 12(b). Figure 14 provides the concentration as a function of z with x and y both = 50 Å (again, because of the structure of the dielectric slab, the solution will be symmetric). As would be expected, the positive ion with valence 1 has a very large concentration on the surface of the slab, whereas the negative ion, valence -1, has a very small concentration on the surface of the slab. As the distance from the slab is increased, the concentration for both ions converges to the bulk value.

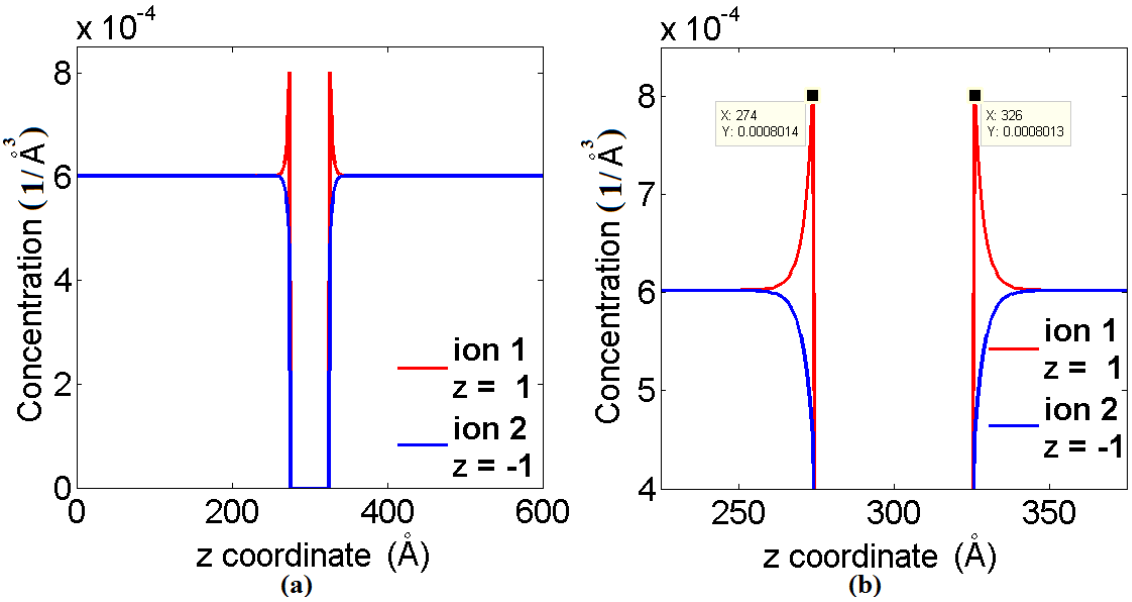

Figure 14: Ionic Concentration vs. z using dielectric slab of length 50 Å for area (a) over entire simulation volume and (b) area focused near the dielectric slab. Red curve is ion with valence +1, blue curve is ion with valence -1.

The potential from the PNP solution is given in Figure 15. As shown, the positive ion that builds on the charged surface greatly reduces the surface potential. Also, as the distance increases from the surface of the slab, the potential approaches zero.

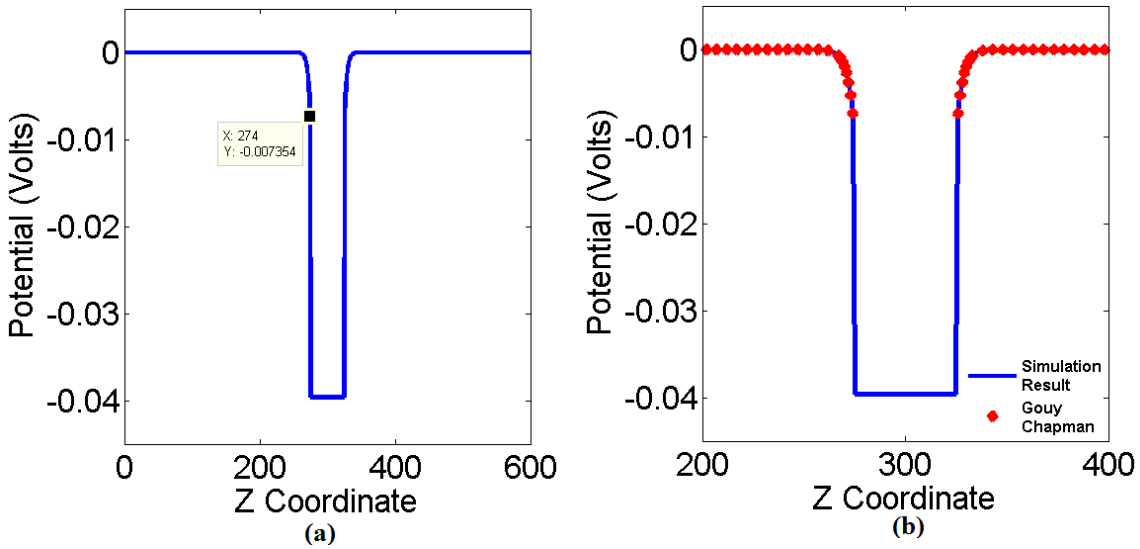

Figure 15: Potential vs. z using dielectric slab of length 50 Å for area (a) Over entire simulation volume and (b) area focused near the dielectric slab. Blue curve is simulated potential. Red points are potential values computed from Gouy-Chapman model.

To test the consistency of the solutions provided in Figures 14 and 15, because there is no applied voltage in these simulations (no ion flow), the ionic concentration should follow a Boltzmann distribution given by Equations (2-42) and (2-43)

$$C_o = C_\infty \exp\left(-\frac{F_c \phi}{RT}\right) \tag{2-42}$$

$$F_c = eN_A \tag{2-43}$$

where C_∞ is the bulk concentration, F_c is Faraday's constant (9.648 x 10^4 C/mol), R is the universal gas constant (8.314 J/K mol), e is the charge on an electron (1.602 x 10^{-19} C),

N_A is the Avogadro constant (6.022 x 10^{-23} mol^{-1}), and C_o is the concentration at the potential given by φ [134]. If I rearrange Equation (2-42) to read:

$$\phi = -\frac{RT}{F}\ln\left(\frac{C_o}{C_\infty}\right) \tag{2-44}$$

and solve for the potential with C_o = 8.014 x 10^{-4} $Å^{-3}$, the concentration at the surface of the slab given in Figure 14 (b), and C_∞ = 6.022 x 10^{-4} $Å^{-3}$, the bulk concentration, the potential is found to be φ = -7.34 x 10^{-3} V, which is approximately equal to the potential given in Figure 15(a) as -7.354 x 10^{-3} V.

To test how the potential curve in Figure 15 compares with theoretical predictions, I computed the Gouy-Chapman (GC) equation [135], as a function of position, and compared those estimates with the simulation results I obtained. The GC equation is given by:

$$\tanh\left[\frac{z_i\psi(z)}{4}\right] = \tanh\left(\frac{z_i\psi_s}{4}\right)\exp(-\kappa z) \tag{2-45}$$

where $\psi(z)$ is the potential as a function of z, $\psi_s = e\psi/kT$, ψ is the surface potential, z_i is the ion valence, and κ is the inverse of the Debye length (λ_D) [135]. With an electrolytic concentration of 1 M, λ_D = 3 Å [135]. Using the surface potential of -7.354 x 10^{-3} V, I plotted the GC equation as a function of z (in Å), given by the discrete red points in

Figure 15 (b). As shown, the points predicted by the GC equation agree very well with my PNP simulation results.

To further test the PNP code, I performed simulations also on the 5 Å slab given in Figure 12(a). And, as shown in Figures 16 and 17, I obtain results similar to the ones obtained with the 50 Å slab. Hence, using these tests, it appears that the results from my PNP calculations agree with theoretical predictions thus proving that my simulation methodology is working properly. Later, in Chapter 5, I will perform PNP simulations on nanopores as well.

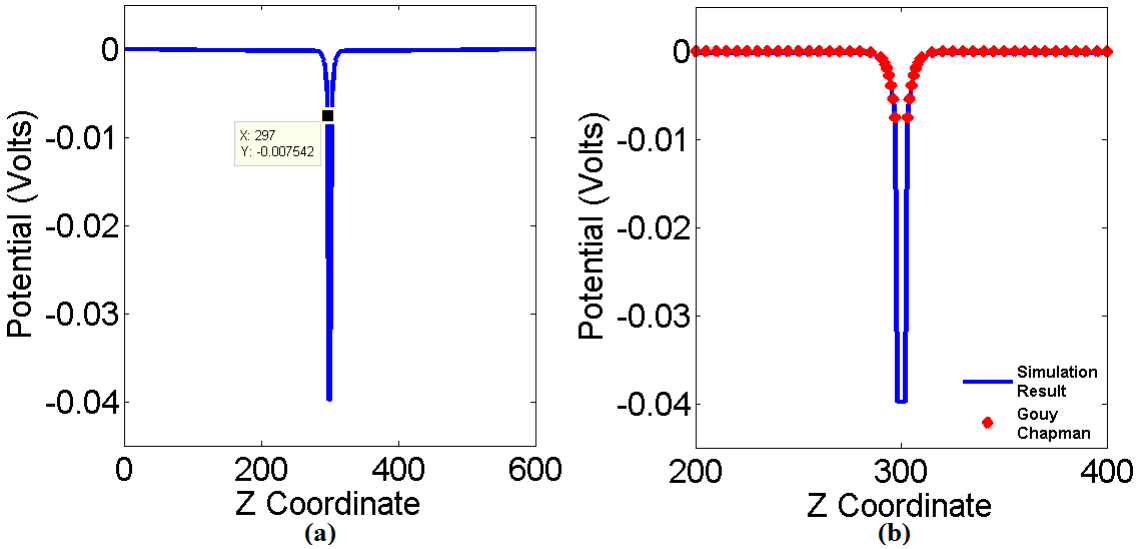

Figure 16: Potential vs. z using dielectric slab of length 5 Å for area (a) Over entire simulation volume and (b) area focused near the dielectric slab. Blue curve is simulated potential. Red points are potential values computed from Gouy-Chapman model.

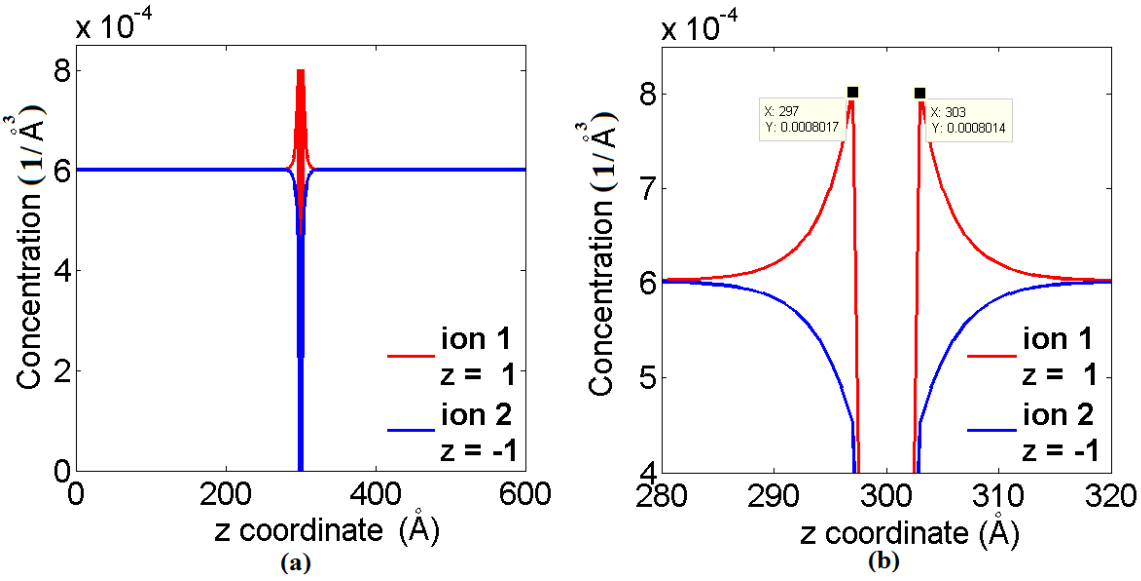

Figure 17: Ionic Concentration vs. z using dielectric slab of length 5 Å for area (a) over entire simulation volume and (b) area focused near the dielectric slab. Red curve is ion with valence +1, blue curve is ion with valence -1.

2.7 Conclusion

The purpose of this chapter was to prove the results obtained from the simulation methodology match theoretical predictions and calculations from fundamental principles. I have shown through MD, using the Velocity Verlet integration method, that my simulation results conserve energy in the NVE ensemble during translocation of polymers through nanopores. Furthermore, I have also demonstrated, using both LD and BD simulation methods, that both the Rouse and Zimm polymer models mimic those in good solvent conditions resulting in proper scaling of radius of gyration, polymer relaxation time, and diffusion coefficient. Finally, using the coupled PNP equations, the calculations from my electrostatic modeling results in the correct theoretical electric field values (in the absence of ions), surface potential, and surface ionic concentration for silicon nitride membranes with the experimental measured surface charge and 1 M

electrolyte, the typical value used in translocation time measurements [9–11,13–15,18,41]. Hence, the methods of integration, electrostatic calculations, and polymer models, are robust, and agree with theoretical predictions and fundamental principles, and are ready to be applied to answer the questions addressed in this thesis.

CHAPTER 3: Rouse Polymer Study

3.1 Introduction

As a first study involving polymer translocation through solid-state nanopore devices, in this chapter I investigate translocation of a Rouse polymer (in the absence of hydrodynamic interactions) through the atomistically detailed silicon nitride nanopores shown in Figure 3, applying the 3-dimensional Langevin dynamics simulations described in section 2.4.2. In particular, this investigation is targeted at understanding the dependence of polymer translocation mechanisms on the chain length, pore geometry (diameter and length), as well as the driving voltage and solvent viscosity.

One main goal of this study is to investigate the translocation time versus chain length scaling exponent α in the expression $\tau \sim N^{\alpha}$. As thoroughly described in section 1.4, finding a universal scaling exponent has not yet been completely resolved [1] and has been the subject of many simulation studies [1,45–71]. Knowing this scaling relationship in advance of a nanopore experiment would make the task of determining the polymer chain length trivial from a translocation time measurement. I also study the effects of the solvent viscosity on the translocation of the polymer through the nanopore. Finally, I investigate the scaling behavior of translocation time versus applied voltage for different polymer and pore lengths. In my analysis, I compare these simulation results to measurement results in the literature to determine if at any time a Rouse polymer is suitable when modeling laboratory systems. It should be noted that all of the simulation studies in this chapter use the minimum energy configuration as the starting point (configuration (1)) as described in section 2.5.

3.2 Unforced Translocation

Figure 18(a) shows the translocation time as a function of polymer length, in an infinitesimally short (0.5 nm length, 0.96 nm diameter) pore with no applied voltage (unforced translocation). To perform these simulations, the polymer was placed with its center monomer in the center of the pore with half of its remaining monomers on the *cis* side of the pore and the other half on the *trans* side of the pore. Each half of the polymer was equilibrated using the MMC procedure described earlier. The polymer was then permitted to translocate in either direction[62]. A successful trial was obtained once the polymer was out of the pore. The translocation time scales as $\tau \sim N^{\alpha}$, where $\alpha = 2.52$, a much stronger scaling behavior than predicted by Chuang *et al.* [45] ($\alpha = 1+2\upsilon = 2.18$, the same scaling exponent as the Rouse relaxation time) and observed in some previous simulation results[59,65,71] in which α varies between 2.2 and 2.33, but which is in good agreement with that predicted by Panja *et al.* [46] ($\alpha = 2+\upsilon = 2.58$) and observed in Dubbeldam *et al.* [70] ($\alpha = 2.5$).

3.3 Scaling Behavior for Forced Translocation vs. Pore Diameter

Figure 18(b) shows the translocation time as a function of polymer length, in the same infinitesimally short pore, using an 80 mV applied voltage, for three different pore diameters (0.96 nm, 1.5 nm, and 3.0 nm), whereas Figure 18(c) shows an example translocation time histogram plot. The translocation time scales as $\tau \sim N^{\alpha}$, where $\alpha = 1.35$ - 1.40, and changes very little with pore diameter. This behavior is in good agreement with the prediction of Vocks *et al.* [48] for translocation through a nanoscale hole, i.e., τ

$\sim N^{(1+2\upsilon)/(1+\upsilon)} \sim N^{(1+2(0.588)/(1+(0.588))} = N^{1.37}$. This is also in good agreement with recent theoretical predictions by Sakaue [78], other simulation methodologies investigating this type of behavior[52,53,55,65] and with measurements from Wanunu *et al.* [18] who observed a crossover behavior with a scaling law exponent of $\alpha = 1.4$ for ds-DNA between 150 - 3500 bp and $\alpha = 2.28$ for longer chains using a 4 nm diameter SiN pore. On the other hand, Storm *et al.* [9] measured a scaling law exponent of $\alpha = 1.27$ for translocation through a 10 nm diameter SiO_2 pore and hypothesized this scaling law was due to the hydrodynamic forces acting on the "blob-like" structure of the DNA outside the nanopore (Figure 19). Interestingly, Fyta *et al.*[57] observed a scaling exponent of $\alpha = 1.36$ in the absence of hydrodynamic interactions, which is in good agreement with my findings, and $\alpha = 1.28$ with hydrodynamic interactions. Because the scaling law in both simulation results as well as the cited experimental results are smaller than the value predicted by Kantor[47] ($\alpha = 1 + \upsilon = 1.588$) it is assumed that the polymer is not in a state of equilibrium during the entire translocation process. It is also seen that these scaling law results are smaller than those predicted from recent MD simulations ($\alpha = 1.47$)[51] and previous works that solve the fractional Fokker-Planck equation and perform subsequent Monte Carlo simulations ($\alpha = 1.5$)[136]. However, as described later in this chapter, by reducing the applied driving force, the polymer flow through the nanopore can be slowed down, allowing the polymer to maintain an equilibrium configuration throughout the translocation process, resulting in larger scaling exponents which approach the values above.

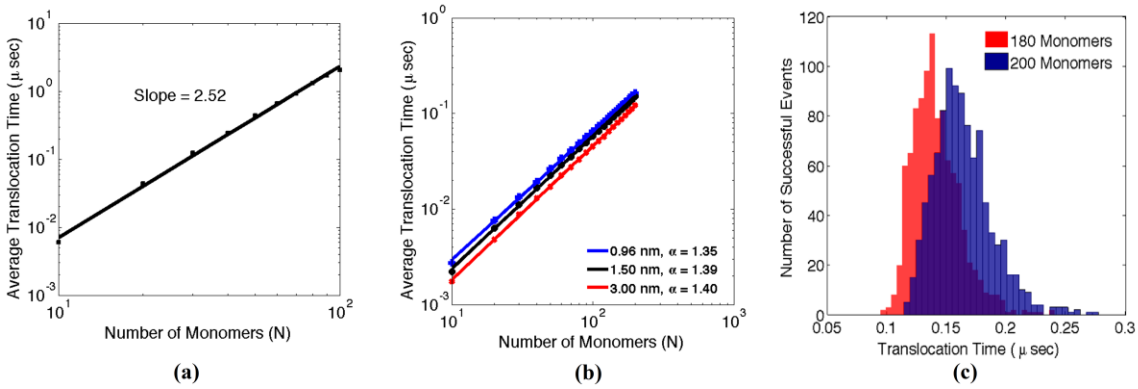

Figure 18: Average translocation time (1000 trials) versus polymer chain length simulations for (a) Unforced (applied voltage = 0V) and (b) applied voltage = 80 mV for three different pore diameters. (c) Example histogram plot for 0.96 nm pore using chain lengths N = 180 and 200.

From my simulations, and previous simulation and measurement results, ds-DNA appears to behave like a Zimm polymer (with hydrodynamic interactions) as in the experiments of Storm *et al.* [9] and like a Rouse polymer (without hydrodynamic interactions) for certain length ranges as in the experiments of Wanunu *et al.* [18] A possible explanation for the discrepancy in the scaling law behavior could be due to electro-osmotic flow inside the nanopore during the translocation process[30]. Recent computational studies[137] have hypothesized that drag forces due to electro-osmotic flow inside a nanopore are more significant that hydrodynamic forces acting on the DNA "blob" outside the nanopore (see Figure 19). If the surface charge of the nanopore has the opposite charge of the polymer flowing through it, the electro-osmotic flow is in the same direction as translocation[138] and vice versa. The silicon nitride pore used by Wanunu *et al.* [18] has a negative surface charge density at high pH[41] which, because DNA is also negatively charged, would result in an electro-osmotic flow in the opposite direction as the translocation process. This leads to an apparent decrease in the velocity of DNA in

the nanopore and reduces the hydrodynamic force caused by the folded DNA chain outside the nanopore. In addition, the pore used by Wanunu *et al.* [18] is also much smaller in diameter than the pore used by Storm *et al.* [9], thereby increasing the effect of the electro-osmotic forces on the translocation process. This behavior is reflected in the translocation time measurements, where it was found that the translocation time through the narrow (4 nm) SiN pore was longer[18] than the translocation time through the much wider (10 nm) SiO_2 pores[9], for DNA chains of similar length.

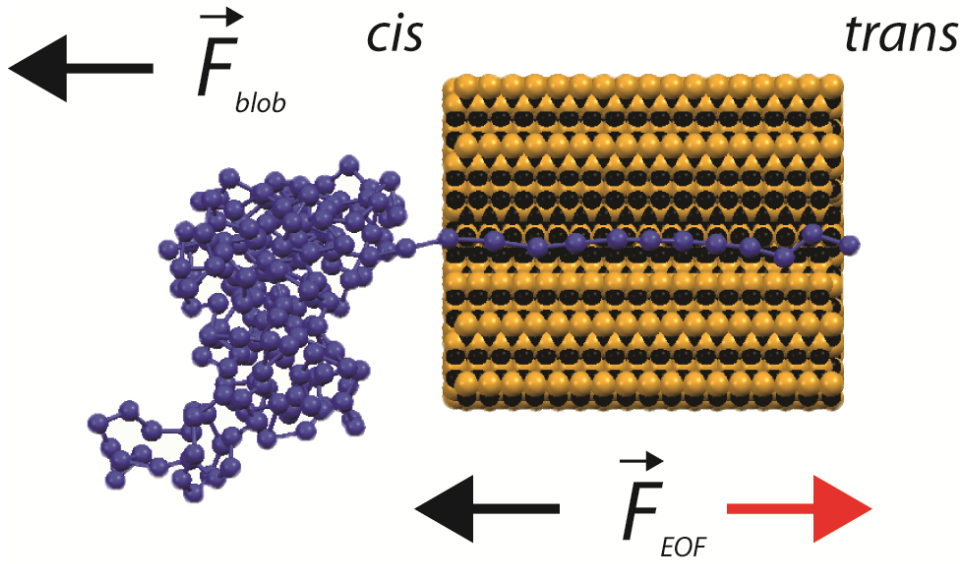

Figure 19: Two hydrodynamic forces involved in a DNA chain translocation through a nanopore. The force due to the "blob like" structure of DNA outside of the nanopore is in the opposite direction of the translocation of the DNA. The direction of the electro-osmotic force is dependent upon the surface charge of the nanopore. If the surface charge of the nanopore is opposite of the surface charge of the polymer, the electro-osmotic flow will be in the same direction as the translocation process (red arrow). If the surface charge of the nanopore is the same as the charge of the polymer, the electro-osmotic flow will be in the opposite direction (black arrow).

3.4 Effects of applied voltage and viscosity

As mentioned earlier, the scaling law exponent for translocation time versus polymer length may vary depending upon how far the polymer is out of equilibrium during the translocation process. In order to verify this, I performed translocation time simulations for several different values of applied voltage and monomer drag coefficient using the same pore that is 0.5 nm in length and has a diameter 0.96 nm. Lowering the voltage and/or increasing the drag coefficient would slow down the translocation process providing more time for the polymer to equilibrate during the translocation process, which should change the scaling law behavior. As shown in Figure 20, whereas increasing the drag coefficient causes a linear increase in the translocation time, the scaling exponent is not affected. This is because even though the translation time is increased due to the higher viscosity, the polymer still does not reach its equilibrium configuration because the relaxation time has also increased. Thus increasing the viscosity does not result in a drastic change in the scaling law with an applied voltage of 80 mV.

On the other hand, when I decrease the applied voltage to 40 mV the scaling law exponent increases from $\alpha = 1.35$ to $\alpha = 1.42$ and increases even more when the applied voltage drops to 10 mV ($\alpha = 1.74$). When the applied voltage is increased from 80 mV to 250 mV, the scaling law remains the same indicating that my simulation results predict a lower limit of $\alpha = 1.35$. This trend of increasing scaling exponent due to lower applied forces has also been observed in other simulation methodologies as well[52,53]. However, it has also been hypothesized by other simulation methodologies that the

scaling law exponent will increase with an increase in driving force[49–51]. The differences in the two results will be further investigated and clarified in the next chapter.

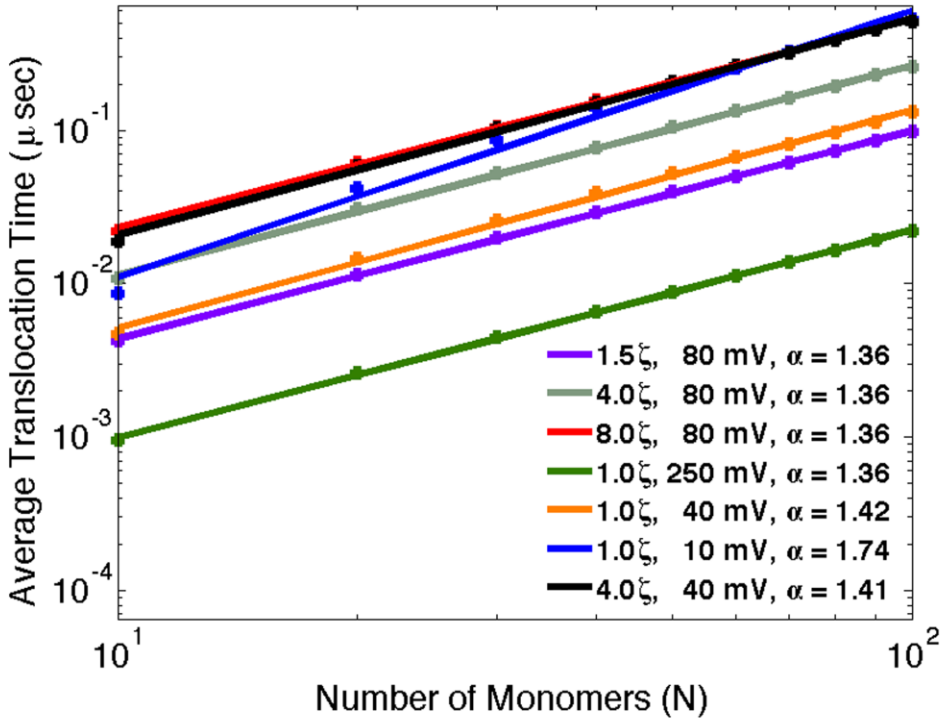

Figure 20: Average translocation time (over 1000 trials) versus number of monomers (N) for different voltages and different multiples of the original drag coefficient using a pore of 0.5 nm in length with a diameter 0.96 nm.

3.5 Translocation in longer pores

When the pore length is increased to 5 nm, the scaling law behavior changes substantially (Figure 21). For polymer lengths between 1 - 30 monomers, the scaling exponent is less than unity, whereas for chain lengths between 40 and 300 monomers the scaling exponent is greater than unity but still lower than the values observed in Figure 18 (b). When the polymer length is increased to N = 320 - 400 monomers the scaling law

exponent becomes 1.39, which is similar to the values observed in Figure 18(b). As shown, the scaling laws appear to be independent of pore diameter. This trend of scaling law dependence on polymer length has also been observed in other simulation methodologies as well [75,86]. A similar scaling law trend is also seen when the diameter and the length of the pore are increased to 4 nm and 10 nm respectively (Figure 22).

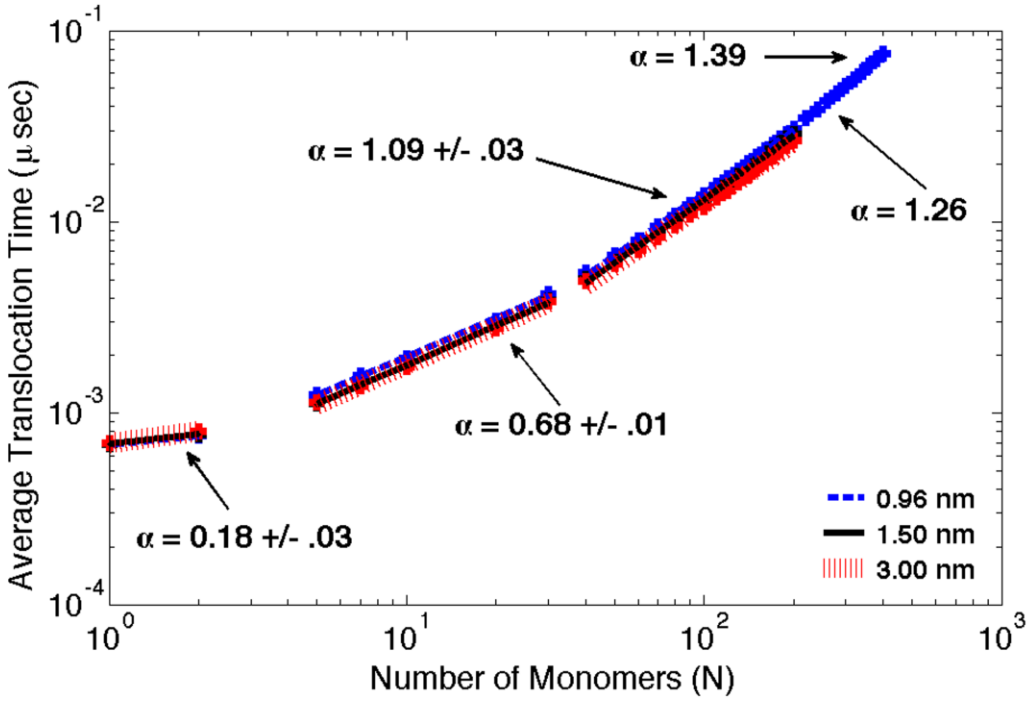

Figure 21: Average Translocation time (over 1000 trials) versus number of monomers (N) for chain lengths N = 1, 2, 5, 7, 10 – 200 monomers for 3 different pore diameters (0.96 nm, 1.5 nm, and 3.0 nm) each with a length of 5 nm. The chain length was increased to N = 220 – 400 monomers for the 0.96 nm pore. The applied voltage for all simulations was 80 mV. As shown, the scaling laws appear to be independent of pore diameter.

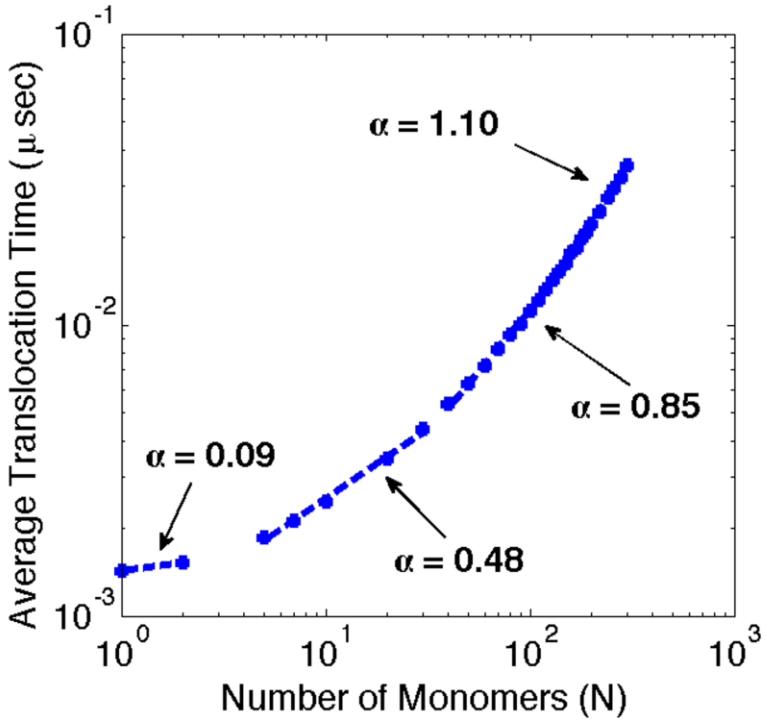

Figure 22: Average Translocation time (over 1000 trials) versus number of monomers (N) for chain lengths N = 1, 2, 5, 7, 10 – 300 monomers using a nanopore of diameter 4 nm and 10 nm length. The applied voltage for all simulations was 80 mV.

To understand why the scaling law exponents are fundamentally different in Figure 18 (b) and Figures 21-22, I examine the differences in the applied force, remembering that the force is only applied to monomers inside the pore. In the situation where the polymer length is on the same order as the pore length, the total force applied to the chain varies as a function of time. This force has its minimum value when only a single monomer is in the pore. The total force increases as more monomers enter the pore, reaching a maximum value when the pore is completely filled with monomers.

Depending upon the length of the chain, the pore force will remain at this maximum value until the last monomer enters the pore. When the polymer has completely exited the pore, the total force returns to zero. This is quite different from the short-pore case in which the force experienced by the monomers remains constant throughout the translocation process. This force profile was also observed by Luo[109] and Gauthier[75]. In the latter work, a scaling behavior of $\tau \sim N$ was observed for chains much smaller than the pore length, whereas $\tau \sim N^{1+\nu}$ was observed for chains much longer than the pore length. The discrepancy between my data and the work of Gauthier is probably due to the state of the polymer during translocation. As mentioned earlier, when the polymer is in equilibrium throughout the translocation process, the translocation time scales as $\tau \sim N^{1+\nu}$. However, as predicted by Vocks *et al.* [48], when the polymer is not in equilibrium, the translocation time scales as $\tau \sim N^{(1+2\nu)/(1+\nu)}$, which is the behavior seen in my simulations. Because the polymers are farther away from equilibrium during the translocation process for both short and long pores, different scaling law exponents are observed. Vocks *et al.* [48] used a conservation of energy approach to predict a lower bound on the translocation time scaling law given by the expression $\tau \sim \eta N^{2\nu}/F$, where η is the viscosity of the solvent. In three dimensions, this would predict a translocation time dependence of $\tau \sim \eta N^{1.176}/F$ whose exponent is substantially larger than that obtained from Figure 21 for chain lengths between 1 - 200 monomers. However, as described earlier, in these simulations the force is now a function of the chain length N, which reduces the scaling exponent to a value lower than 2ν, indicating an even lower bound when the chain length is on the order of the pore length.

For the situation when the polymer length is much greater than the pore length (Figure 18(b)), it was observed from the scaling behavior that the polymer is not in equilibrium throughout the translocation process. This observation helps explain why the scaling exponent for intermediate chain lengths (5 – 30 monomers) in Figures 21 and 22 are much less than unity. Due to the longer pore length, the applied force is larger and, as a result, the translocation time is much shorter than the Rouse relaxation time. The polymer is therefore now farther from equilibrium during the translocation process. This phenomenon is also demonstrated by the increase in crowding of monomers at the exit of the pore as demonstrated in Figure 23(c).

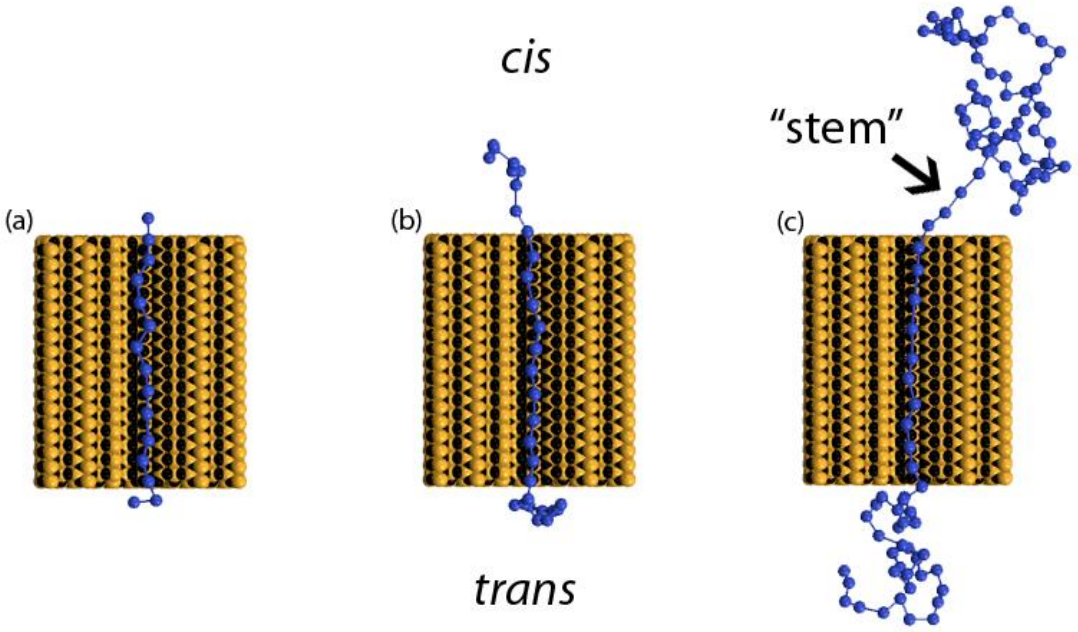

Figure 23: Snapshot of translocation through a nanopore of 0.96 nm diameter and 5 nm in length for (a) N = 15, (b) N = 30, and (c) N = 100 monomers using an applied voltage of 80 mV. In order to view the polymer inside the nanopore, half of the nanopore has been removed in the figures. Because of the repulsive nature of the energy equation that describes the interaction between non-adjacent monomers (Equation 2-3), in equilibrium, the polymer should have minimum overlap and possess a very large radius of gyration. However, as shown in figures (b) and (c), there is crowding of monomers on the trans side of the nanopore during the translocation process indicating the polymer is not in equilibrium. In addition, as shown in figure (c), a 4 monomer "stem" region has developed at the entrance of the pore due to the presence of a large driving force.

As described by Sakaue[78] and more recently in Dubbeldam *et al.* [51], the total translocation time can be broken down into two individual time components: an initial period, τ_1, where the tension caused by the applied force propagates down the polymer resulting in a decreasing chain velocity, and a second period, τ_2, in which the tension propagation has reached the end of the chain and thus the velocity of the polymer remains constant throughout the remaining translocation process. Furthermore, Dubbeldam *et al.* [51] described three possible formations ('trumpet', 'stem-trumpet', and 'stem') of the

polymer on the *cis* side of the pore, and two different translocation time versus chain length scaling law regions. Both the polymer shape and scaling law are dependent upon the strength of the applied force. In the force strengths used in this work (intermediate to strong), the scaling laws for the two different time regions are: $\tau_1 \sim N^{1+\nu}/F \sim N^{1.588}/F$ and $\tau_2 \sim N^{2\nu}/F \sim N^{1.176}/F$, which correspond to the 'stem-trumpet' or 'stem' polymer shapes. This can be seen in Figure 23(c), where a "stem" of 4 monomers is seen to exist at the pore entrance. In addition, the scaling law behavior - albeit with different scaling exponents - is demonstrated in Figures 21-22. When the length of the chain is very short, the time required for the tension to reach the end of the chain is very small, and thus the velocity during translocation is essentially constant, thereby resulting in small scaling exponents with the dominant time period being τ_2. When the length of the chain is increased, the time required for the tension to reach the end of the chain increases, thus causing the chain velocity to decrease and resulting in a larger influence of τ_1 and higher scaling exponents. Finally, when the length of the chain is long enough, a maximum scaling exponent is reached. Even though the scaling exponent in Figure 21 ($\alpha = 1.39$) is smaller than the exponent obtained by Dubbeldam *et al.* [51] ($\alpha = 1.47$), the results in Figure 20 show that the applied voltage could be varied until the observed scaling law is reached, which occurs at ~35 mV. I investigate the scaling exponent versus applied voltage further in Chapter 4.

3.6 Translocation Time vs. Applied Voltage: Scaling Behavior

Next, I investigate the scaling behavior of translocation time on the applied voltage (60 mV – 750 mV) for several different chain lengths, through both a short (0.5 nm) and long (5 nm) nanopore. Figure 24 shows the voltage dependence of the translocation time for chains of different lengths in a very short pore (0.5 nm). For N = 1, the voltage scaling exponent is weak (about -0.3), because the single monomer travels very quickly through the pore without being significantly accelerated by the applied voltage. As the chain length increases, the time required for the polymer to pass through the pore increases. This permits a longer duration to which the electrical force will be applied to the polymer chain. Because the force is applied for a longer period of time, the velocity of the chain now has ample time to increase during the translocation process. This increase in velocity is dependent upon the strength of the applied voltage. If the applied voltage is increased, the velocity is increased, which reduces the translocation time. Hence, when the length of the polymer is increased, the dependence of translocation time on voltage is increased as shown in Figure 24. The theoretical inverse proportionality $\tau \sim V^{-1}$ [47] sets in after N = 10. At higher voltages (~500 mV), a crossover behavior for all chain lengths is observed. For example, in the case of N = 50, the scaling exponent changes from -0.96 to -0.72 as the voltage is increased from 400 mV to 500 mV. This behavior has also been observed in previous simulations[52,53] and was hypothesized to be a manifestation of the polymer being far away from its equilibrium state. An example of this phenomenon is given in Figure 25 which shows a snapshot of the translocation of a polymer chain with length N = 50 for: (a) V = 80 mV and (b) V = 750 mV. At (a) V = 80 mV, the chain at the *trans* side of the pore has a large radius of

gyration with minimum folding whereas at (b) V = 750 mV there is a lot of monomer crowding indicating the polymer is far from its equilibrium state during the translocation process.

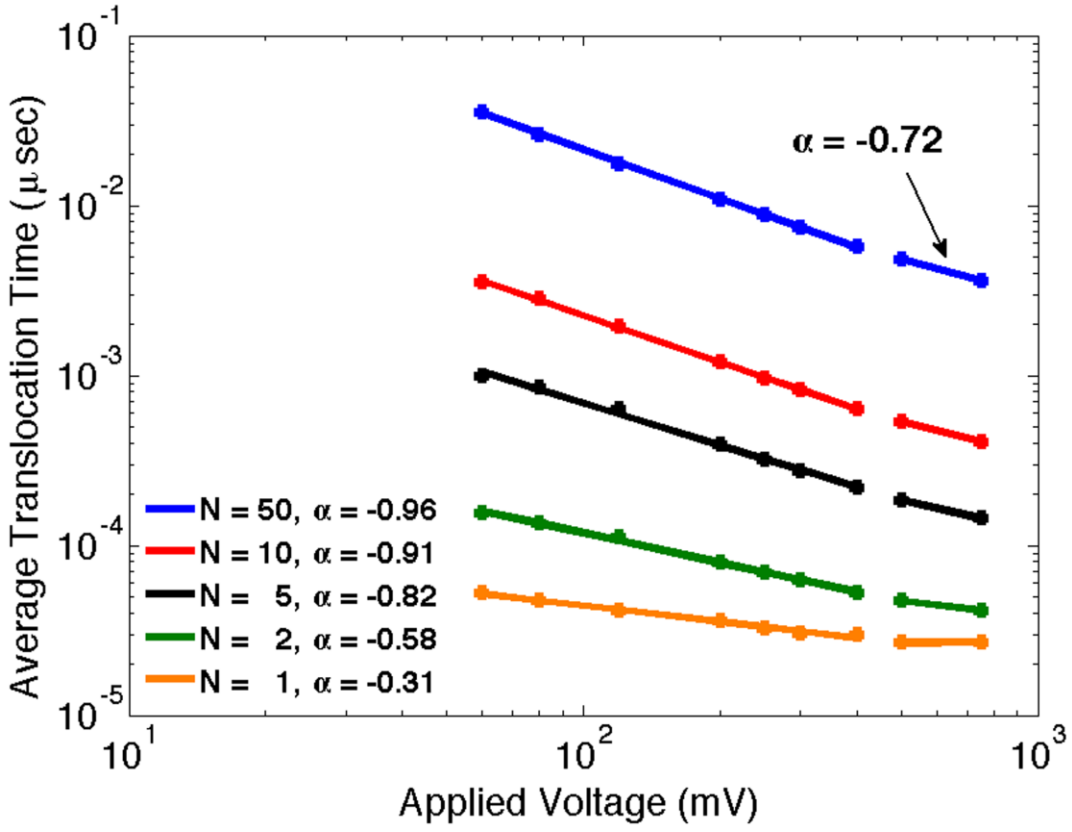

Figure 24: Average translocation time (over 1000 trials) versus applied voltage (60 mV – 750 mV) for different chain lengths (N), using a pore of 0.96 nm diameter and length 0.5 nm. The scaling exponent reaches -0.96 for 50 monomers. This is in good agreement with the theory that predicts $\tau \sim V^{-1}$. As the chain length decreases, the scaling exponent weakens. The values in the legend represent the slopes of the curves before the crossover region. The crossover scaling exponents occurring at 500 mV are: -0.72 (N = 50), -0.66 (N = 10), -0.62 (N = 5), -0.34 (N = 2), and -0.01 (N = 1).

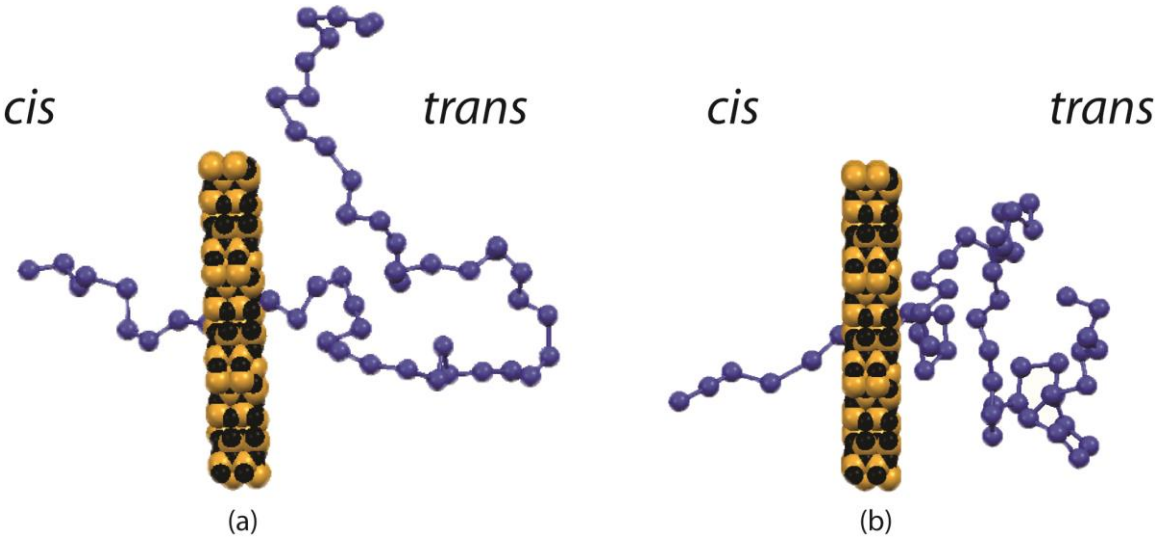

Figure 25: Snapshot of translocation simulation using a nanopore of 0.96 nm diameter and 0.5 nm in length for a polymer length N = 50 and applied voltages of (a) 80 mV and (b) 750 mV. As shown, the polymer at the trans side of the nanopore for the small voltage of (a) 80 mV is spread far apart with minimal folding whereas the polymer at the trans side of the nanopore for the large voltage of (b) 750 mV possesses a lot of monomer crowding during the translocation process indicating the polymer is far from its equilibrium state.

Figure 26 shows the scaling behavior of translocation time versus voltage for translocation through a long (5 nm) pore. Unlike the case of the short pore, the scaling exponents for all chain lengths are approximately -1 and do not vary significantly with chain length. In addition, there are no voltages in which the slope changes from one value to another as seen in the short pore simulations. The key differences in voltage scaling between the short and long pores can be explained by remembering that the force due to the applied voltage is non-zero only inside the pore. For short pores and short polymer lengths, the polymer is present inside the pore briefly and therefore will only experience the applied force for a small amount of time, thus increasing the applied voltage only results in a slight increase in velocity and, as a result, a small change in translocation

time. When the polymer length becomes longer, even though each monomer only experiences the applied force for a short amount of time, the overall force on the polymer will increase because the time required for the polymer to fully translocate through the pore will increase. Similarly, when the length of the pore is increased, because more time is required for each monomer to translocate through the nanopore, the polymer will also experience the applied force for a greater period of time and, consequently, increases in the applied voltage result in increases in the polymer velocity and decreases in translocation time.

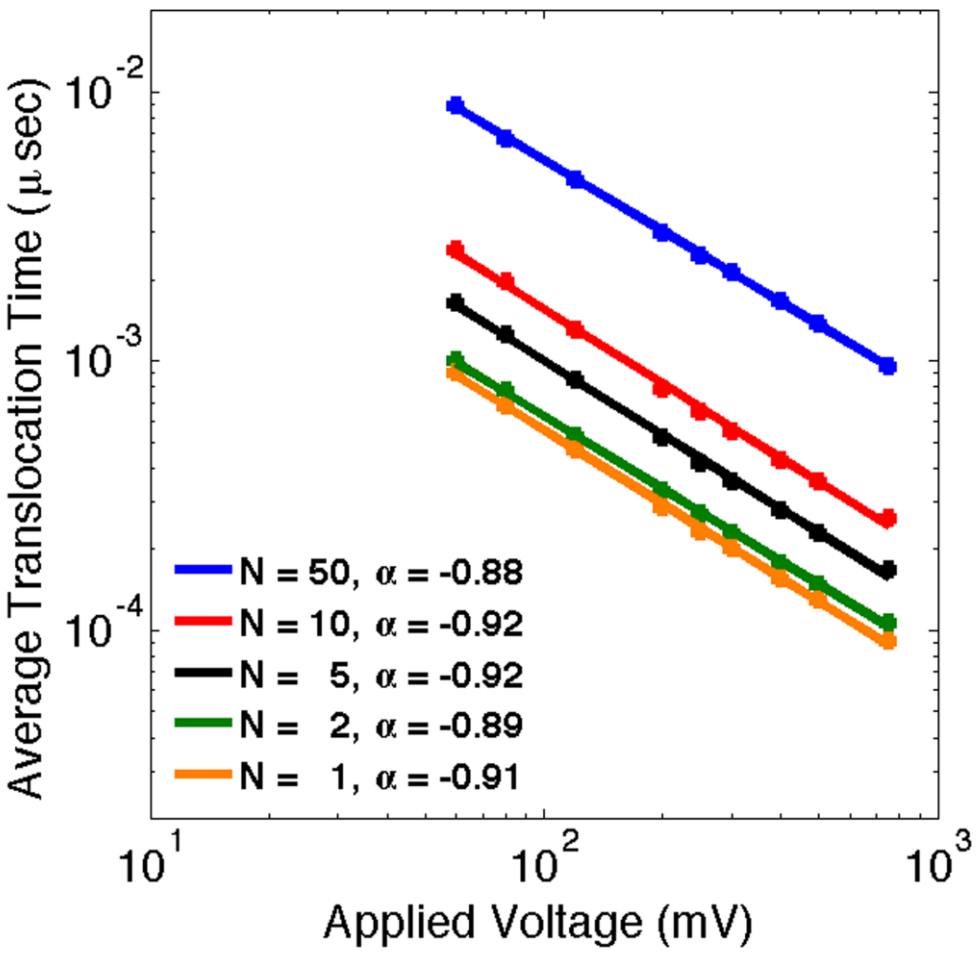

Figure 26: Average translocation time (over 1000 trials) versus applied voltage (60 mV – 750 mV) for different chain lengths (N) using a pore of 0.96 nm diameter and length 5 nm. Depending upon the chain length, the scaling law α varies slightly between -0.88 and -0.92. These values are in good agreement with the theoretical values which predict $\tau \sim V^{-1}$.

3.7 Conclusion

I have investigated the translocation time scaling laws, for both polymer length and applied voltage, for a Rouse polymer in atomistically detailed silicon nitride nanopores of varying diameter and length using realistic parameters rather than traditional dimensionless quantities. I found that in the case of short nanopores and long

polymers, the translocation time versus chain length N scales as $\tau \sim N^{\alpha}$, where α = 1.35-1.40, in good agreement with predictions by Vocks *et al.* [48] and Sakaue[78], previous simulation results[52,53,55,57,65], and measurements of ds-DNA with lengths between 150 – 3500 bp[18]. My results also clarify the dependence of the scaling exponent upon the applied voltage. When the voltage is reduced below 80 mV, the scaling exponent increases and approaches the value for the unforced case, α = 2.52, in good agreement with Panja *et al.* [46] When the pore length increases, a continuous scaling law does not exist, but the scaling exponent increases as the length of the polymer increases which converges to the same value obtained in the short pore simulations for very long polymers. In addition, my simulation results mimic the theoretical predictions for translocation time dependence on applied voltage ($\tau \sim V^{-1}$) for the case of long pore lengths. When the pore length is very short, the scaling law is dependent not only on the polymer length, but also the applied voltage. The differences in the scaling laws can be attributed to the duration of the applied force on the polymer. In the case of the short pores, the duration of the applied force on the polymer is much smaller than the situation of long pores. This smaller duration, especially for the case of short polymers, results in smaller changes in velocity even for increased applied voltages. I found that when the polymer length (N = 10) is approximately 10 times the length of the short pore (L = 0.5 nm), the $\tau \sim V^{-1}$ scaling law is recovered. However, I found that in the case of short pores, a threshold voltage exists in which larger voltages result in smaller changes in translocation time. Finally, I found that using an atomistically detailed nanopore provided similar simulation results obtained from other simulation methodologies which modeled the nanopore as a simple homogenous lattice of atoms. This is probably due to the

repulsive interaction between the polymer and pore (Equation 2-3) used in my and other simulation methodologies which guarantees the polymer will flow in a single file fashion (no folding) through the nanopore during the translocation process.

CHAPTER 4: Zimm Polymer Study

4.1 Introduction

In this chapter I investigate polymer translocation through solid-state nanopore devices, using both Rouse (no hydrodynamic interactions) and Zimm (with hydrodynamic interactions) polymer models, applying the 3-dimensional Brownian dynamics simulation methodology described in section 2.4.3. As described earlier in Chapter 3, the diffusion of one monomer of a Rouse polymer does not affect the diffusion of another. As a result, the center-of-mass diffusion coefficient scales as $D \sim N^{-1}$ and the polymer relaxation time scales as $\tau_R \sim N^{1+2\upsilon}$ [74]. On the other hand, when hydrodynamic interactions are introduced - as modeled by a Zimm polymer - the diffusion of each monomer is affected by every other monomer in the chain through solvent interactions, resulting in a center-of-mass diffusion coefficient scaling law $D \sim R_g \sim N^{-\upsilon}$ and a relaxation time scaling law of $\tau_Z \sim N^{3\upsilon}$ [74].

The assumption of Rouse behavior is likely valid inside a nanopore as long as minimal folding occurs during the translocation process or if very little water is present inside the pore as would be the case for a very narrow nanopore. However, because many polymers such as double-stranded DNA (ds-DNA) behave as Zimm polymers in bulk solution [88–90], it would seem that assuming Rouse behavior would underestimate the diffusivity of the polymer, especially in the case of studies involving unforced translocation through a nanopore. To complicate matters, hydrodynamic interactions are long ranged in bulk solution [91], but have shown to be screened for polymers moving near a wall or inside a channel [45,68,91]. Hence, the effect of hydrodynamic interactions

in translocation time simulation studies is not trivial and should not be omitted in any thorough investigation.

The main goal of this chapter is to investigate the effect of hydrodynamic interactions on the translocation time scaling exponent and compare these results to Rouse polymer simulations. More specifically, this chapter is targeted at understanding the dependence of polymer translocation mechanisms on the chain length, pore diameter, as well as the driving voltage and solvent viscosity for both Rouse and Zimm polymer models. In addition, I also investigate the dependence of the translocation time on the initial polymer configuration using two different configurations: minimum energy configuration (described in section 2.5), and 'steady-state' configuration (described in section 4.3). Finally, I also investigate the effects of polymer-pore interactions on polymer translocation through nanopores without an applied voltage (or unforced). As shown in the previous chapter, the pore diameter has little effect on the scaling exponent for polymer translocation through nanopores with an applied force. However, as will be discovered in section 4.9, the pore diameter greatly affects the scaling exponent in unforced translocation time simulations.

4.2 Translocation time vs. Chain Length: Minimum Energy Configuration

Figure 27 shows the scaling of translocation time with N for three different applied voltages, with and without HI, for a polymer initially in configuration (1) using a pore with diameter 0.96 nm and length of 0.5 nm, which is the length for all nanopores used in this chapter. As shown in Figure 27(a) for an applied voltage of 80 mV, in the

absence of hydrodynamic interactions, the translocation time scales as $\tau \sim N^{1.35}$, which is in good agreement with my previous simulation results [54] using the integration algorithm by Ermak and Buckholz [104], as well as other previous simulations results [52,53,55,57], results using the BDTP theory [82,83], and with the prediction of Vocks *et al.* [48] ($\tau \sim N^{1.37}$). All translocation time versus chain length studies presented in this thesis resulted in a maximum variation of $\alpha = \pm 0.01$ using the standard error formulation [139].

Figure 27 also shows that the scaling exponent α increases with decreasing voltage. This trend is in good agreement with previous simulation results [52–54] as well as predictions with the BDTP model [76,82]. Based upon the findings in references [45–48], the scaling exponent is larger for unforced translocation than for forced translocation, indicating as the applied force is decreased α should increase. This trend agrees with my simulation results given in Figure 27. On the other hand, there are other simulation methodologies that predict the opposite trend [49–51]. It should be noted that nothing was done in these simulations to prevent the polymer from escaping out of the pore into the *cis* reservoir, as was done by Dubbeldam *et al*. [51] in which the radius of the first monomer was given a value larger than the pore diameter. As discussed by Ikonen *et al.* [76] implementing this "reflective boundary condition" could be responsible for the discrepancy in trends between scaling exponents and driving force.

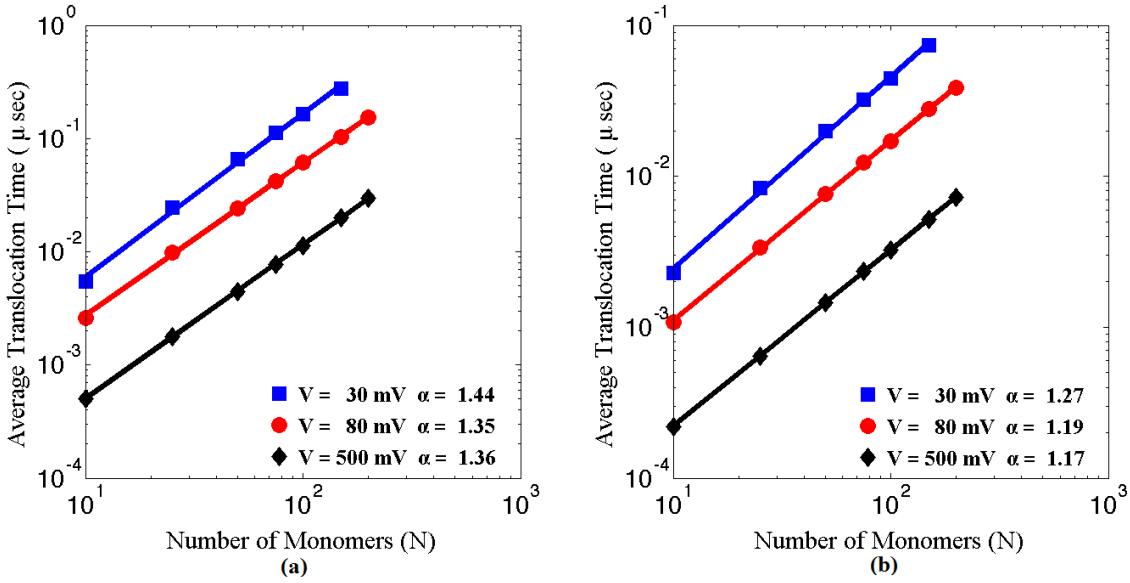

Figure 27: Average translocation time (500 trials) vs. chain length (N) for simulations (a) without HI and (b) with HI, for three voltages: 30 mV, 80 mV, and 500 mV, for initial configuration (1) using a pore with diameter 0.96 nm.

A question exists as to why the scaling law for the non-HI simulations does not match the value of $\alpha = 1.588$ derived by Kantor and Kardar [47]. Figure 28 shows $\langle R_g^2 \rangle$ of the polymer as a function of N on the *cis* side before the translocation process has begun (time zero) and on the *trans* side at the conclusion of the translocation process. As mentioned earlier, one of my goals is to investigate how the initial polymer configuration affects the translocation time scaling law. Interestingly, because of the abrupt cutoff in the WCA potential (Equation (2-3)) when the distance of the non-adjacent monomers is greater than $2^{1/6}\sigma$, the 'equilibrium' (or steady-state) polymer configuration is very different than the minimum energy state. For the calculations shown in Figures 27 and 28, the polymer is placed in its minimum energy state using a MMC procedure [118] for 50,000 trials before the translocation process begins. As shown in Figure 28, on the *cis* side, the radius of gyration scales as $\langle R_g^2 \rangle \sim N^{0.85}$ which is much smaller than the scaling

for a polymer in a good solvent with high excluded volume interactions [74]: $N^{2\upsilon} \sim N^{1.18}$. In addition, as also shown in Figure 28, on the *trans* side, the radius of gyration scales as $\langle R_g^2 \rangle \sim N^{1.03}$ after the translocation process has ended, which is also much smaller than the theoretical scaling. This is a clear indication of crowding of the polymer at the exit of the nanopore after the translocation process has ended, observed during forced translocation [49–54,56]. In order to obtain the scaling exponent predicted by Kantor and Kardar [47], the polymer must be in equilibrium throughout the entire translocation process. This does not occur in these simulations.

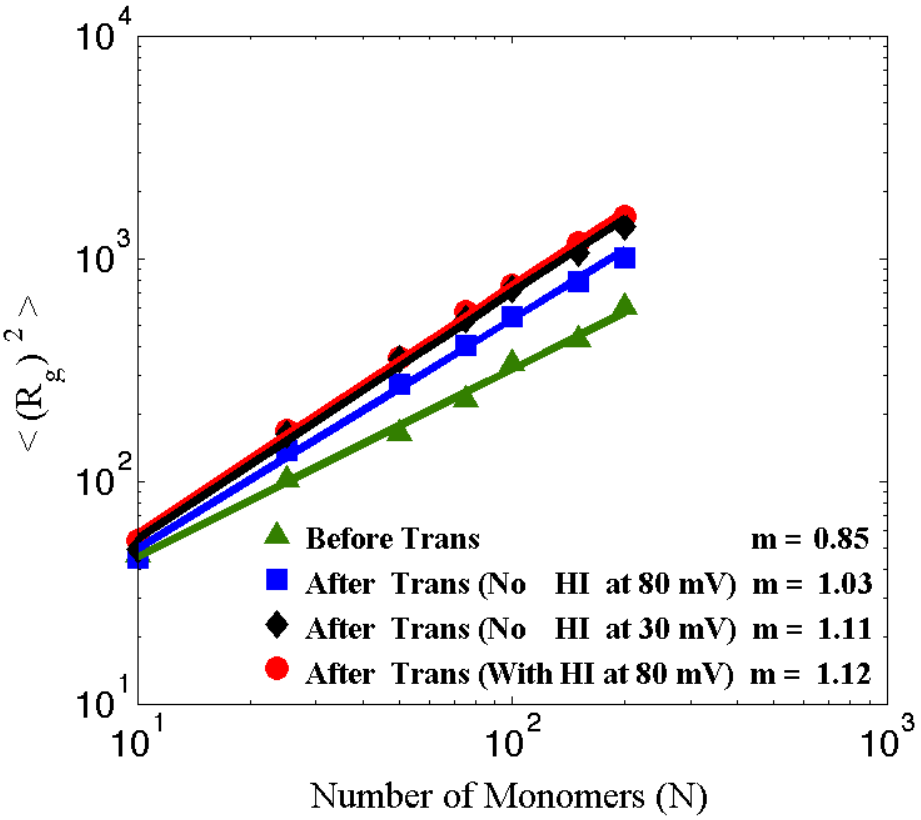

Figure 28: $\langle R_g^2 \rangle$ (100 trials) versus N measured at time t = 0 (green), and after completion of the translocation process for: No HI at 80 mV (blue), No HI at 30 mV (black), and with HI at 80 mV (red).

When the applied voltage is decreased to 30 mV, I find that $<R_g^2> \sim N^{1.11}$ on the *trans* side, indicating less crowding at the exit of the nanopore. As a result, the translocation time scaling exponent increases to $\alpha = 1.44$, a value still different than the scaling exponent predicted by Kantor and Kardar [47]. Figure 27 (b) shows simulation data using the same polymer configuration with hydrodynamic interactions (HI) included. Not only do the HI interactions decrease the translocation time [49,57], but the scaling exponent is reduced to $\alpha = 1.19$ at 80 mV. This value is in good agreement with the predictions in references [9,57,78] wherein $\alpha = 2\upsilon = 2(0.588) = 1.18$ and slightly higher than the prediction by Vocks *et al*. [48] ($\alpha = 3\upsilon/(1+\upsilon) = 1.11$). My results are also in good agreement with results obtained using dissipative particle dynamics (DPD) in reference [60] ($\alpha = 1.2$) and only slightly lower than the results obtained from lattice Boltzmann techniques ($\alpha = 1.28$) [57,58]. Just as in the non-HI polymer model, the scaling exponent α increases with decreasing voltage when hydrodynamic interactions are included. Finally, as shown in Figure 28, the radius of gyration for the Zimm model after the translocation has completed scales as $<R_g^2> \sim N^{1.12}$ on the *trans* side for an applied voltage of 80 mV, indicating less crowding at the exit of the nanopore than for the Rouse polymer with the same applied voltage. As stated earlier, the theoretical Zimm polymer relaxation time, which scales as $\tau_Z \sim N^{3\upsilon}$ is much shorter than the Rouse polymer relaxation time, which scales as $\tau_R \sim N^{1+2\upsilon}$ [74]. Hence, my simulations show that once the Zimm polymer exits the nanopore, due to secondary polymer-solvent interactions, it begins to equilibrate to the steady-state configuration much faster than the Rouse polymer.

4.3 Translocation time vs. Chain Length: 'Steady-State Configuration'

To gain a better understanding of how the initial polymer configuration affects the scaling exponents, I performed another set of simulations with configuration (2), *i.e.*, after the MMC procedure is performed, the first monomer is kept inside the pore while the other monomers are free to move on the *cis* side of the pore for a time period determined by the values in Figure 7(b). This is referred to this as the 'steady-state' configuration. After the steady-state time expires, the chain is then free to translocate.

As shown in Figure 29 (a), the scaling exponent α for the non-HI polymer has increased from 1.35 to 1.44. This is in good agreement with the predictions of Saito and Sakaue [78,79] (1.43), MD simulation results by Dubbeldam *et al.* [51] (1.47), and MD and LD simulations by Luo *et al.* [65] (1.42 ± 0.01 and 1.41 ± 0.01 respectively). Again, the scaling exponent is smaller than the value predicted by Kantor and Kardar [47]. Once again, I measured $\langle R_g^2 \rangle$ on the *cis* side of the nanopore (after the steady-state time period but before the translocation process begins). As shown in Figure 30 (a), $\langle R_g^2 \rangle \sim N^{1.20}$, which agrees very well with the theoretical $\langle R_g^2 \rangle \sim N^{2\upsilon} = N^{1.18}$ obtained for a polymer in a good solvent. However, as shown in Figure 30 (b), at 80 mV I obtain $\langle R_g^2 \rangle \sim N^{1.08}$ on the *trans* side after translocation, once again indicating crowding at the exit. On the other hand, at 30 mV the radius of gyration scales as $\langle R_g^2 \rangle \sim N^{1.15}$, which is in good agreement for a polymer in a good solvent. As a result, the translocation time scaling exponent increases to $\alpha = 1.52$, which is in good agreement with the prediction by Kantor and Kardar [47] of $\alpha = 1 + \upsilon = 1.588$. Hence, my model indicates that in order to obtain the prediction by Kantor and Kardar [47], the polymer must be in its steady-state configuration throughout the translocation process. In addition, when comparing results

from Figure 29 (a) with results from Figure 27 (a), it can be seen that the translocation time is larger for the 'steady-state' configuration polymer than the minimum energy polymer. This is because, as shown in Figure 28, the initial radius of gyration for the minimum energy configuration is smaller than the radius of gyration for the 'steady state' configuration given in Figure 30 (a), thus the polymer must travel a longer distance which results in a longer translocation time.

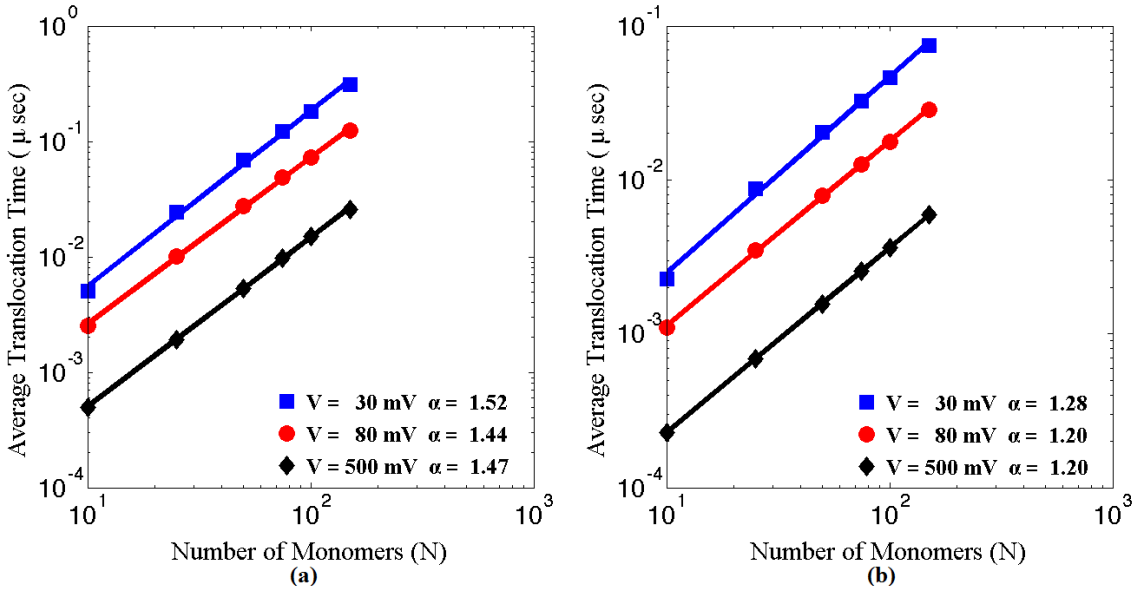

Figure 29: Average translocation time (500 trials) vs. chain length (N) for simulations (a) without HI and (b) with HI, for three voltages: 30 mV, 80 mV, and 500 mV, for initial configuration (2) using a pore with diameter 0.96 nm.

In Figures 27 and 29 it is shown that increasing the voltage from 80 mV to 500 mV (more than six times) does not change the scaling significantly. Lowering the voltage to 30 mV, however, does increase the scaling exponent, agreeing with the earlier assessment that α should increase as the applied force decreases. Hence, from these results, it appears that the lower bound on the scaling exponent is determined by the initial polymer configuration, whereas the upper bound is set by the applied voltage. The

role of the initial polymer configuration was investigated by Lehtola *et al.* [50]. They hypothesized that when the applied force is large the translocation process is dictated by a force balance between the applied driving force and the drag force felt by the monomers in the *cis* reservoir as they move towards the pore entrance. Lehtola *et al.* [50] performed translocation time simulations using a polymer with an initially linear configuration and obtained a scaling law of $\alpha = 2$, which is very different from any prediction or previous simulation results. It was further stated that the diffusive motion of the monomers has no impact on the translocation time scaling. This would seem to explain why the scaling law changes very little from 80 mV to 500 mV. In other words, a driving force of 80 mV is large enough that the effects of diffusion are insignificant and the scaling is dictated by the initial polymer configuration.

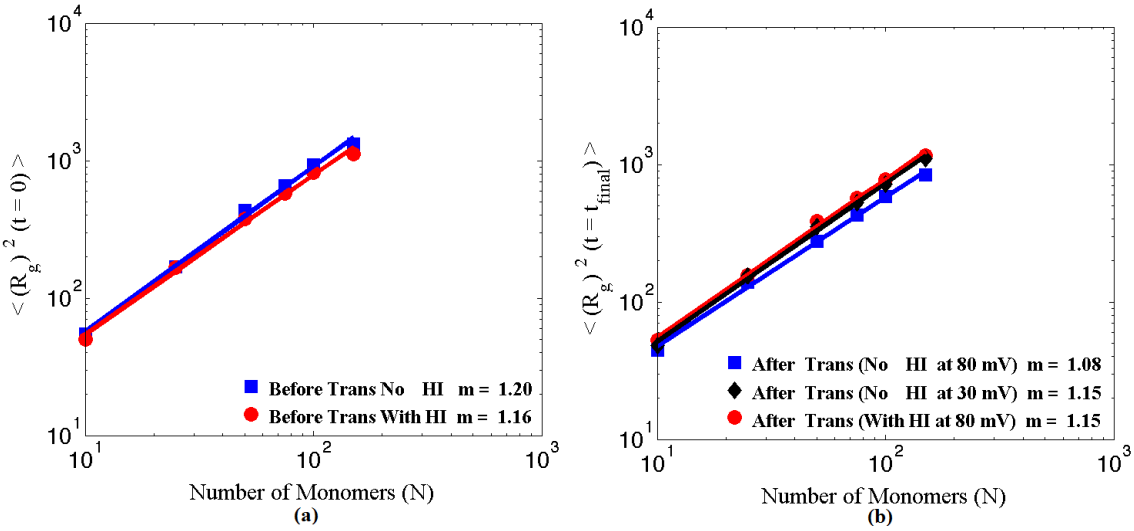

Figure 30: $<R_g^2>$ (100 trials) versus N on (a) the *cis* side after the steady-state time has expired (but before translocation begins) for non-HI (blue) and HI (red) polymers, and (b) on the *trans* side after complete translocation, for the non-HI case at 80 mV (blue), the non-HI case at 30 mV (black), and the HI case at 80 mV (red).

Figure 29 (b) shows the effects of including HI using a steady-state initial polymer configuration (2). Similar to the findings with the minimum energy configuration, when comparing Figure 29 (b) to Figure 29 (a), the Zimm polymer translocates faster than the Rouse polymer for configuration (2) as well. Also shown in Figure 29 (b) is $\alpha = 1.20$ at 80 mV, which, interestingly, is not significantly different from that obtained in the minimum energy configuration (1) given in Figure 27 (b). In fact, the translocation times and scaling laws for all voltages for both configurations are approximately the same. This can be explained by noting the time required to equilibrate from the minimum energy configuration to the steady-state configuration is much shorter for the Zimm polymer than the Rouse polymer, as shown in Figure 7 (b). As a result, due to the secondary polymer-solvent interactions, Zimm polymers that begin in the minimum energy configuration immediately expand and approach the equilibrium steady-state radius of gyration during the translocation process. In addition, it can be seen from both Figure 28 and Figure 30 (b) that the radius of gyration at the exit of the nanopore for the Zimm polymer is only slightly different than the theoretical value for both the minimum energy (~5%) and for the steady-state (~2%) configurations, indicating very little crowding at the exit of the nanopore. As stated before, this reduction in crowding in the Zimm model as compared to the Rouse is due to the Zimm model having a shorter relaxation time as a result of secondary polymer-solvent interactions (i.e. hydrodynamic interactions) and, hence it can more quickly reach its steady-state radius of gyration after it exits the nanopore. Finally, just as in the case for the minimum energy configuration (1), it is also observed for the steady-state configuration (2) that increasing

the applied voltage from 80 mV to 500 mV does not change α, whereas reducing the voltage increases α significantly.

4.4 Translocation time vs. Chain Length: Effect of pore diameter (Zimm Polymer)

To gain a better understanding in how pore dimensions affect the translocation process, I next performed translocation time versus chain length simulations and varied the pore diameter as shown in Figure 31. In each of these simulations, I used the steady-state initial polymer configuration (2) and included hydrodynamic interactions as well. From Figure 31 it is observed that as the pore diameter increases the translocation time decreases as well as the scaling exponent α slightly increases. Both of these same trends were also observed in Chapter 3 for Rouse polymers as shown in Figure 18 (b) [54]. One explanation for the decrease in translocation time is due to the decrease in polymer-pore interactions. In my initial simulations, I used a narrow pore (0.96 nm) with a highly repulsive potential energy function to ensure 'single-file' translocation of the polymer with no folding inside the pore. In wider nanopores, the monomers inside the pore no longer experience a strongly repulsive polymer-pore potential and can more easily translocate through the pore.

In addition, in forced translocation time simulations with moderately high applied voltages, as mentioned before, the effect of diffusion on the translocation process is negligible and hence, the scaling exponent α changes very little with an increase in pore diameter. This is very different from unforced simulations in which diffusion is the primary mechanism for translocation through a pore. In those simulations a reduction in polymer-pore interactions allow for polymers to diffuse more freely inside the pore increasing the stochasticity of the process and, as a result, increasing the scaling law

exponent α as shown in the work of de Haan and Slater [66]. I investigate unforced translocation time simulations in section 4.9 later in this chapter.

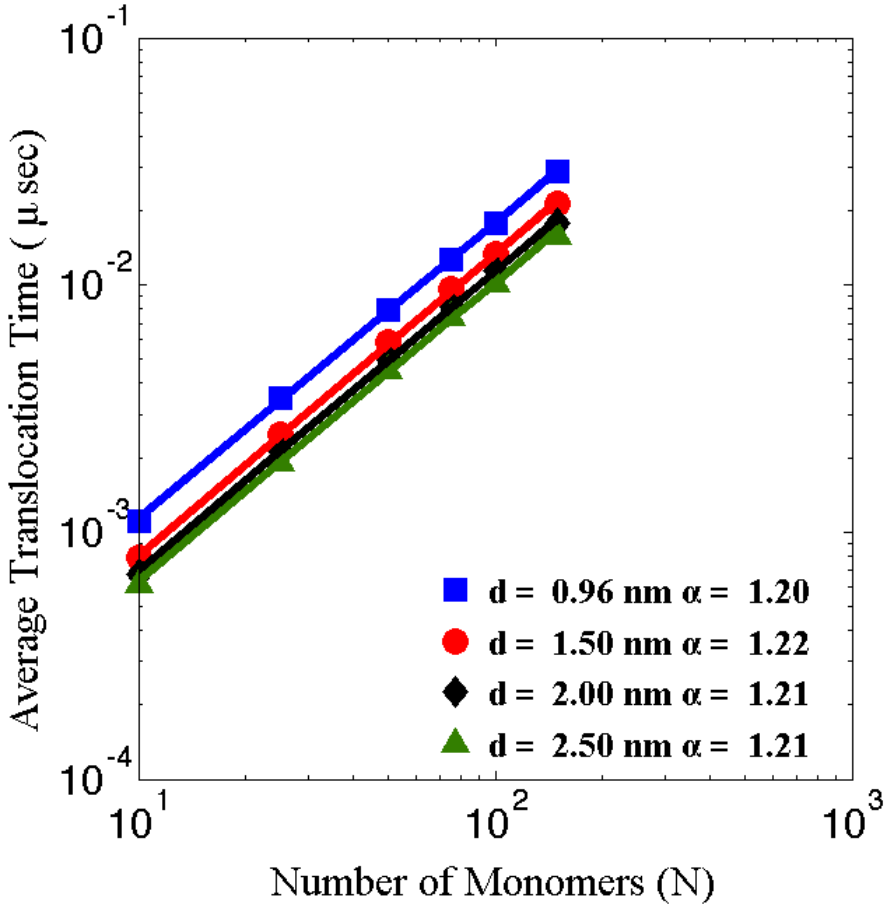

Figure 31: Average translocation time (500 trials) vs. chain length (N) for varying pore diameters for initial configuration (2) with hydrodynamic interactions with an applied voltage of 80 mV.

4.5 Waiting Time Simulations

One way to observe the behavior of the polymer during translocation is by measuring the waiting time, defined as the time each monomer remains inside the pore during translocation. As shown in Figure 32, I measured waiting times for the Minimum

Energy configuration and for the ‘steady-state’ configuration for both Rouse (a) and Zimm (b) polymers using a 0.96 nm diameter pore for a chain length No = 100. First, observing Figure 32 (a), the waiting time increases to a maximum value about three quarters down the chain before reaching a minimum value at the end of the chain. This same behavior, observed in previous simulation methodologies [50,62,76,82,86], indicates that the polymer does not translocate with a constant velocity. But rather, as described by Ikonen *et al.* [76,82] as the tension front propagates down the chain, more monomers contribute to the overall drag force, thus slowing down the translocation process. After the tension reaches the back of the chain, the drag force is now only determined by the number of monomers on the *cis* side of the nanopore. Since this number continually decreases during the translocation process (as more monomers move from the *cis* side to the *trans* side of the nanopore) the drag force continually decreases which results in the increase of monomer velocity, thus the waiting times of the monomers in the back of the chain go down. Hence, the translocation process speeds up until all monomers reach the *trans* side of the nanopore. The peak in the waiting time curve represents when the tension front has reached the back of the chain [76,82]. Interestingly, the waiting times are much smaller for the minimum energy configuration than the ‘steady-state’ configuration. This could be due to one of two reasons. First, because the minimum energy configuration has a much smaller radius of gyration, the polymer has to travel a shorter distance than the polymer in the ‘steady-state’ configuration, and thus, a shorter translocation time and waiting times are observed. This result is also observed when comparing translocation time simulations in Figure 27 (a) and Figure 29 (a). A second reason for the two different waiting times could be a result of

smaller drag forces in the direction of translocation, observed in the minimum energy configuration. As described earlier, at moderate driving forces, the translocation time process can be thought of as a force balance between the driving force and the drag force of the monomers moving towards the pore. The drag force can be thought of as having two components, one parallel to the direction of translocation and one perpendicular. It would appear that a polymer with a smaller radius of gyration, like a curled "blob", would have less drag force in the direction parallel to translocation than a polymer with a large radius of gyration with a long-drawn out configuration. Hence, the monomers in the minimum energy configuration have a larger drag force in the perpendicular direction of translocation and less drag force in the parallel direction of translocation than does the 'steady state' polymer configuration.

Interestingly, as shown in Figure 32 (b), the waiting time curve for the Zimm polymer is essentially flat, indicating a constant velocity translocation. This same behavior was also predicted by Fyta *et al.* [57], whom stated that during translocation, due to the size of the polymer on the *cis* side of the nanopore decreasing, the amount of work done by the fluid also decreases, whereas on the *trans* side of the nanopore the amount of work done by the fluid increases because of the increase in size of the polymer. Hence, during translocation, the amount of work done by the fluid remains constant. Coupled with the fact that the work done by the electric field is also constant, Fyta *et al.* [57] came to the conclusion that the monomers should translocate through the pore with the same velocity, which agrees with my simulation results given in Figure 32 (b). Finally, the waiting times are almost the same values for both initial configurations

for Zimm polymers, also reflected in the translocation time simulations given in Figure 27 (b) and Figure 29 (b).

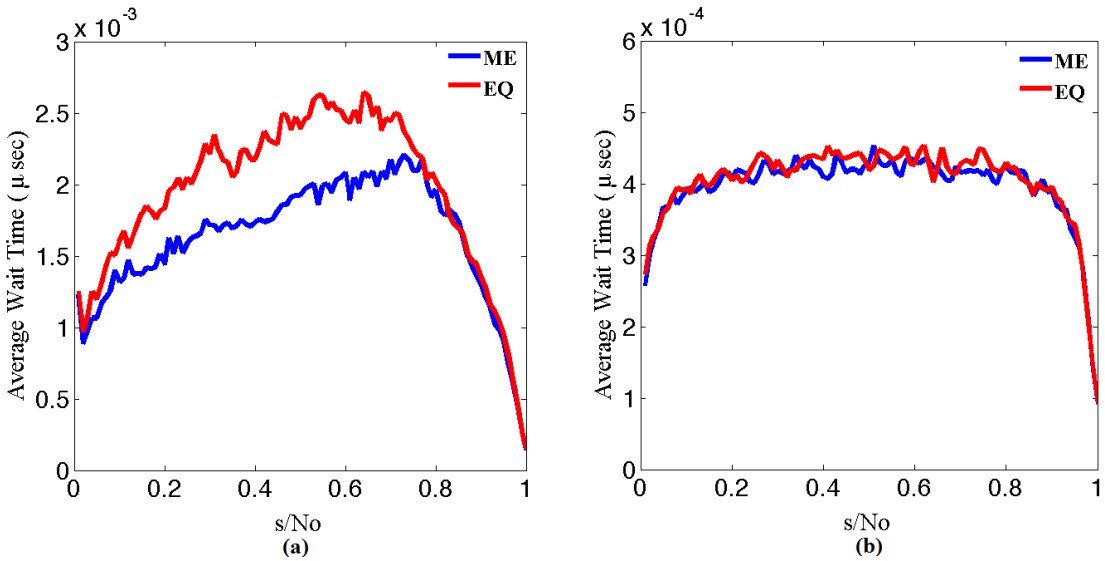

Figure 32: Average waiting time, for monomer s, for both the minimum energy (ME) and the 'steady-state' equilibrium (EQ) configurations over 500 trials for (a) Rouse and (b) Zimm polymer models using a pore with diameter 0.96 nm for polymer chain No = 100.

4.6 Simulation Results compared with Measured Values

I now summarize how my computational results compare to experiments. Before I begin these comparisons, I need to address the question whether it is feasible to compare my coarse-grained simulation results with those from experiments. Whereas some of the simulation model parameters do not exactly match those existing in experiments, I do use parameters that realistically depict relationships between polymer and pore dimensions used in translocation time experiments with ds-DNA. For example, the measurements performed by Storm *et al.* [9,10] investigate the translocation time of ds-DNA, which has an approximate diameter [9] of 2 nm, using a 10 nm-diameter SiO_2 nanopore. Hence, the

ratio between the diameter of the ds-DNA and nanopore is approximately 5, which is approximately the same ratio as the polymer (0.43 nm) to the nanopore of diameter 2.0 nm used in the simulation results given in Figure 31. In addition, in the translocation time versus chain length scaling law studies, Storm *et al.* [9,10] uses ds-DNA chain lengths, the shortest containing approximately 6.6 kbp (length per base ~ 0.34 nm [140], total length ~ 2250 nm) much longer than the length of the nanopore used in their experiments (approximately 20 nm). Similarly, the polymer chains used in my simulations, the smallest being 10 monomers (length per monomer = 0.43nm, total length 4.3 nm) are also much longer than the length of the nanopore (0.5 nm). Finally, as given in Figures 7 and 8, with hydrodynamic interactions implemented, the polymer model behaves as ds-DNA in bulk solution.

As shown in Figure 31, the translocation time versus chain length scaling law (α) is 1.21 which agrees very well with experiments performed by Storm *et al.* [9,10] (α = 1.26 – 1.27) using an applied voltage of 120 mV. Hence, because this scaling law is very different from the values obtained without HI (α = 1.44) as shown in Figure 29 (a), it can be concluded that HI interactions are required to accurately model the physics involved in these translocation time measurements. It was shown in previous experimental results ds-DNA diffuses as $D \sim N^{-\upsilon}$, where υ is between 0.57-0.611 [88–90]. As mentioned earlier, the translocation time was predicted to scale as $\tau \sim N^{2\upsilon}$ [9,57,78], which would result in a translocation time scaling exponent that could vary between α = 1.14 – 1.22. This is in good agreement with my simulation results and only slightly lower than the values obtained by Storm *et al.* [9,10].

In a second example experiment, Wanunu *et al.* [18] used a 4 nm wide, 10 nm thick SiN nanopore to observe $\alpha = 1.40$ for ds-DNA chain lengths of 0.150–3.5 kbp at 300 mV. This is vastly different from my simulation results that include HI, but similar to my simulation results without HI ($\alpha = 1.44$) as shown in Figure 29 (a). One hypothesis that could be made as to why hydrodynamic interactions are not required for the accurate modeling of these experimental results is due to higher polymer-pore interactions due to a smaller diameter pore. Due to the smaller diameter of the nanopore used in their experiments, polymer-pore interactions heavily influence the dynamics in the translocation process. This is also evident from the higher voltage required for translocation. In addition, unlike what is demonstrated from my simulation results shown in Figures 24, 26, and 34, and experiments using very large nanopores (30 nm diameter)[14], both of which agree with predictions [47] of $\tau \sim V^{-1}$, Wanunu *et al.* [18] obtained experimentally an exponential relationship for translocation time versus voltage a further indicator how polymer-pore interactions greatly influence the translocation process. One other possible cause for this exponential relationship between the voltage and the translocation time seen for smaller diameter pores, is related to the higher entropic barrier that must be overcome in order for the polymer to translocate through the pore[30].

4.7 Translocation time vs. Chain Length: Effect of Viscosity

One drawback of using solid state nanopore devices in translocation measurements is the high rate at which the polymers flow through them when using an applied voltage. For example, ds-DNA flows through a silicon nitride nanopore at

approximately 20 – 30 base pairs per μsec when applying potentials in the 120 mV-200 mV range[11,12,141]. Unfortunately, this high velocity requires measurement instruments to have detector bandwidth values in the MHz range which makes it very difficult to measure changes in current on a pico-ampere scale[22]. It was shown in previous experiments that it is possible to increase the translocation of DNA through silicon nitride nanopores, while keeping a good signal-to-noise ratio (SNR) [13], when increasing the viscosity of the solvent by adding glycerol. In order to study the effects on solvent viscosity on the translocation physics, I performed translocation time simulations for different polymer lengths, with an applied voltage of 80 mV, while varying the solvent viscosity using a 0.96 nm diameter pore. In these studies, the initial polymer was equilibrated to its 'steady-state' configuration.

As shown on Figure 33, the translocation time simulations increase when increasing the solvent viscosity in a linear fashion. In other words, if the viscosity is increased by a factor of 4, the translocation time is increased by a factor of 4. This linear relationship between the solvent viscosity and the translocation time was also observed in measurement results as well [13].

Interestingly, as shown in Figure 33 (a) there is not a drastic change in the scaling law when the solvent viscosity is increased for Rouse polymers. One might hypothesize that due to the increase in translocation time, crowding at the exit of the nanopore will be reduced because the portion of the polymer on the *trans* side of the nanopore will have more time to relax, and, thus, the resultant scaling exponent will begin to approach the theoretical prediction of $\alpha = 1 + \upsilon = 1.588$[47]. However, by increasing the viscosity of the solvent, the relaxation time of the polymer has also increased, thus, crowding at the

exit of the nanopore is still present resulting in scaling exponents smaller than α = 1.588, as shown in Figure 33 (a). In addition, as shown in Figure 33 (b), there is not a drastic change in the scaling law for Zimm polymers either. But, as discussed earlier, because of the smaller relaxation time of a Zimm polymer, there is less crowding at the exit of the nanopore than for Rouse polymers.

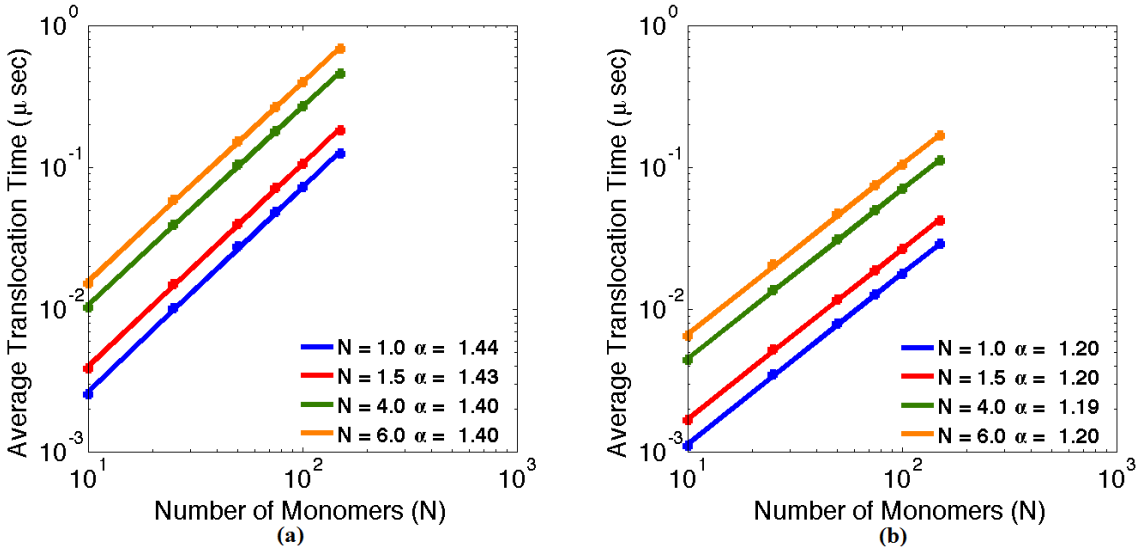

Figure 33: Average translocation time (500 trials) vs. chain length (N) for simulations (a) without HI and (b) with HI, for four different viscosity values using initial configuration (2) with an applied voltage of 80 mV using a pore with diameter 0.96 nm.

4.8 Translocation time vs. Applied Voltage

Another important issue in the physics of translocation is how the translocation time scales with applied voltage. I earlier demonstrated (Chapter 3, Figure 24)) results for a Rouse polymer in an initial polymer configuration obtained using the MMC procedure. In this chapter, in order to investigate this relationship further, I performed translocation

time simulations, while varying the voltage from 30 mV to 750 mV, using a polymer chain of N = 50 for both Rouse and Zimm polymer models with the polymer initially in the 'steady-state' configuration using a 0.96 nm diameter pore.

As shown for both polymer models, the translocation time scales as approximately the theoretical scaling behavior of $\tau \sim V^{-1}$ [47] up until an applied voltage of 400 mV, which is similar to the results obtained in Figure 24. In addition, this scaling behavior has also been observed in experiments using very large nanopores (30 nm diameter)[14]. And, just as shown in Figure 24, the scaling exponent is increased from -1 for both polymer models at voltages 500 mV and higher. As mentioned before, and shown in Figure 25, the reduction in scaling exponent is due to extreme crowding at the exit of the nanopore [52,53]. Interestingly, the reduction in the scaling exponent for the Zimm polymer (m = -0.80) is much less than for the Rouse polymer (m = -0.65). This would be in agreement with the findings that there is less crowding at the exit of the nanopore for Zimm polymers than for Rouse polymers due to the smaller relaxation time.

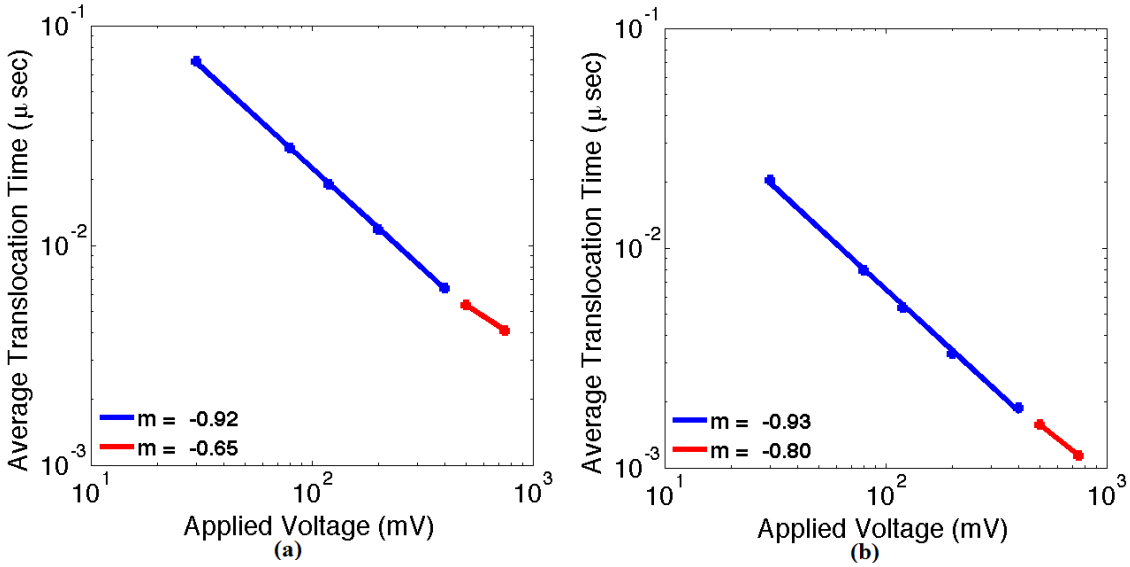

Figure 34: Average translocation time (500 trials) vs. voltage for simulations (a) without HI and (b) with HI, using polymer chain N = 50 using initial configuration (2) using a pore with diameter 0.96 nm.

4.9 Translocation time vs. Chain Length unforced simulations

Finally, I examine the translocation time scaling behavior in unforced translocation, for both HI and non-HI models. To study the effects of polymer-pore interactions, I also vary the diameter of the pore from 0.6 nm to 5.0 nm and perform simulations with the pore removed. In these unforced simulations, the middle monomer is initially placed in the center of the pore and the two halves of the chain are placed in the *cis* and *trans* reservoirs respectively. To put the polymer in the 'steady-state' configuration, the chain is allowed to relax, using the values given in Figure 7 (b), and then permitted to translocate in either direction. A successful translocation event occurs when the chain has exited to either side of the nanopore.

As shown in Figure 35, for the 0.96 nm pore, the translocation time for the HI case scales with $\alpha = 2.30$. These results are in good agreement with previous works that explicitly include polymer-solvent interactions *via* molecular dynamics (MD) ($\alpha = 2.27–2.30$) [67–69], stochastic rotation dynamics (SRD) (2.30)[59], and dissipative particle dynamics DPD (2.24)[60] methods. Interestingly, the scaling law obtained is very similar to the scaling prediction for unforced translocation derived by Chuang *et al.* [45] in the absence of hydrodynamic interactions ($\tau \sim N^{1+2\upsilon} \sim N^{2.176}$), a result also obtained by Panja *et al.* [46] who hypothesized that any relationship between the two is pure coincidence. On the other hand, as described by Guillouzic and Slater [67], due to the small diameter of the pore, the strong polymer-pore interactions heavily influence the translocation process whereas the hydrodynamic interactions have a negligible effect. This could be because the strong polymer-pore interactions slow down the polymer velocity thus significantly reducing the hydrodynamic drag. In addition, as discussed earlier and pointed out by Gauthier and Slater [68], hydrodynamic interactions have shown to be screened for polymers moving near a wall or inside a channel [91]. Hence, by observing the scaling exponents, this screening effect is shown playing a major role in these unforced translocation time simulations.

To further test this hypothesis, I simulated the unforced case for a smaller pore diameter of 0.60 nm. As shown in Figure 35, not only is the translocation time significantly increased, but the scaling exponent ($\alpha = 2.14$) resembles even more the scaling exponent derived by Chuang *et al.* [45] for unforced translocation in the absence of HI. Hence, for very small pores, polymer-pore interactions become very large and the effects of hydrodynamic interactions are greatly reduced.

To complete my study on the effects of polymer-pore interactions on the scaling exponent, I performed simulations for pore diameters ranging from 0.6 nm to 5.0 nm. As shown in Figure 35, as the nanopore size increases, the polymer-pore interactions decrease resulting in a decrease in the translocation time. In addition, the data demonstrates that when the size of the nanopore is increased, the scaling exponent first begins to increase to a maximum value of $\alpha = 2.35$ for a pore diameter = 1.5 nm and then reduces to a value of $\alpha = 1.64$ when the pore is removed.

This scaling exponent, which has been observed in other simulation methodologies [68], agrees with theoretical findings and intuition. As first reported by Chuang *et al.* [45] the time required for a polymer to translocate through a nanopore without the assistance of an applied force can be estimated as the time required for a polymer to diffuse its own radius of gyration. This is also defined as the polymer relaxation time [45,53]. As described earlier, when the pore diameter is very small, polymer-pore interactions dominate the translocation process, and hence, the Zimm polymer translocates through the pore as a Rouse polymer with a scaling exponent of approximately $\tau \sim N^{1+2\upsilon} \sim N^{2.176}$. Interestingly, this is the same scaling behavior for the relaxation time of a Rouse polymer [74]. When the pore is removed, the effects of hydrodynamic interactions become dominant, and, theoretically, the time required for the polymer to translocate through this "imaginary" pore, should be the same as the Zimm polymer relaxation time of $\tau_Z \sim N^{3\upsilon} \sim N^{1.76}$ [74]. As shown in Figure 35, my simulation results obtain a scaling exponent only slightly smaller than this theoretical value when the pore is removed ($\alpha = 1.64$). Hence, these are the scaling exponent limits for a Zimm polymer translocating through a pore without an applied force. For intermediate pore

diameters, the polymer no longer translocates in a single-file fashion, but rather folds inside the pore [66]. In addition, when the polymer-pore interactions become weaker through the increase in the pore diameter, diffusion forces become greater thus increasing stochasticity of the process which results in a larger scaling exponent. As the pore size becomes larger (and finally removed) the scaling exponent converges to the same scaling exponent as the Zimm polymer relaxation time.

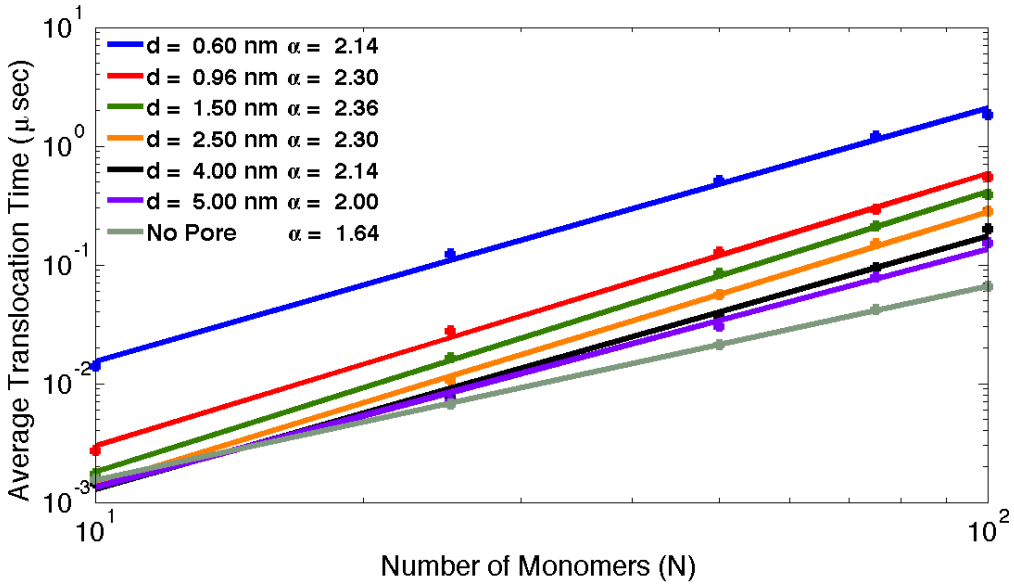

Figure 35: Average unforced translocation time (over 500 trials) vs. N for different pore diameters with HI effects (Zimm polymer).

In addition to the simulation results using Zimm polymers, I also performed simulations with Rouse polymers, with the results provide in Figure 36. As shown, with the 0.96 nm pore, I obtained $\alpha = 2.52$ for the non-HI case. This is in good agreement with my previous simulation results reported in Chapter 3, Figure 18 (a) [54], the predictions

by Panja *et al*. (2.59) [46], and those of Dubbeldam *et al.* (2.52) [70] and Gauthier *et al*. [75]. However, this scaling law is larger than the prediction of Chuang *et al.* [45] and other previous simulations in which $\alpha = 2.22\text{-}2.23$ [65,71] or 2.33 [59]. In addition to the previous simulations with a HI model by Gauthier and Slater [68], de Haan and Slater [66] performed unforced translocation simulations using a non-HI polymer model and varying the pore diameter. For a pore with diameter of 2σ, which approximately corresponds to the 0.96 nm pore used above, they obtained $\alpha = 2.5$, which is in good agreement with the scaling law that I obtained.

To further investigate the effects of polymer-pore interactions using Rouse polymers, I also performed translocation time simulations using the same pore diameters as the Zimm polymer studies. When using a very narrow nanopore (0.60 nm diameter) I obtained a smaller value of $\alpha = 2.23$, which is in good agreement with the prediction of Chuang *et al.* [45] ($\alpha = 2.176$) and simulations by de Haan and Slater [66] (2.19). As is the case in the simulations using a Zimm polymer, the scaling law is greatly affected by the pore diameter (i.e. polymer-pore interactions). In addition, just as in the case of unforced Zimm polymer translocation, there are scaling exponent limits for a Rouse polymer translocation as well. Although, for the Rouse polymer, the beginning and ending limits are the same, $\tau \sim N^{1+2\upsilon} \sim N^{2.176}$, which is its relaxation time [74]. And, as shown in Figure 36, I obtain scaling exponents in good agreement with these limits (i.e. $\alpha = 2.23$ for narrow pore and $\alpha = 2.02$ for no pore). In addition, the same behaviors as observed for Zimm polymers given in Figure 35 are also seen for the Rouse polymer in Figure 36. In other words, when the pore size is increased, the polymer-pore interactions

decrease resulting in not only a decrease in the translocation time but also an increase in the scaling exponent.

As discussed earlier, one of elusive goals of many researchers studying polymer translocation through nanopores has been to find a universal translocation time scaling exponent. What I have shown in this section is the importance of polymer-pore interactions on translocation time simulation results by varying the pore diameter. If a universal scaling law is to be obtained, it is important that there must be a consistency of polymer-pore interactions between all theoretical and computational studies.

One final interesting observation is that the unforced translocation scaling law for a pore diameter of 0.96 nm (Figure 36) using the 'steady-state' configuration is the same as found in Figure 18 (a) [54] which considered the polymer to initially be in a minimum energy configuration. Both cases result in the same scaling law in unforced translocation because, unlike in forced translocation, the translocation time is much longer than the relaxation time.

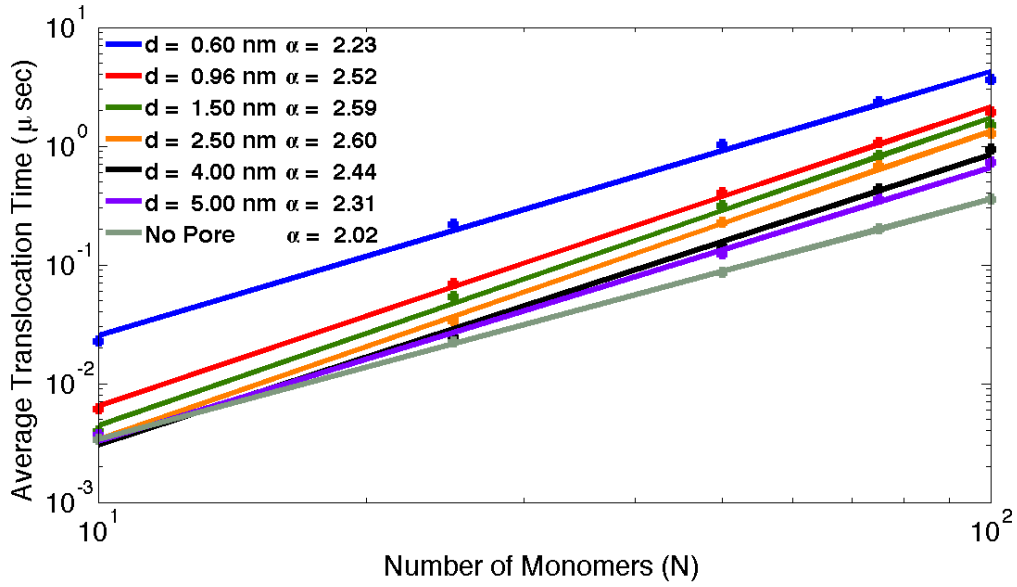

Figure 36: Average unforced translocation time (over 500 trials) vs. N for different pore diameters without HI effects (Rouse polymer).

4.10 Why Minimum Energy Configuration?

One of the important questions that I sought to answer is the effect of the initial polymer configuration on the translocation process, which has been hypothesized by some to heavily influence the scaling exponent, α, observed in the literature [50,58]. Based upon my findings above, I demonstrated that α does indeed differ depending upon which initial polymer configuration (minimum energy or 'steady-state') is used in the simulation. Of course, one may ask why perform simulations using the minimum energy convention as the starting initial polymer configuration, as there may not be a direct correlation between this configuration and experimental findings.

Whereas there may not be a direct relationship to experimental findings and the minimum energy convention that I use in these simulations, I feel that this initial polymer configuration is a scientifically based theoretical configuration, unlike a chain of

monomers in a totally random configuration. In addition, theoretically the minimum energy configuration, due to the WCA potential energy function used for non-adjacent monomers and the initial placement of monomers being σ_{poly} (0.43 nm) apart, should result in the smallest radius of gyration (R_g) possible for this polymer model. Hence, one could argue that by comparing the minimum energy configuration with the 'steady-state' configuration, I am comparing the smallest and largest possible values of R_g using the WCA potential energy functions. This can be seen in my simulation results when comparing R_g in Figure 28 and Figure 30(a).

Finally, by comparing the minimum energy to the 'steady-state' configuration I may have identified a potential source of discrepancy between scaling exponents listed in the literature. As described above, the often used polymer model in these coarse grained simulation methods is the WCA potential, Equation (2-3). Upon observation of this model, one can see that, due to the cutoff in the potential energy function at distances greater than $2^{1/6}\sigma$, the potential energy of the polymer in both the minimum energy configuration and the 'steady-state' configuration are equal even though the radius of gyration of each are very different. This would not be the case if, for example, the potential energy function was modeled with a full 6-12 Lennard-Jones potential (Equation 2-4) in which the minimum energy configuration would also be the equilibrium configuration. As shown in Figure 27 (a) and Figure 29 (a), I obtain values of α found in the previous simulation results using either the minimum energy configuration or the 'steady-state' configuration. It must be made clear that I am not suggesting that other findings in previous research are incorrect or proper equilibration procedures were not

followed, my purpose is to point out a potential source of discrepancy in the values of α could lie in this oddity of the WCA potential energy function.

Of course, one way to remove this potential discrepancy source would be to simply add a bond-angle potential as was done by Kong and Muthukumar [98]. However, because of the parabolic nature of this potential energy function and the requirement to keep the bond stiff to ensure a polymer with high excluded volume interactions, resulting in a large spring constant, a small simulation time step would be required thus limiting both the overall simulation time and the number of monomers in the simulation. One way to ensure that this discrepancy does not occur is to follow the 'start-up' procedures that I used to obtain the 'steady-state' polymer configuration in which I first assign random monomer positions, then place the polymer in its minimum energy configuration, and finally equilibrate the polymer to its 'steady-state' configuration. I believe this initialization procedure could possibly reduce any source of inconsistency related to the initial polymer configurations in simulation studies.

The 'steady-state' polymer configuration (2) is the more realistic polymer configuration that would be observed in an experimental result. This is because, in an experiment, the time required for the polymer to arrive at the entrance of the nanopore (before translocation) would be much larger than the polymer relaxation time. Hence, the polymer on the *cis* side of the nanopore would scale as $\langle R_g^2 \rangle \sim N^{2\upsilon}$ (Figure 30 (a)).

4.11 Conclusion

I have investigated the translocation time versus polymer chain length scaling behavior, for both Rouse and Zimm polymers, using a computationally efficient simulation methodology - the TEA algorithm [105] - in both forced and unforced

translocation studies. For forced translocation, using Rouse polymers, I obtained different scaling exponents depending upon the initial polymer configuration and the strength of the applied voltage. I demonstrate that if the radius of gyration of the initial polymer configuration deviates from its theoretical value in a good solvent ($<R_g^2> \sim N^{2\upsilon}$), the scaling exponent will also deviate from $\alpha = 1 + \upsilon$ as predicted by Kantor and Kardar [47].

In addition, if the applied voltage is large enough that it causes the translocation time to be much shorter than the polymer relaxation time, the polymer will crowd the nanopore exit and also cause the scaling law to differ as well. However, if the radius of gyration of the polymer begins and ends at its theoretical value, I find that the scaling exponent is in accordance with the value of $\alpha = 1 + \upsilon$ as predicted by Kantor and Kardar [47]. Because of the strongly repulsive nature of the WCA potential often used in translocation simulations, the radius of gyration is vastly different depending upon how long the polymer is permitted to relax. As I show in this chapter, the radius of gyration for the minimum energy configuration is different from the 'steady-state' radius of gyration. Hence, care must be taken in defining the initial polymer configuration before a translocation time simulation is performed and also in comparing simulations results from different studies.

Furthermore, I found the scaling law α increases with decreasing voltage, which is in good agreement with previous simulation results [52–54] as well as predictions with the recently developed Brownian Dynamics Tension Propagation model [76,82]. Based upon the findings in references [45–48], the scaling exponent is larger for unforced translocation than for forced translocation, indicating as the applied force is decreased α should increase, which agrees with my findings given in Figures 27 and 29. From these

results, I observed the lower bound on the scaling exponent was determined by the initial polymer configuration, whereas the upper bound was set by the voltage.

In the presence of HI, as with Zimm polymers, I obtained scaling laws that agree very well with the predictions of $\alpha = 2\upsilon$ [9,57,78] and also with the measurements of Storm *et al.* [9,10]. I also found that, since the relaxation time in the presence of HI is much shorter than in the absence of HI, there was less crowding at the exit of the nanopore. In addition, just as in my previous studies of forced translocation of Rouse polymers through nanopores with increasing diameters [54], translocation of Zimm polymers also results in small changes in α and decreases in translocation time due to the reduction in polymer-pore interactions. Just as in the case with Rouse polymers, I also found the scaling exponent increases with decreasing voltage using Zimm polymers.

In addition, I also show that whereas increasing the viscosity will result in longer translocation times, it has no effect on the translocation time scaling exponent α. I also find that the translocation time versus applied voltage using both Rouse and Zimm polymer models results in the theoretical inverse proportionality $\tau \sim V^{-1}$ [47] for low to intermediate voltages (~ 400 mV). Larger voltages results in an increase in the scaling exponent from -1 caused by extreme crowding at the exit of the nanopore. Due to the smaller relaxation time of Zimm polymers, this scaling law increase is much less than in the Rouse polymer model.

Finally, I performed unforced translocation simulations with and without HI for several different pore diameters. When the pore width is very small, the polymer-pore interactions dominate the translocation process, resulting in approximately the scaling law for Rouse polymers as predicted by Chuang *et al.* [45] ($\alpha = 1 + 2\upsilon$) for both polymer

models. When the pore diameter is increased, the polymer-pore interactions are decreased, the translocation time is decreased, and, due to the increased stochasticity of the process, the scaling exponent also increases. When the pore is removed from the simulation, the scaling exponent for both the Rouse and Zimm both polymers approach the same scaling as their relaxation time, $\alpha = 1 + 2\upsilon$ for Rouse polymer and $\alpha = 3\upsilon$ for Zimm polymer [74]. These simulation findings are important because they provide the scaling law bounds for unforced translocation time simulations for both polymer models.

CHAPTER 5: ELECTROSTATICS IN NANOPORE DEVICES

5.1 Introduction

In most previous coarse-grained simulation studies of biomolecule translocation, including the studies presented in Chapters 3 and 4, the electrostatic effects due to the surface charge on the nanopore and ions in the electrolytic solution were not considered. This may lead to significant deviations in the predictions from physical reality. In this chapter, I present a preliminary investigation of the electrostatics inside silicon nitride nanopores for pore diameters of 25 Å, 30 Å, and 40 Å, using the coupled Poisson-Nernst-Planck (PNP) equations described in Chapter 2. The goal of this study is to make a preliminary assessment (based upon rigorously-obtained computational data) of the electrostatic effects inside nanopores with and without a biopolymer present. In each of the simulations, I assume the nanopore has a negative surface charge density of σ_{Si3N4} = -0.02 C/m^2, the measured value for silicon nitride at pH between 7-8 [41], which are typical levels for translocation time measurements [9–11,13–15,41]. I also employ Dirichlet Boundary conditions, both at the top and bottom of the simulation volume in which the voltage is assigned to 0, and periodic boundary conditions in x and y. To find the potential and ion concentration, as described in chapter 2, Equations (2-36) and (2-37) are solved in an iterative fashion by the Successive Over-Relaxation (SOR) method[123,124] using the six point "nearest neighbors" summation at each grid point in a checkerboard pattern[125] for 200,000 trials. The dielectric slab results given in Figures 14 and 15 serve as the initial condition for the ion concentrations and potential.

5.2 PNP Computations with No Monomers

To begin investigating the effects of electrostatics inside silicon nitride nanopores, I first performed PNP simulations in an open pore (i.e. with no monomers present). Figures 37, 39, and 41 provide the results for the potential, whereas Figures 38, 40, and 42 provide the results for the ionic concentration, for nanopores with diameters of 25 Å, 30 Å, and 40 Å respectively. As shown, the potential inside the membrane is approximately the same value for the membrane when no pore was present as shown in Figure 15 (~ -0.04 V). In addition, the potential quickly decays to zero outside the nanopore, which is expected due to the short Debye length of 3 Å as a result of the 1 M electrolyte solution. Also, as shown in Figures 38, 40, and 42, the ionic concentration for the positive valence ion is very high near the surface of the nanopores, due to the negative surface charge of the silicon nitride, whereas the negative valence ion is very small at the surface. Inside the membrane the concentration is zero, and, at distances far away from the pore, the concentration approaches the bulk value of
$C_\infty = 6.022 \times 10^{-4}$ Å^{-3}.

The potential inside the nanopore does not decay to zero in the center (x = y = 50 Å) for the 25 Å pore. This is reflected in the fact that the ionic concentration is not the bulk value in the center either. However, as the diameter of the pore is increased, the concentration for both ions at the center of the nanopore approaches the bulk concentration of $C_\infty = 6.022 \times 10^{-4}$ Å^{-3}, and, as a result, the potential inside the nanopore becomes zero.

In addition, the surface potential for the 25 Å pore is lower (or more negative) than the potential, -7.354×10^{-3} V, obtained in Figure 15 (a) for the charged silicon

nitride slab. However, as the pore size is increased, this surface potential increases and at 40 Å, as shown in Figure 41 (b), the surface potential of -7.75 x 10^{-3} V better agrees with the values obtained in Figure 15(b). This same behavior is also observed in the ionic concentration at the surface of the pore as well. The surface concentration for the positive valence ion for the 25 Å pore is higher than the concentration obtained for the charged silicon nitride slab in Figure 14 (b) of C_o = 8.014 x 10^{-4} $Å^{-3}$. However, as the pore diameter is increased to 40 Å, as shown in Figure 42 (c) the surface concentration decreases to a value of C_o = 8.144 x 10^{-4} $Å^{-3}$, which agrees very well with the value obtained in Figure 14. Hence, it can be seen in these simulations that the pore diameter does have an effect on the ionic concentration and, as a result, the potential inside the pore.

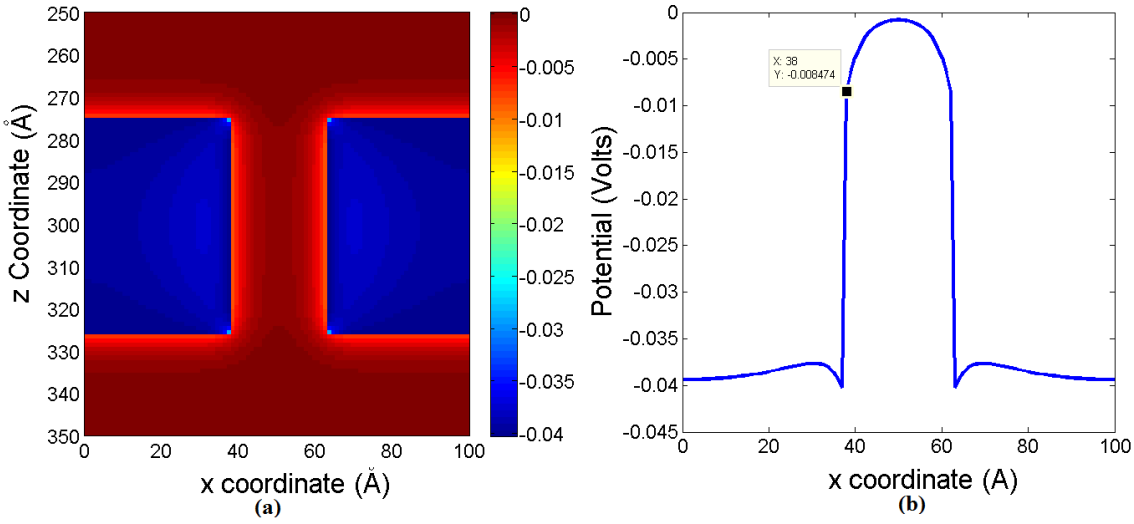

Figure 37: Potential (in Volts) in nanopore with diameter 25 Å and length 50 Å. (a) Potential as a function of both x and z with y held constant at 50 Å. (b) Potential in center of nanopore with z = 300 Å and y = 50 Å, with surface potential labeled at x = 38 Å, with a value of -8.474 x 10^{-3} V.

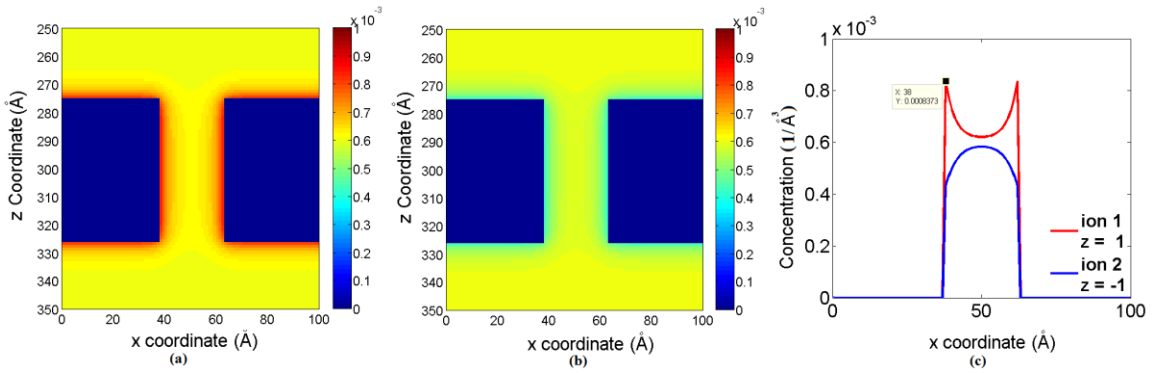

Figure 38: Concentration (in $1/Å^3$) in nanopore with diameter 25 Å and length 50 Å. (a) Concentration of positive valence ion as a function of both x and z with y held constant at 50 Å. (b) Concentration of negative valence ion as a function of both x and z with y held constant at 50 Å. (c) Concentration in nanopore with z = 300 Å and y = 50 Å**,** with concentration at surface of nanopore of $C_o = 8.373 \times 10^{-4}$ $Å^{-3}$.

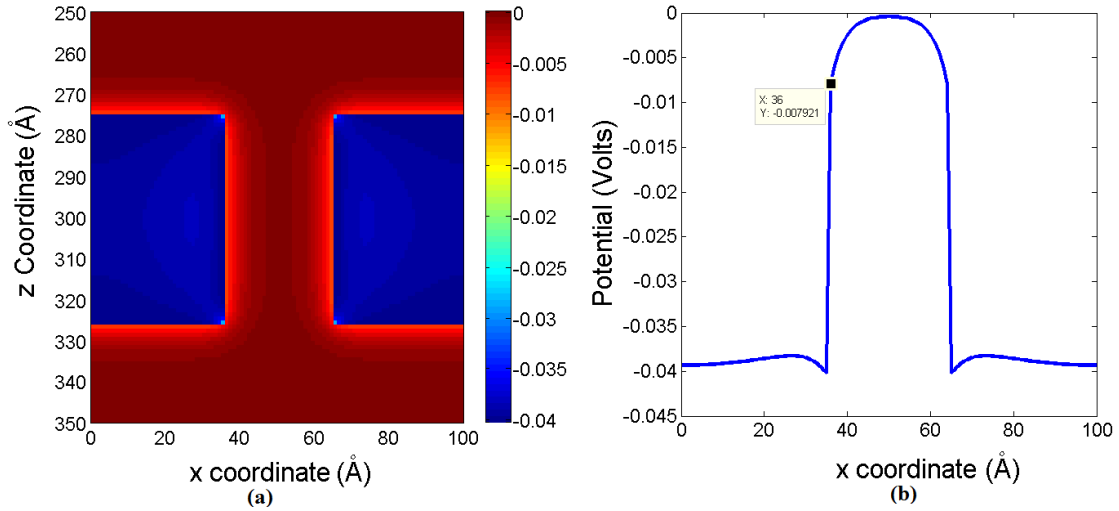

Figure 39: Potential (in Volts) in nanopore with diameter 30 Å and length 50 Å. (a) Potential as a function of both x and z with y held constant at 50 Å. (b) Potential in center of nanopore with z = 300 Å and y = 50 Å with surface potential labeled with a value of -7.921×10^{-3} V.

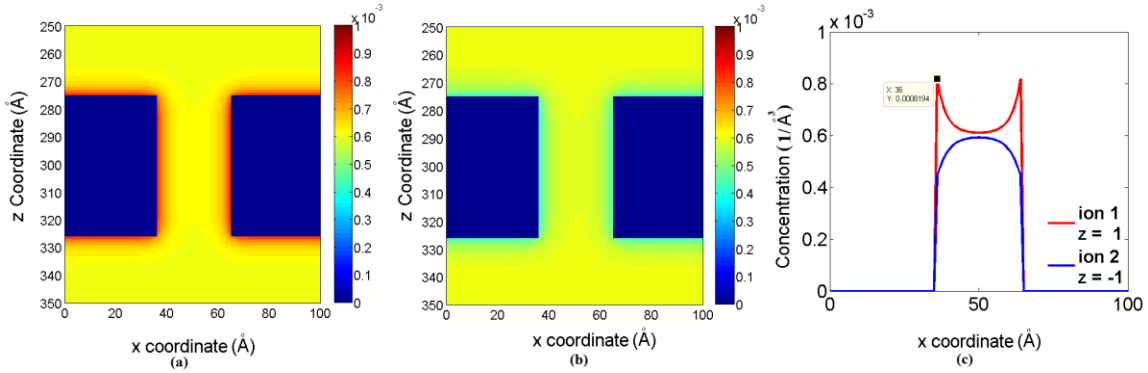

Figure 40: Concentration (in $1/Å^3$) in nanopore with diameter 30 Å and length 50 Å. (a) Concentration of positive valence ion as a function of both x and z with y held constant at 50 Å. (b) Concentration of negative valence ion as a function of both x and z with y held constant at 50 Å. (c) Concentration in nanopore with z = 300 Å and y = 50 Å with concentration at surface of nanopore of $C_o = 8.194 \times 10^{-4}$ $Å^{-3}$.

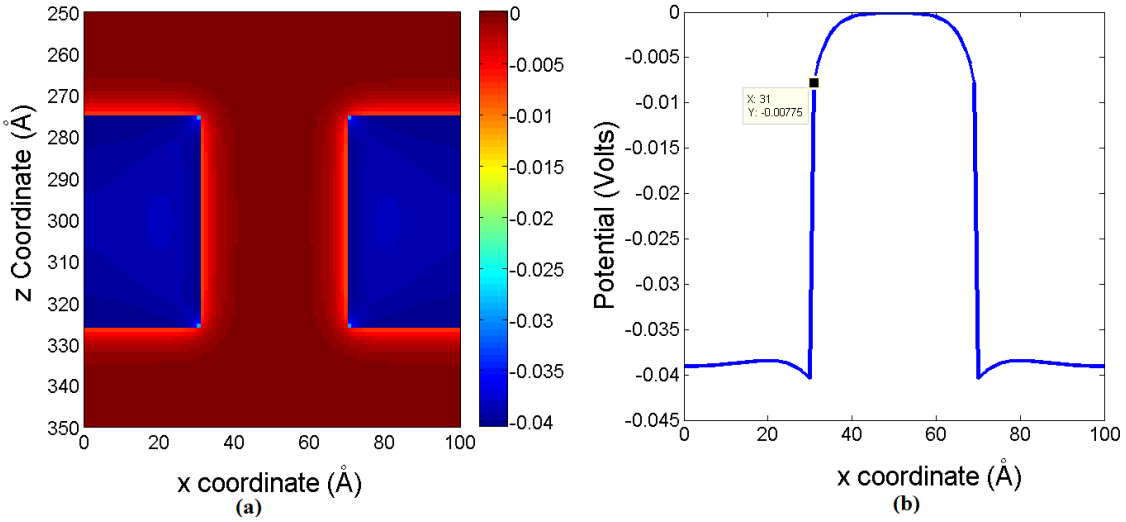

Figure 41: Potential (in Volts) in nanopore with diameter 40 Å and length 50 Å. (a) Potential as a function of both x and z with y held constant at 50 Å. (b) Potential in center of nanopore with z = 300 Å and y = 50 Å with surface potential labeled with a value of -7.75×10^{-3} V.

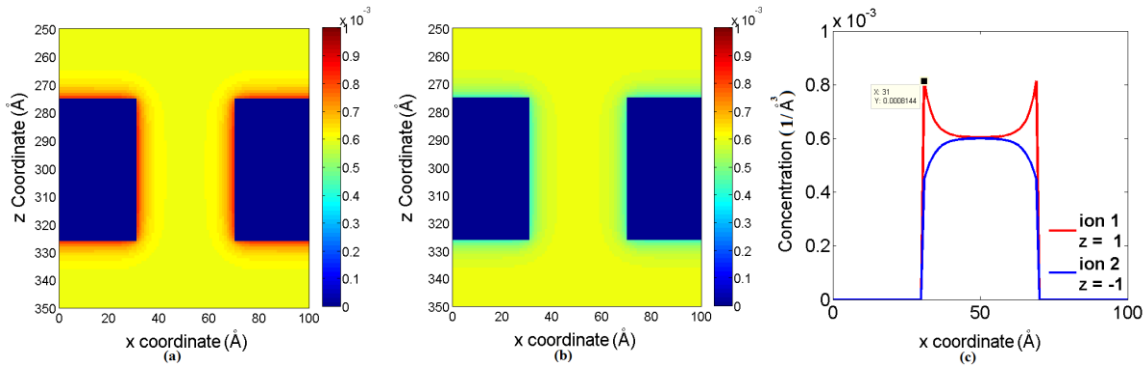

Figure 42: Concentration (in $1/Å^3$) in nanopore with diameter 40 Å and length 50 Å. (a) Concentration of positive valence ion as a function of both x and z with y held constant at 50 Å. (b) Concentration of negative valence ion as a function of both x and z with y held constant at 50 Å. (c) Concentration in nanopore with z = 300 Å and y = 50 with concentration at surface of nanopore of $C_o = 8.144 \times 10^{-4}$ $Å^{-3}$.

5.3 PNP Computations with Uncharged Monomers

The next set of simulations sought to investigate the effects of monomers being present inside the nanopore. To do this, I performed simulations on the same nanopores above, but this time threaded the pore with a 17 monomer chain. Each monomer, which was represented by an approximate 5 Å sphere with dielectric constant of 2 [127], did not have an associated charge. The chain was placed in the center of the pore and ions were not permitted to flow inside the monomers.

Figures 43, 45, and 47 show the results for the potential, whereas Figures 44, 46, and 48 provide the results for the ionic concentration, for nanopores with diameters of 25 Å, 30 Å, and 40 Å respectively. The surface potential does not change significantly from the simulations without the monomers. Whereas there a very small change in the potential in the center of the 25 Å pore, there is no difference in the potential in the middle of the pore for the 30 Å and 40 Å pores. Hence, it can be concluded that the

presence of the uncharged monomers does not significantly alter the electrostatic potential.

As shown in Figures 44, 46, and 48, whereas the concentration in the middle of the pore is reduced to zero due to the presence of the monomers in the center of the pore, the concentration at the surface of the pore walls, just as in the surface potential, did not change significantly from earlier results in which monomers were not present inside the pore. The importance of these simulation results demonstrate that the presence of a uncharged monomer with a different dielectric constant will not alter the potential inside the nanopore and only slightly change the concentration profile.

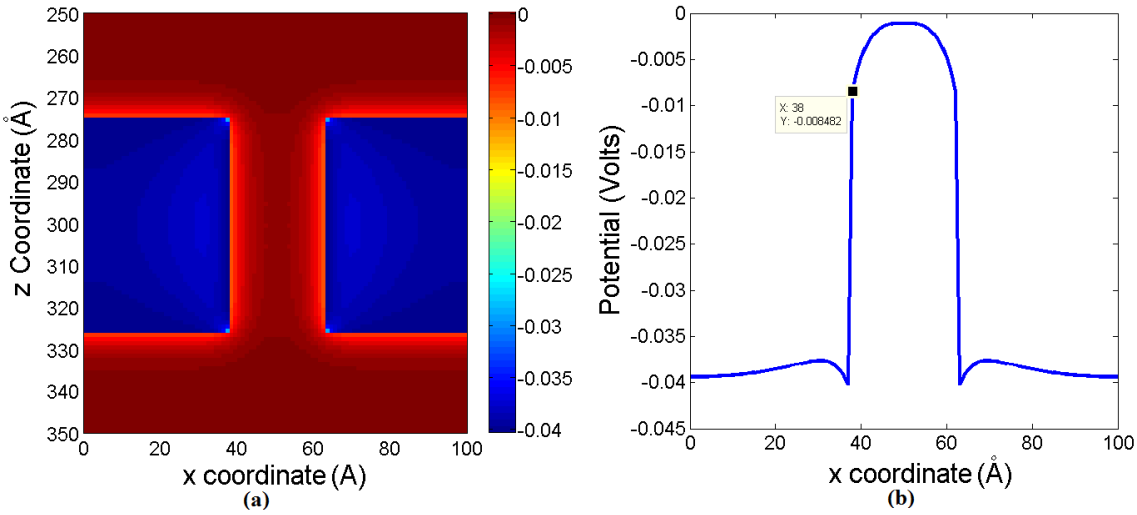

Figure 43: Potential (in Volts) in nanopore with diameter 25 Å and length 50 Å with polymer chain containing 17 uncharged monomers threading the pore. (a) Potential as a function of both x and z with y held constant at 50 Å. (b) Potential in center of nanopore with z = 300 Å and y = 50 Å with surface potential labeled with a value of -8.482 x 10^{-3} V.

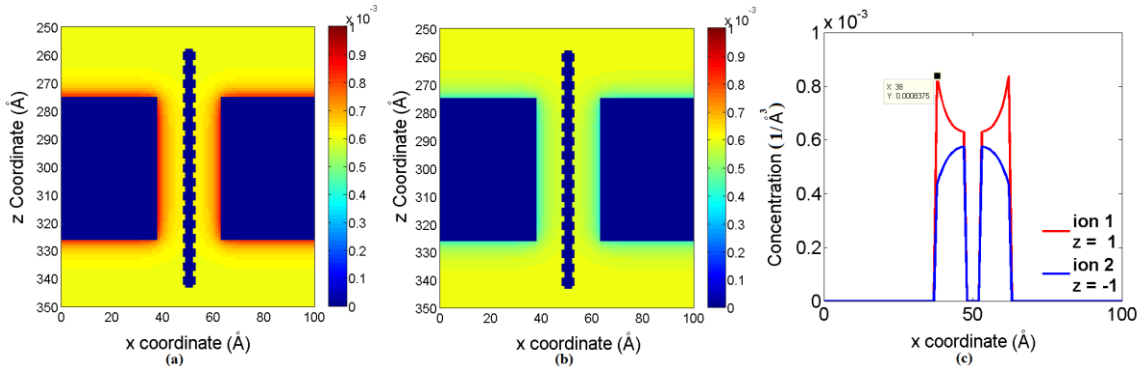

Figure 44: Concentration (in $1/Å^3$) in nanopore with diameter 25 Å and length 50 Å with polymer chain containing 17 uncharged monomers threading the pore. (a) Concentration of positive valence ion as a function of both x and z with y held constant at 50 Å. (b) Concentration of negative valence ion as a function of both x and z with y held constant at 50 Å. (c) Concentration in nanopore with z = 300 Å and y = 50 with concentration at surface of nanopore of $C_o = 8.375 \times 10^{-4}$ $Å^{-3}$

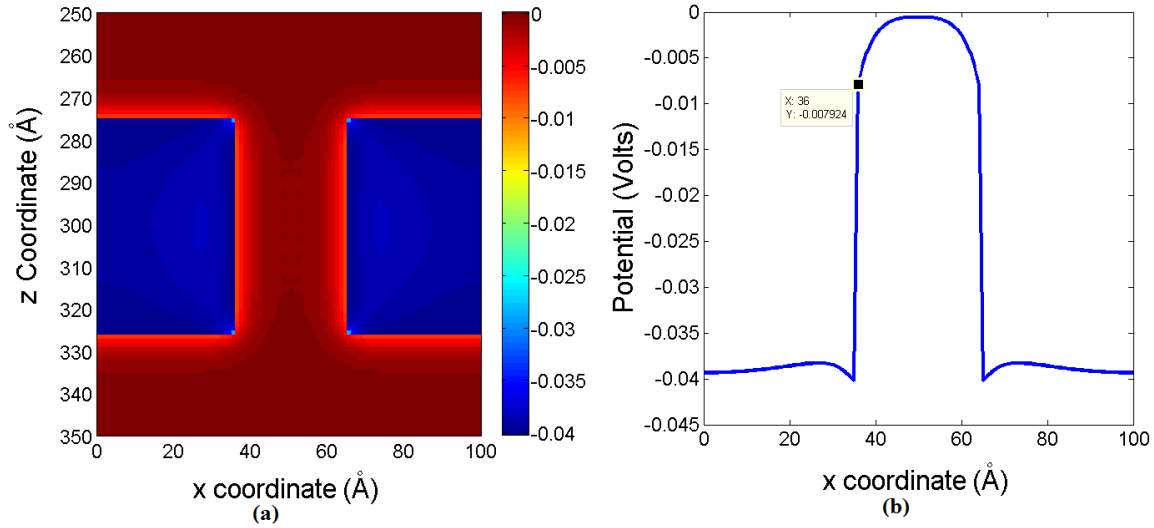

Figure 45: Potential (in Volts) in nanopore with diameter 30 Å and length 50 Å with polymer chain containing 17 uncharged monomers threading the pore. (a) Potential as a function of both x and z with y held constant at 50 Å. (b) Potential in center of nanopore with z = 300 Å and y = 50 Å with surface potential labeled with a value of -7.942×10^{-3} V.

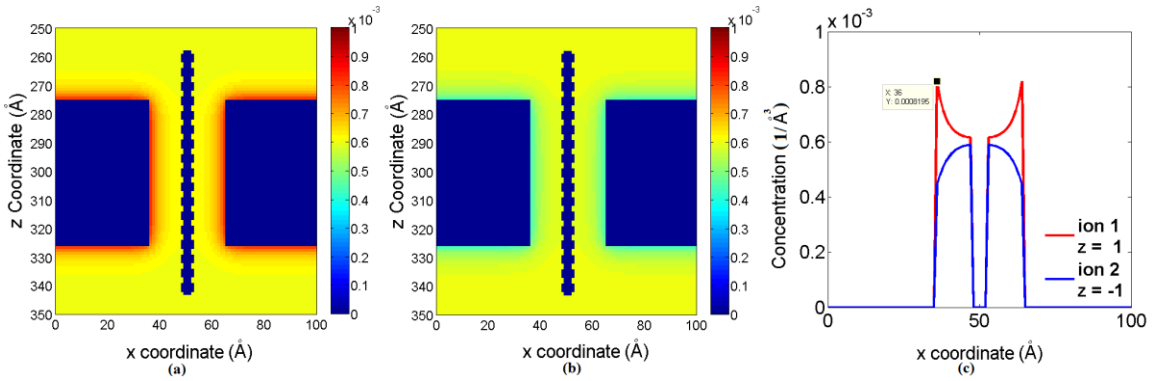

Figure 46: Concentration (in $1/Å^3$) in nanopore with diameter 30 Å and length 50 Å with polymer chain containing 17 uncharged monomers threading the pore. (a) Concentration of positive valence ion as a function of both x and z with y held constant at 50 Å. (b) Concentration of negative valence ion as a function of both x and z with y held constant at 50 Å. (c) Concentration in nanopore with z = 300 Å and y = 50 with concentration at surface of nanopore of $C_o = 8.195 \times 10^{-4}$ $Å^{-3}$

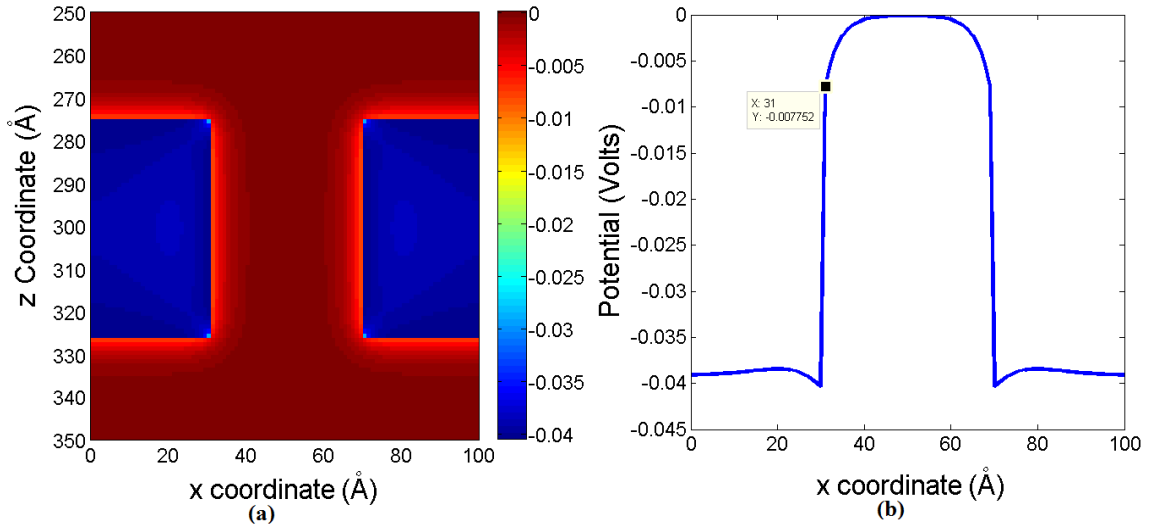

Figure 47: Potential (in Volts) in nanopore with diameter 40 Å and length 50 Å with polymer chain containing 17 uncharged monomers threading the pore.(a) Potential as a function of both x and z with y held constant at 50 Å. (b) Potential in center of nanopore with z = 300 Å and y = 50 Å with surface potential labeled with a value of -7.752×10^{-3} V.

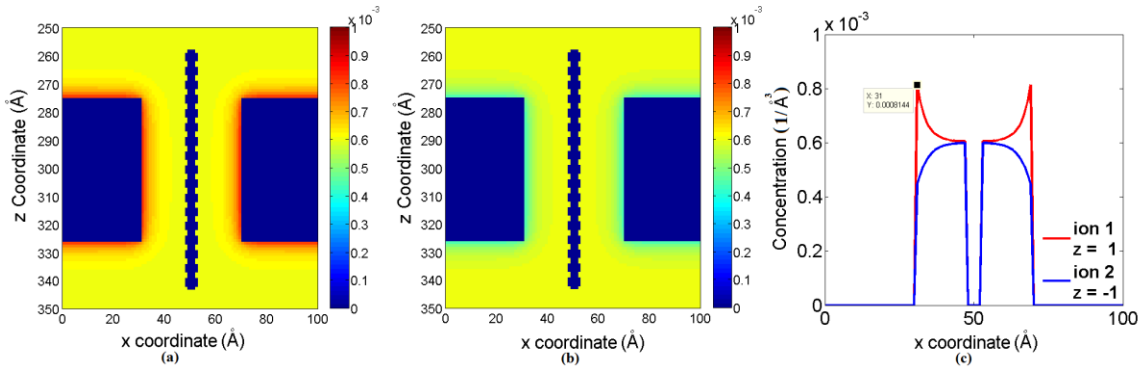

Figure 48: Concentration (in $1/Å^3$) in nanopore with diameter 40 Å and length 50 Å with polymer chain containing 17 uncharged monomers threading the pore. (a) Concentration of positive valence ion as a function of both x and z with y held constant at 50 Å. (b) Concentration of negative valence ion as a function of both x and z with y held constant at 50 Å. (c) Concentration in nanopore with z = 300 Å and y = 50 with concentration at surface of nanopore of $C_o = 8.144 \times 10^{-4}$ $Å^{-3}$

5.4 PNP Computations with Center-Charged monomers

In the next set of simulations, the same 17-monomer chain threaded the pore as in the previous section, but instead of an uncharged monomer being used, a point charge of -1*e* [97,98] was placed at the center of each monomer. Figures 49, 51, and 53 shows the results for the potential, whereas Figures 50, 52, and 54 provide the results for the electrolyte ion concentration, for nanopores with diameters of 25 Å, 30 Å, and 40 Å respectively. As shown, the electrostatic potential significantly changes from previous simulation results, and, as expected theoretically, mimics a delta function in the center of each monomer. The negative center charge on each monomer causes a large build-up of positive ions on the surface of each monomer, thus significantly reducing the monomer surface potential, as shown in Figures 51(b) – 53 (b). As mentioned earlier, the surface charge of the silicon nitride nanopore is $\sigma_{Si3N4} = -0.02$ C/m^2, which results in a total

charge of -2 x 10^{-22} C for a 1 $Å^2$ box. Because each monomer possess a charge of -1e (or -1.6 x 10^{-19} C), there is a larger absorbed positive valence ion concentration on the monomers than the pore surface. Whereas the pore diameter has no effect on the ionic concentration on the surface of each monomer, it results in a slightly higher concentration at the surface of the pore for both the 25 Å and 30 Å pores. However, for the 40 Å pore, the surface concentration is very similar to the concentrations obtained for both previous studies in which there were no monomers or uncharged monomers. The importance of these findings indicates that introducing a charge on each monomer greatly affects the ion concentration inside the pore, causing a large buildup of ions on the surface of each monomer, which, in a translocation time experiment, would result in a large electro-osmotic force along the backbone of the polymer. In addition, the presence of the large concentration of ions also greatly reduces the potential at short distances away from the monomer and the nanopore surface. Thus, when using very high electrolytic concentrations, such as 1 M used in the present simulations, it would appear that the effects of surface charge on the nanopore and the monomer would be largely "screened" by the electrolytic solution.

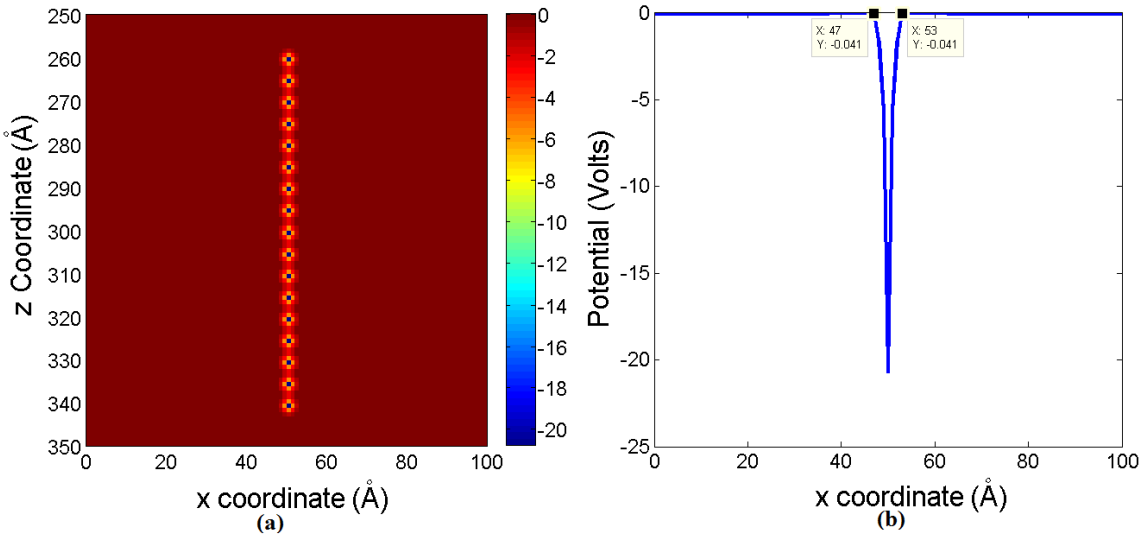

Figure 49: Potential (in Volts) in nanopore with diameter 25 Å and length 50 Å with polymer chain containing 17 monomers threading the pore. Each monomer has a negative charge of -1e assigned to its center. (a) Potential as a function of both x and z with y held constant at 50 Å. (b) Potential nanopore with z = 300 Å and y = 50 Å. Labels on the surface of the monomer (at x = 47 Å and x = 53 Å) indicate the potential is "screened" at short distances due to the high buildup of positive ions.

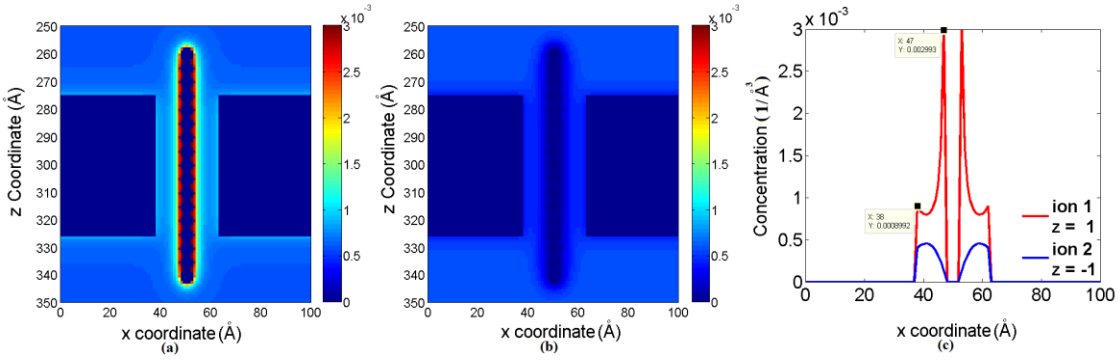

Figure 50: Concentration (in $1/Å^3$) in nanopore with diameter 25 Å and length 50 Å with polymer chain containing 17 monomers threading the pore. Each monomer has a negative charge of -1e assigned to its center. (a) Concentration of positive valence ion as a function of both x and z with y held constant at 50 Å. (b) Concentration of negative valence ion as a function of both x and z with y held constant at 50 Å. (c) Concentration in nanopore with z = 300 Å and y = 50 Å. Concentration at surface of nanopore (x = 38 Å) is C = 8.992 x 10^{-4} $Å^{-3}$, whereas the concentration at the surface of the monomer (x = 47 Å) is C = 2.993 x 10^{-3} $Å^{-3}$.

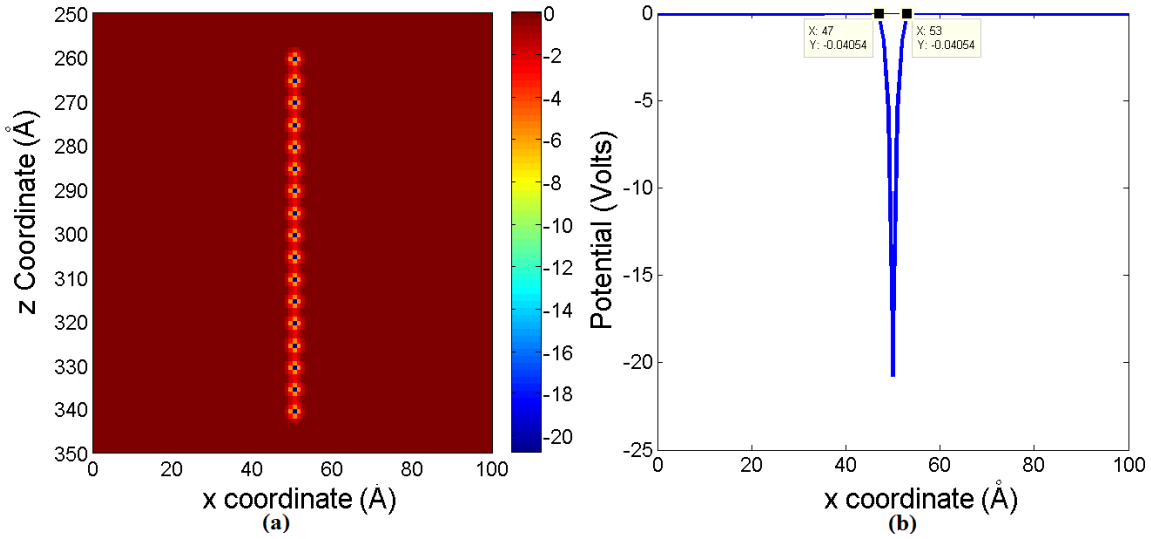

Figure 51: Potential (in Volts) in nanopore with diameter 30 Å and length 50 Å with polymer chain containing 17 monomers threading the pore. Each monomer has a negative charge of -1e assigned to its center. (a) Potential as a function of both x and z with y held constant at 50 Å. (b) Potential in nanopore with z = 300 Å and y = 50 Å. Labels on the surface of the monomer (at x = 47 Å and x = 53 Å) indicate the potential is "screened" at short distances due to the high buildup of positive ions.

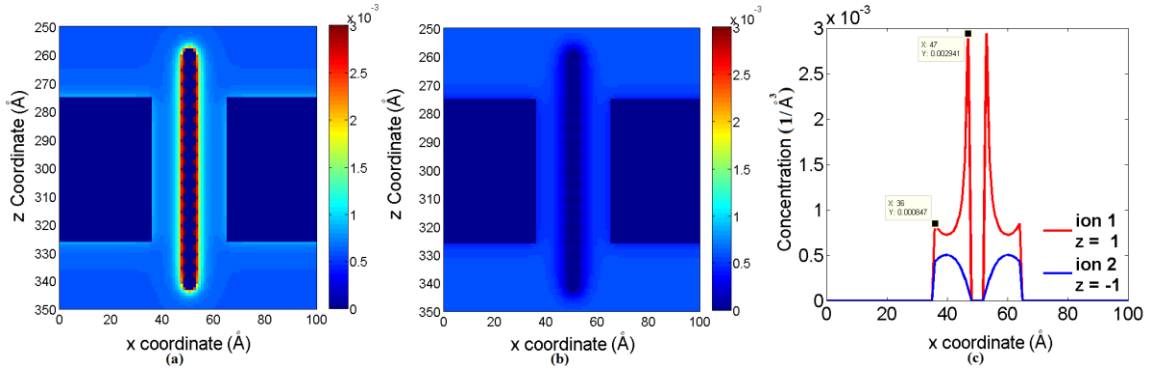

Figure 52: Concentration (in $1/Å^3$) in nanopore with diameter 30 Å and length 50 Å with polymer chain containing 17 monomers threading the pore. Each monomer has a negative charge of -1e assigned to its center. (a) Concentration of positive valence ion as a function of both x and z with y held constant at 50 Å. (b) Concentration of negative valence ion as a function of both x and z with y held constant at 50 Å. (c) Concentration in nanopore with z = 300 Å and y = 50 Å. Concentration at surface of nanopore (x = 36 Å) is C = 8.47 x 10^{-4} $Å^{-3}$, whereas the concentration at the surface of the monomer (x = 47 Å) is C = 2.941 x 10^{-3} $Å^{-3}$.

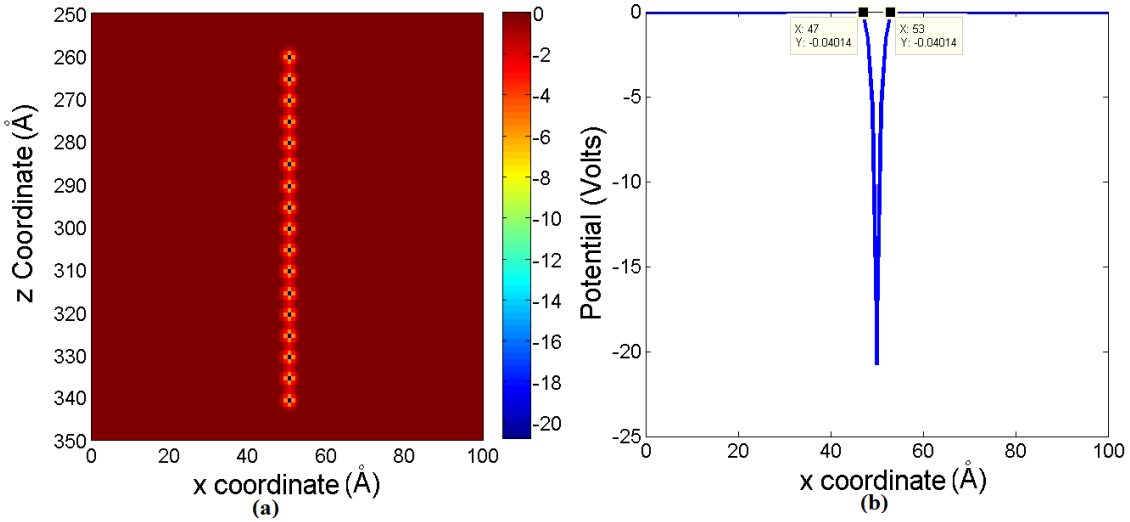

Figure 53: Potential (in Volts) in nanopore with diameter 40 Å and length 50 Å with polymer chain containing 17 monomers threading the pore. Each monomer has a negative charge of -1e assigned to its center. (a) Potential as a function of both x and z with y held constant at 50 Å. (b) Potential in nanopore with z = 300 Å and y = 50 Å. Labels on the surface of the monomer (at x = 47 Å and x = 53 Å) indicate the potential is "screened" at short distances due to the high buildup of positive ions.

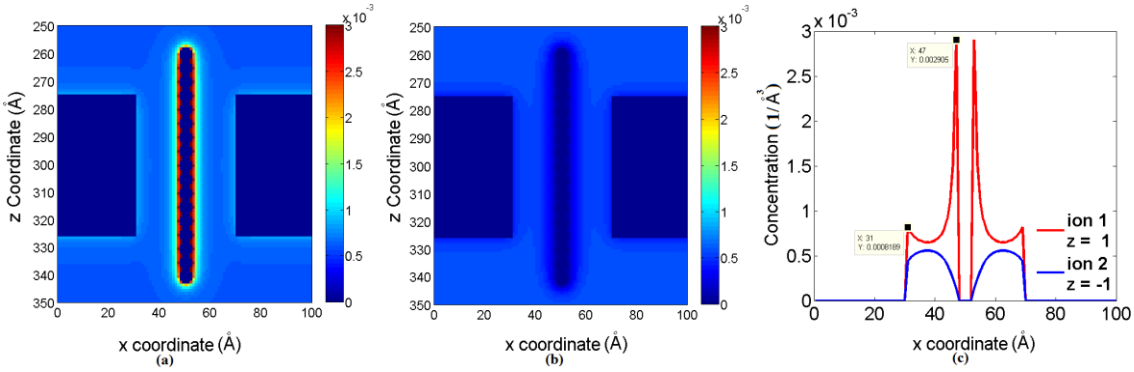

Figure 54: Concentration (in $1/Å^3$) in nanopore with diameter 40 Å and length 50 Å with polymer chain containing 17 monomers threading the pore. Each monomer has a negative charge of -1e assigned to its center. (a) Concentration of positive valence ion as a function of both x and z with y held constant at 50 Å. (b) Concentration of negative valence ion as a function of both x and z with y held constant at 50 Å. (c) Concentration in nanopore with z = 300 Å and y = 50 Å. Concentration at surface of nanopore (x = 31 Å) is C = 8.189 x 10^{-4} $Å^{-3}$, whereas the concentration at the surface of the monomer (x = 47 Å) is C = 2.905 x 10^{-3} $Å^{-3}$.

5.5 PNP Computations with Surface-Charged Monomers

Finally, as opposed to assigning the center of each monomer a charge of -1*e*, the charge was instead spread evenly over the entire surface of each monomer. Figures 55, 57, and 59 provide the results for the potential, whereas Figures 56, 58, and 60 provide the results for the ionic concentration, for nanopores with diameters of 25 Å, 30 Å, and 40 Å respectively. As shown, instead of a delta function shape, the potential is now spread across the diameter of the monomer. Just as in the center charge monomer solution, there is also a high concentration of positive valence ions on the surface of each monomer which, again, drastically reduces the potential on the surface of each monomer. Again, these simulation results confirm that for biopolymers, such as ds-DNA, that have an associated charge, electro-osmotic forces could greatly affect the translocation dynamics when the presence of a high concentration electrolyte.

One other observation is that because the charge is spread out over the surface of the monomer, the ion concentration is slightly smaller than the previous center charge values. In addition, just as in all of the cases above, the surface concentration does not approach the values observed in the earlier slab simulations until the diameter of the pore is 40 Å. Finally, in reviewing the simulation results from both the center-charged monomer model and the surface-charged monomer model, it would appear that the latter is more physically reasonable. This can be seen by noting that the large delta potential function as shown in Figures 49, 51, and 53, significantly weakens other surface potential effects that could possibly be important when modeling translocation time simulations. As shown in Figures 55(b), 57(b), and 59 (b), potential effects due to the negative surface

charge on the silicon nitride and the resultant positive ion build up, are shown as variations in the potential energy. Hence, these effects are not "drowned out" by distributing the polymer charge on the surface of each monomer.

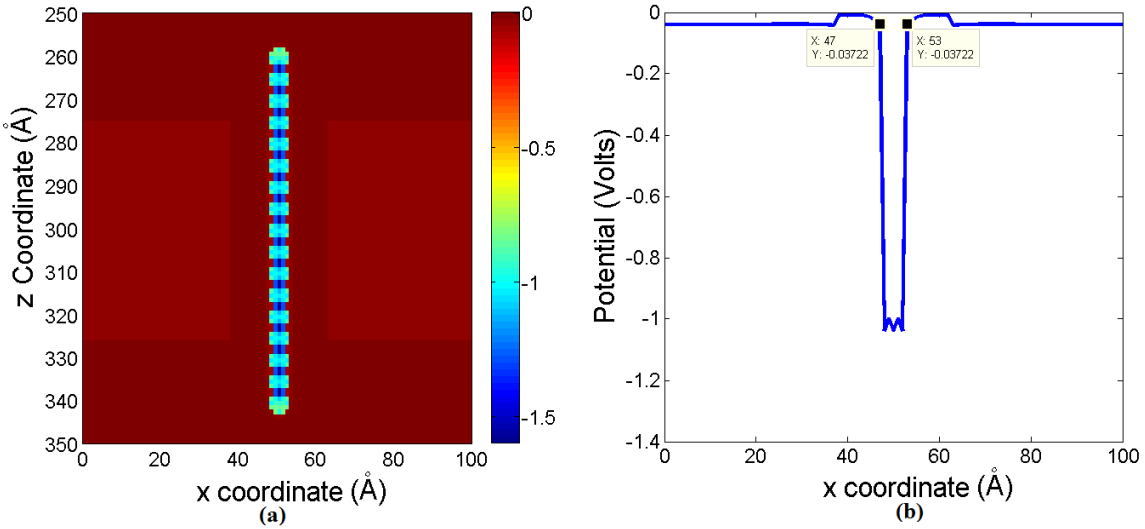

Figure 55: Potential (in Volts) in nanopore with diameter 25 Å and length 50 Å with polymer chain containing 17 monomers threading the pore. Each monomer has an equally distributed negative charge on the surface.(a) Potential as a function of both x and z with y held constant at 50 Å. (b) Potential in nanopore with z = 300 Å and y = 50 Å. Labels on the surface of the monomer (at x = 47 Å and x = 53 Å) indicate the potential is "screened" at short distances due to the high buildup of positive ions.

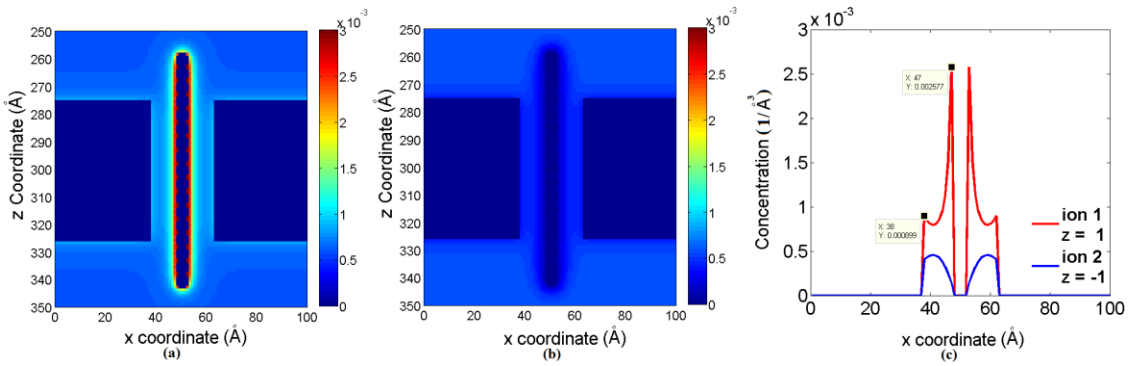

Figure 56: Concentration (in $1/Å^3$) in nanopore with diameter 25 Å and length 50 Å with polymer chain containing 17 monomers threading the pore. Each monomer has an equally distributed negative charge on the surface. (a) Concentration of positive valence ion as a function of both x and z with y held constant at 50 Å. (b) Concentration of negative valence ion as a function of both x and z with y held constant at 50 Å. (c) Concentration in of nanopore with z = 300 Å and y = 50 Å. Concentration at surface of nanopore (x = 38 Å) is C = 8.99 x 10^{-4} $Å^{-3}$, whereas the concentration at the surface of the monomer (x = 47 Å) is C = 2.577 x 10^{-3} $Å^{-3}$.

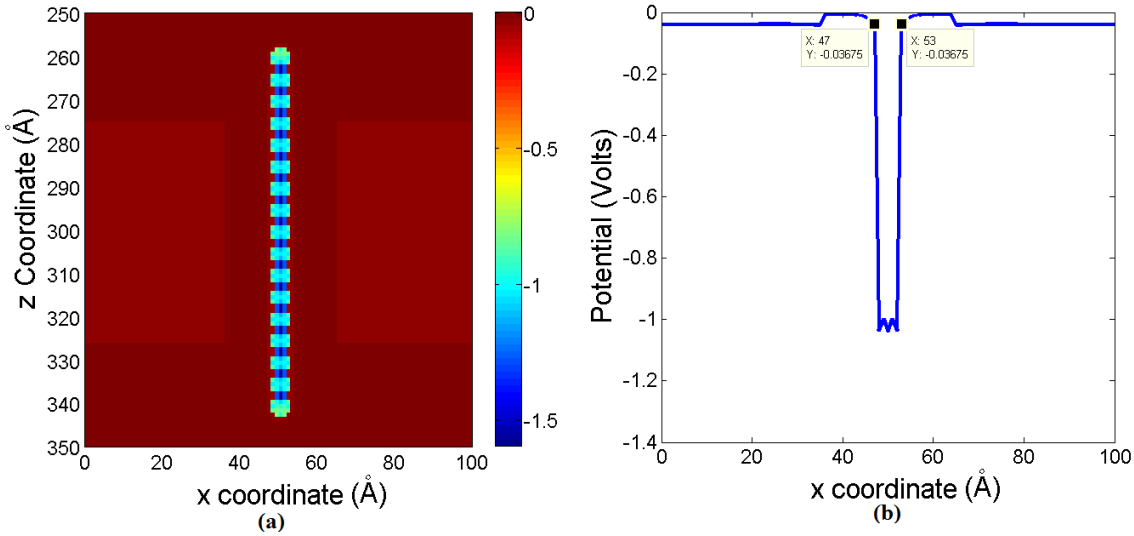

Figure 57: Potential (in Volts) in nanopore with diameter 30 Å and length 50 Å with polymer chain containing 17 monomers threading the pore. Each monomer has an equally distributed negative charge on the surface.(a) Potential as a function of both x and z with y held constant at 50 Å. (b) Potential in center of nanopore with z = 300 Å and y = 50 Å with surface potential labeled. Labels on the surface of the monomer (at x = 47 Å and x = 53 Å) indicate the potential is "screened" at short distances due to the high buildup of positive ions.

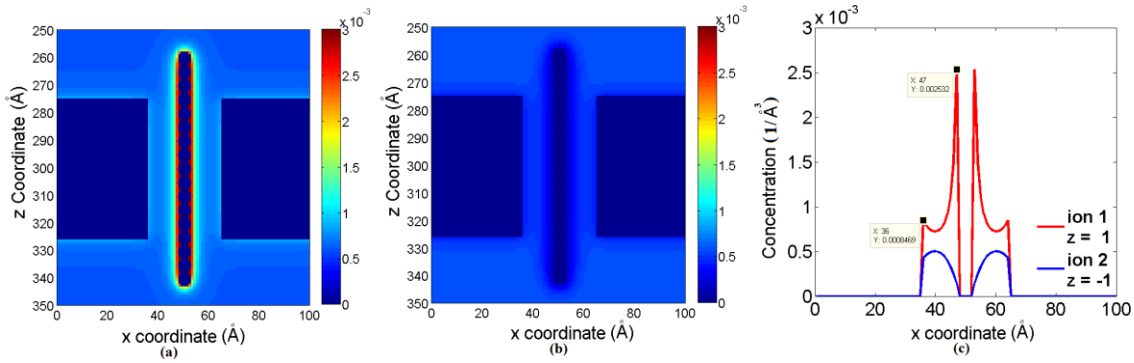

Figure 58: Concentration (in $1/Å^3$) in nanopore with diameter 30 Å and length 50 Å with polymer chain containing 17 monomers threading the pore. Each monomer has an equally distributed negative charge on the surface.(a) Concentration of positive valence ion as a function of both x and z with y held constant at 50 Å. (b) Concentration of negative valence ion as a function of both x and z with y held constant at 50 Å. (c) Concentration in nanopore with z = 300 Å and y = 50 Å. Concentration at surface of nanopore (x = 36 Å) is C = 8.469 x 10^{-4} $Å^{-3}$, whereas the concentration at the surface of the monomer (x = 47 Å) is C = 2.532 x 10^{-3} $Å^{-3}$.

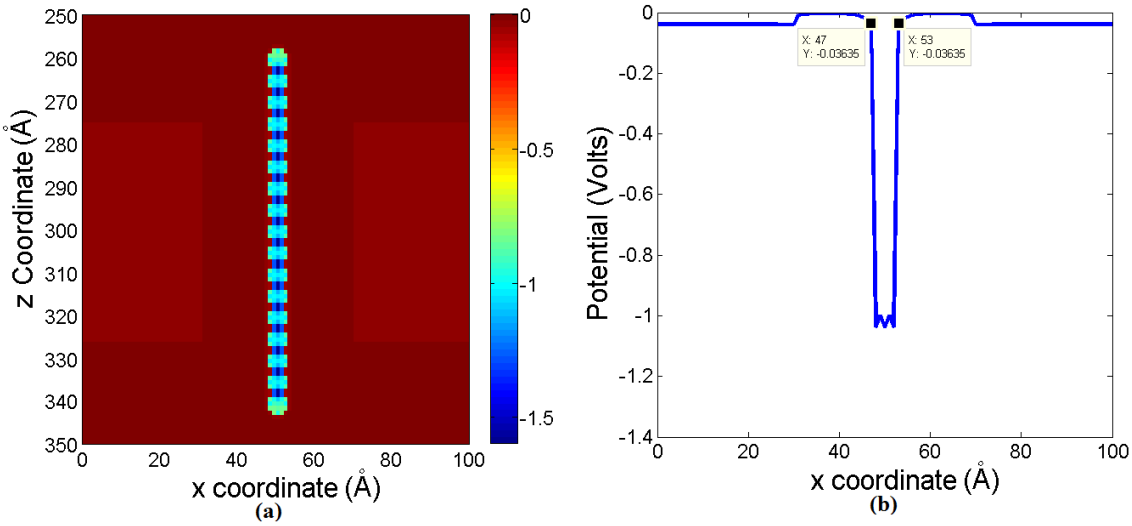

Figure 59: Potential (in Volts) in nanopore with diameter 40 Å and length 50 Å with polymer chain containing 17 monomers threading the pore. Each monomer has an equally distributed negative charge on the surface.(a) Potential as a function of both x and z with y held constant at 50 Å. (b) Potential in center of nanopore with z = 300 Å and y = 50 Å with surface potential labeled. Labels on the surface of the monomer (at x = 47 Å and x = 53 Å) indicate the potential is "screened" at short distances due to the high buildup of positive ions.

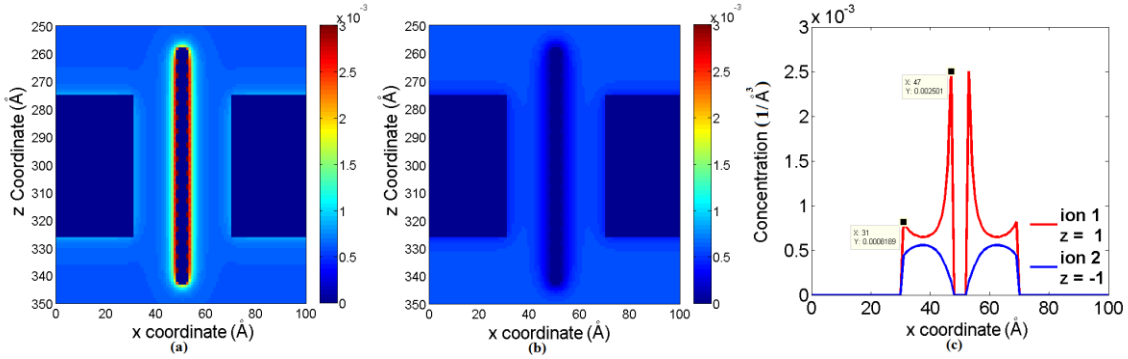

Figure 60: Concentration (in $1/Å^3$) in nanopore with diameter 40 Å and length 50 Å with polymer chain containing 17 monomers threading the pore. Each monomer has an equally distributed negative charge on the surface.(a) Concentration of positive valence ion as a function of both x and z with y held constant at 50 Å. (b) Concentration of negative valence ion as a function of both x and z with y held constant at 50 Å. (c) Concentration in nanopore with z = 300 Å and y = 50 Å. Concentration at surface of nanopore (x = 31 Å) is C = 8.189 x 10^{-4} $Å^{-3}$, whereas the concentration at the surface of the monomer (x = 47 Å) is C = 2.501 x 10^{-3} $Å^{-3}$.

5.6 Limitations of the PNP model

One of the limitations of using the PNP mean field approximation to model the electrostatics in a nanopore simulation, is the assumption that each ion has a zero self-energy. This self-energy term, which has been shown to be important in ion channel modeling, arises when a charge induces an image charge at a dielectric boundary resulting in a repulsive energy that scales as $\sim q^2$ [128]. This repulsive energy term limits ion flow into a channel. Because continuum models do not compute discrete ion-ion interactions, this self-energy term is zero. However, it has been shown using Brownian Dynamics (BD) simulations to model ion flow through channels that the solution to continuum methods such as the Poisson-Nernst-Planck and Poisson-Boltzmann converges to the BD results when the radius of the ion channel is 2 Debye lengths or greater [128–130]. I note that, in these simulations, a 1 M solution is used as the electrolyte resulting in an approximate Debye length of 3 Å. The smallest radius in which I performed PNP simulations was 12.5 Å (or diameter = 25 Å), which is 4 times the Debye length well within the limitations specified in references [128–130].

5.7 Conclusions

In this section, using the coupled Poisson-Nernst-Planck equations, I investigated the electrostatic effects inside silicon nitride nanopores using measured quantities for both surface charge and electrolytic concentrations used in translocation time studies. I also studied how the presence of both uncharged and charged monomers affects the ion concentration and potential distribution inside a nanopore. When either monomers are absent or uncharged monomers are present, the potential does not change significantly,

although the concentration will change due to the prevention of ions from flowing inside a monomer.

On the other hand, when a monomer is charged, a large concentration of oppositely charged ions will build on the surface, which reduces the potential at short distances away from the monomer. In addition, a large concentration of ions also builds on the surface of the nanopore. As a result, when using very high electrolytic concentrations, such as 1 M used in these simulation results, it would appear that the effects of surface charge on the nanopore and the monomer would be "screened" by the electrolytic solution. One could hypothesize, due to the large ion concentrations in close proximity to the polymer, that electro-osmotic forces along the backbone of the polymer would greatly affect the translocation dynamics in an experiment with a charged biopolymer such as ds-DNA. The importance of these findings indicates how important it is to include the electrolytic solution for not only electrostatic effects but possible electro-osmotic effects as well.

CHAPTER 6: CONCLUSIONS AND RELATED FUTURE WORK

6.1 Main Findings

This thesis has thoroughly investigated polymer translocation through solid-state nanopores in order to gain a better understanding of the underlying physics. This present work investigated several important issues, including the elusive and important translocation time versus chain length scaling exponent ($\tau \sim N^{\alpha}$)[1]. If the scaling exponent α is known, determining the length of the polymer chain is trivial from the measured translocation time. In order to gain a better understanding of how the scaling parameter α may change under different conditions, I performed simulations varying key physical parameters such as nanopore dimensions, applied voltage strength, solvent viscosity, and the configuration of the polymer before the translocation begins. In addition, I also studied the potential inside silicon nitride nanopores of varying diameter with the inclusion of surface charge and ions due to an applied electrolytic solution used in translocation time measurements. The results from my simulation studies can assist in not only proper nanopore design, but also help determine the proper experimental environments and operational parameters for nanopore operation.

As a first objective of this thesis, I developed a computationally efficient, physically accurate simulation methodology in order to study the underlying physics involved in a translocation time measurement. My simulation methodology, which allowed for both the inclusion (Zimm polymer) and the omission (Rouse polymer) of hydrodynamic interactions, used highly accurate atomistically detailed silicon nitride nanopores of varying diameters and lengths. In addition, I used coarse-grained simulation

techniques (i.e. Brownian and Langevin Dynamics) in my studies, permitting the use of higher time steps and longer simulation times and polymer chain lengths, which allowed for a more thorough and detailed study of polymer translocation. Finally, using the coupled Poisson-Nernst-Planck equations, I was able to determine the potential and ionic concentration distribution inside the nanopore, as a result of the ions present in the electrolytic solution and surface charge of the silicon nitride nanopore, for both situations of when a polymer is present or absent from the nanopore.

Using my simulation methodology, I first investigated forced Rouse polymer translocation through silicon nitride nanopores using two different initial polymer configurations for different applied voltages. Whereas most polymers behave as Zimm polymers in bulk solution [88–90], hydrodynamic interactions have shown to be screened for polymers moving near a wall or inside a channel [45,68,91]. Thus my study of Rouse polymers is very applicable in polymer translocation through nanopores especially in measurement conditions where the pore diameter is very small. In my first studies, using polymer lengths much longer than the length of the pore, which is often the situation in a typical translocation time measurement, I found the only way to obtain the theoretical scaling exponent derived by Kantor and Kardar [47] ($\alpha = 1 + \upsilon = 1.588$) was if the radius of gyration of the polymer scaled as $R_g \sim N^{\upsilon}$ throughout the translocation process. Any deviation from this scaling, either through the initial polymer configuration or polymer crowding at the exit of the nanopore (due to the translocation time being much shorter than the polymer relaxation time for large applied voltages), resulted in scaling exponents smaller than the theoretical prediction. Thus, for nanopore operation, the only way to obtain the theoretical value for the scaling exponent (thus making it trivial to determine

the polymer chain length from the measured translocation time) would be to use an applied voltage that allows the translocation time to be shorter than the polymer relaxation time. On the other hand, when the polymer length is on the same order as the pore length, a continuous scaling exponent did not exist, but rather increased as the length of the polymer increased, converging to the same value obtained in the short pore simulations for very long polymers. As discussed earlier, one of the drawbacks of using solid state nanopore devices in translocation measurements is the high rate at which the polymers flow through them when using an applied voltage [11,12,141] putting very demanding requirements on measurement equipment [22]. It was shown in previous experiments that it is possible to increase the translocation of DNA through silicon nitride nanopores, while keeping a good SNR[13], when increasing the viscosity of the solvent by adding glycerol. Hence, I studied the effects of increasing the solvent viscosity using my simulation methodology and found, whereas increasing the viscosity of the solvent increases the translocation time through the pore, it had no effect on the scaling exponent α due to the increase in polymer relaxation time. Thus, my findings indicate that decreasing the applied voltage, and not increasing the solvent viscosity, leads to the scaling exponent agreeing with the theoretical predictions. Finally, my simulation results for Rouse polymers shown in Figure 29 (a) (α = 1.44) are very similar to the measurement values obtained by Wanunu *et al.* [18] using a 4 nm wide, 10 nm thick SiN nanopore with ds-DNA chain lengths of 0.150–3.5 kbp (α = 1.40). These findings indicate that Rouse polymers may be appropriate for accurate modeling of polymer translocation through narrow nanopores due to polymer-pore interactions heavily

influencing the dynamics of the translocation process and weakening the effects of hydrodynamic interactions.

As a next objective, I investigated how hydrodynamic interactions (HI) affect the translocation process by studying Zimm polymer translocation through silicon nitride nanopores using the same two initial polymer configurations as in the Rouse polymer case. As mentioned before, most polymers behave as Zimm polymers in bulk solution [88–90] indicating hydrodynamic interactions are vital for any thorough investigation of polymer translocation through nanopores. In my simulation results, I found that not only do the secondary polymer-solvent interactions caused by HI decrease the translocation time from the Rouse polymer translocation, but also decrease the relaxation time for the Zimm polymer. This shorter relaxation time reduces polymer crowding at the exit of the nanopore resulting in scaling exponents that agree with theoretical predictions of $\alpha = 2\upsilon$ even at high voltages. For smaller voltages, the scaling exponent becomes larger, agreeing with intuition since the scaling exponent for unforced translocation is always larger than for forced translocation. In addition, as shown in Figure 31, the translocation time versus chain length scaling law (α) is 1.21, which agrees very well with experiments performed by Storm *et al.* [9,10] (α = 1.26 – 1.27) using a 10 nm-diameter SiO_2 nanopore. These findings indicate that for larger nanopores, due to weaker polymer-pore interactions, hydrodynamic interactions are more prominent than for narrow pores. Finally, just as was observed with Rouse polymers, I demonstrated that increasing the solvent viscosity will increase the translocation time, but have no effect on the scaling exponent α.

Not only did I study the effect of polymer length, but I also studied the scaling relationship between the translocation time and the applied voltage. For both Rouse and Zimm polymers, I obtained the theoretical scaling relationship of $\tau \sim V^{-1}$ [47], which has also been observed in experiments using very large nanopores (30 nm diameter)[14], for low to intermediate applied voltages. For much higher voltages, beginning at 500 mV, the scaling exponent was greater than -1. This change in scaling exponent is due to the extreme polymer crowding at the exit of the nanopore when using high applied voltages. Not surprising, the deviation from the theoretical scaling exponent was less in the Zimm polymer model due to the shorter relaxation time than the Rouse model. The importance of this finding is that this scaling relationship of $\tau \sim V^{-1}$ does not hold for all voltages further indicating that large applied voltages are responsible for extreme polymer crowding at the nanopore exit and deviations from theoretical derivations.

Whereas most translocation time laboratory experiments involve driving biopolymers through nanopores with an applied voltage, I investigated an equally important situation in which the applied voltage is absent, or unforced, translocation. In these simulations, I studied the effect on the polymer-pore interactions on the translocation time by varying the pore diameter. For very narrow pores, I found that for both the Rouse and Zimm polymer models, the translocation time scales as the Rouse relaxation time defined as the time required for a polymer to diffuse its radius of gyration, $\tau \sim N^{1+2\upsilon}$. This important result indicates that, even though hydrodynamic interactions are long ranged in bulk solution [91], the effects are screened for polymers moving near a wall or inside a channel [45,68,91]. And, as demonstrated in my simulation results, if the polymer-pore interactions are strong enough, HI affects are removed. Once the pore

diameter is increased, the polymer-pore interactions are weakened and the scaling exponent increases. When the pore is removed from the simulation results, the scaling law for both the Rouse and Zimm models converges to their polymer relaxation times, $\tau \sim N^{1+2\upsilon}$ and $\tau \sim N^{3\upsilon}$ respectively. These studies emphasize the importance of polymer-pore interactions on translocation time simulation studies. As stated earlier, if a universal scaling law is to be obtained, it is important that there must be a consistency of polymer-pore interactions between all theoretical and computational studies.

Finally, I conducted preliminary investigations of the effects of electrostatic interactions caused by the ions in the electrolytic solution and the charge on the surface of the silicon nitride nanopore, using the coupled Poisson-Nernst-Planck equations. I found that, due to the negative surface charge on the silicon nitride nanopore, there is a large positive valence ion build up on the pore surface which causes the potential to decrease to zero at small distances from the nanopore surfaces. In addition, the ionic concentration also decreases further away from the pore surface, and only reaches the bulk value for large nanopore diameters. Hence, an important result is that pore diameter greatly affects the ion concentration inside the pore. I also showed that, whereas uncharged monomers have little impact on the potential inside a nanopore, negatively charged monomers attract positive ions to the surface and thus change the ion distribution. Just as is the case for the pore surface, the cation buildup on the surface of the negatively charged monomers also reduces the potential at very short distances. These key findings indicate two important results. First, due to the high electrolytic concentration (1 M) and very short Debye length (~ 3 Å), the potential as a result of the surface charge of both the nanopore and polymer is largely screened even at very short

distances. Second, due to the buildup of ions on the surface of each monomer, which would indeed be the case for a charged biopolymer such as DNA, electro-osmotic forces could possibly have a large impact on the translocation process. The need for models that include electro-osmotic forces is discussed in the future works section of this thesis.

6.2 Related future works and challenges

6.2.1 Controlling DNA/Translocation Time Resolution

One of the current drawbacks to using nanopores in translocation time measurements is, due to polymer-pore interactions[18], random thermal forces, and interactions between solute and solvent molecules resulting in viscous drag forces, the time required for a particular DNA chain to pass through a solid state nanopore can vary widely from trial to trial making it difficult to know the exact length of the DNA chain, thus decreasing the sensitivity of the measurement [22]. In addition, as discussed earlier, another difficulty when using solid state nanopore devices is due to the high rate at which the polymers flow through them when using an applied voltage [11,12,141]. This high velocity requires measurement instruments to have detector bandwidth values in the MHz range which makes it very difficult to measure changes in current on a pico-ampere scale[22]. Hence, controlling DNA flow through nanopore devices would seem to be an important next step at arriving at a sequencing solution.

One possible way to reduce the stochasticity of the translocation process, thus improving the sensitivity of the DNA chain length measurement, is to control the DNA-nanopore interactions by changing the nanopore surface composition with either atomic layer deposition [16,142] or coating the surface with an organic material [143]. It was also shown in previous experiments that it is possible to decrease the translocation time

by a factor of 10 while keeping a good SNR[13] by decreasing the temperature of the measurement system, increasing the salt concentration, increasing the viscosity of the solvent by adding glycerol, and lowering the applied potential. Unfortunately, these steps also reduce the ionic current signal[13], which could cause potential problems when making more sensitive measurements.

Another method that could potentially be used to decrease the velocity of the DNA in a nanopore device is, instead of using DC applied potentials to facilitate translocation, use time varying, or AC, applied potentials. Intuitively, one can imagine that by using an AC stimulus, the DNA would remain in the nanopore for longer periods of time due to the oscillatory nature of the resultant electric field [39,43]. Finally, nanopores fabricated with different topologies such as p-n junctions [144–148] or stacked layers of metal and oxide materials [149,150] can be used to vary the electric field inside the nanopore thus either slowing down the DNA or trapping it for possible base by base measurements. Hence, computational investigations of each of the methods discussed above would be extremely helpful in determining if any of these are viable options for better controlling of DNA translocating through nanopore devices, before undertaking the difficult and costly experimental work required to build and measure these types of nanopore devices.

6.2.2 Polymer model improvement

Currently, most coarse-grained simulation methodologies, including the ones presented in this work, use the combination of the FENE [99] (Equation (2-2)) and the WCA [100] (Equation (2-3)) potential energy functions to model a polymer with high excluded volume interactions as would be seen in a good solvent conditions. As I stated

before, because of the abrupt cutoff in the WCA potential when the distance of the non-adjacent monomers is greater than $2^{1/6}\sigma$, the 'equilibrium' (or steady-state) polymer configuration is very different than the minimum energy state. And, as I showed in Chapter 4, translocation time versus chain length scaling exponents, α, vary differently depending upon the configuration of the polymer. One way to remove this potential discrepancy source would be to simply add a bond-angle potential to the potential energy function [98]. However, because of the parabolic nature of this potential energy function and the requirement to keep the bond stiff to ensure a polymer with high excluded volume interactions, resulting in a large spring constant, a small simulation time step would be required thus limiting both the overall simulation time and the number of monomers in the simulation.

Another limitation to this FENE-WCA polymer model is the lack of full characterization of the different physical effects seen in translocation time measurements. For example, in the experiments performed using a 4 nm diameter SiN pore, by Wanunu *et al* [18] observed a crossover behavior with a scaling law exponent of $\alpha = 1.4$ for ds-DNA between 150 - 3500 bp and $\alpha = 2.28$ for longer chains. This larger scaling exponent was hypothesized to be due to the polymer interacting with the SiN membrane outside the pore, which has not been observed in the literature in any coarse-grained simulation studies. One possible reason for this is computational limitations that bead-spring polymer models present due to the required small time step needed to keep the configuration stable. In addition, unlike what is demonstrated from the simulation results shown in Figures 24, 26, and 34, and experiments using very large nanopores (30 nm diameter)[14], both of which agree with predictions [47] of $\tau \sim V^{-1}$, Wanunu *et al.* [18]

obtained experimentally an exponential relationship for translocation time versus voltage. One possible cause for this exponential relationship between the voltage and the translocation time that is seen for smaller diameter pores could be related to the higher entropic barrier that must be overcome in order for the polymer to translocate through the pore[30]. Again, this exponential scaling relationship has also not been observed using the FENE-WCA polymer model. One possible reason for this is due to the lack of a bond-angle potential term in the potential energy which would limit the number of configurations the polymer can achieve thus increasing the entropy barrier. However, as stated before, using a bond-angle potential would limit the time step, and thus not only the number of monomers used in a simulation study, but also the overall simulation duration.

Hence, whereas the FENE-WCA model does a good job in modeling many of the properties of polymers in good solvent conditions, there are some improvements that are needed in order to fully model all aspects of translocation through solid-state nanopores. This new model must address the issues stated above while also permitting the use of high time steps and longer simulation durations and chain lengths which would allow for simulations to more accurately model translocation time measurements.

6.2.3 Electro-osmotic Force Modeling

Another improvement that needs to be addressed more thoroughly in translocation time simulation studies is the effect of electro-osmotic forces. Recent computational studies have hypothesized that drag forces due to electro-osmotic flow inside a nanopore are much more significant that hydrodynamic forces acting on the DNA “blob” outside the nanopore when driven with an applied voltage [137]. If laminar flow similar to a pipe

is assumed in nanopores, then narrow pores should have stronger electro-osmotic forces than wider pores. If so, this may explain why the scaling law in the studies of Wanunu *et al.* [18] using 4 nm pores are much more different than those observed by Storm *et al.* [9] in larger (10 nm) pore studies.

In addition, it has also been hypothesized using computational studies that the direction of electro-osmotic forces is dependent on the surface charge of the nanopore [138]. If the surface charge of the nanopore has the opposite charge of the polymer flowing through it, the electro-osmotic flow is in the same direction as translocation and vice versa. Hence, electro-osmotic forces can either hinder or assist in the translocation process. In the latter, when the flow is in the same direction as translocation, the electro-osmotic forces have been hypothesized to stretch the polymer and thus reduce the entropic barrier required for translocation [138].

Most, if not all, of the current simulation methodologies do not include the effects of electro-osmotic forces. Whereas computational studies state electro-osmotic forces do contribute to the overall drag involved in a translocation time simulation, there is no studies to indicate how electro-osmotic forces may contribute to the scaling exponent α. Hence, future simulation methodologies could include electro-osmotic effects in order to study their impact on α.

6.2.4 Electrostatic Interactions

In many of the translocation time computational studies including the one presented in this thesis[127,131,144–146,151], the electrostatic effects are computed assuming the ions are treated as a continuum either through the Poisson-Boltzmann (PB) or Poisson-Nernst-Planck (PNP) equations. Whereas the continuum models reduce

computational requirements for a solution, there are some approximations made that could be improved upon in order to obtain a more accurate model. For example, when treating the electrolytic solution as a continuum, there is no associated size with each ion, thus steric effects are omitted. This could lead to extremely high, and unrealistic, ion concentrations at charged surfaces (although I did not observe this in my simulation results shown in Chapters 2 and 5). There have been studies which have modified the PB or the PNP equations to include steric effects[152–154]. However, a computationally efficient finite-difference algorithm for both the PB and PNP equations that includes steric effects has yet to be fully developed and tested. Such an algorithm would be very beneficial in studying electrostatic effects in nanopore simulations.

Another limitation of using a continuum method, such as the PNP mean field theory approximation, to model the electrostatics in a nanopore simulation, is the assumption that each ion has a zero self-energy. This self-energy term, which has been shown to be important in ion channel modeling, arises when a charge induces an image charge at a dielectric boundary resulting in a repulsive energy that scales as ~ q^2 [128]. This repulsive energy term limits ion flow into a channel. An approximation to the change in self energy when moving from an area of dielectric constant ε_{R1} to an area with dielectric constant ε_{R2} can be found from [155]:

$$\Delta U_{self} = \frac{q^2}{8\pi\varepsilon_o \mathrm{a}}\left(\frac{1}{\varepsilon_{R1}} - \frac{1}{\varepsilon_{R2}}\right) \tag{6-1}$$

where a is the ion radius and ε_o is the permittivity of free space. Because continuum models do not compute discrete ion-ion interactions, this self-energy term is zero. However, it has been shown using Brownian Dynamics (BD) simulations to model ion flow through channels that the solution to continuum methods such as the Poisson-Nernst-Planck and Poisson-Boltzmann converges to the BD results when the radius of the ion channel is 2 Debye lengths or greater [128–130]. In the simulations reported in thesis as well as most translocation time measurements, a 1 M solution is used as the electrolyte resulting in an approximate Debye length of 3 Å. In other words, in order to accurately omit the self-energy term, the radius of a pore must be at least 6 Å. Hence, another way to improve upon the electrostatic modeling would be to include self-energy terms that limit the amount of ions that are present in nanopores, especially those with small diameters.

APPENDIX

A.1 Fraenkel and FENE-WCA bead-spring models

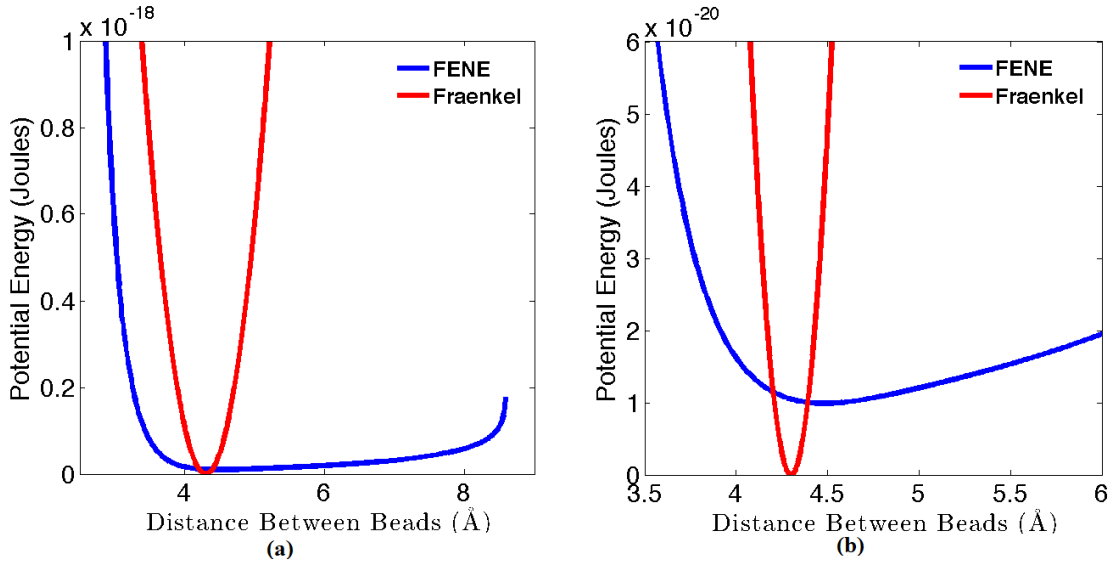

Figure 61 Potential energy curves for both the Fraenkel (red) and FENE (blue) spring models. (a) Expanded Curve (b) Focused at Minimum Energy Distance.

As shown in Figure 61 (b), for the polymer model parameters described in Chapter 2, the minimum energy point for the Fraenkel model is 4.3 Å, whereas the minimum energy point for the FENE-WCA model is 4.48 Å. The two graphs above indicate there are several differences between the Fraenkel and FENE-WCA models. For example, the Fraenkel model has a sharper potential energy curve indicating that it possesses stronger bead-to-bead forces and higher vibrational frequencies than the FENE-WCA model. In addition, the Fraenkel model has a continuous potential energy curve and is infinitely expandable. The FENE-WCA spring model, on the other hand, has a singularity in it its potential energy function at R_o (8.3 Å in Figure 61(a) above) indicating a finite bead-to-bead distance that it can reach[156]. It is interesting to note

that, upon comparison, the force-extension curve for DNA more resembles the FENE-WCA spring model than the Fraenkel model[156,157]. In reality, DNA, just like the FENE-WCA spring model, has a finite distance to which it can be extended to[157]. However, many other research simulation projects choose to use the Fraenkel model as a way to model bead-to-bead interactions[98,127,158] and, to increase the flexibility of my code, I choose to incorporate this model as well.

A.2 Metropolis Monte Carlo (MMC) simulation flow chart

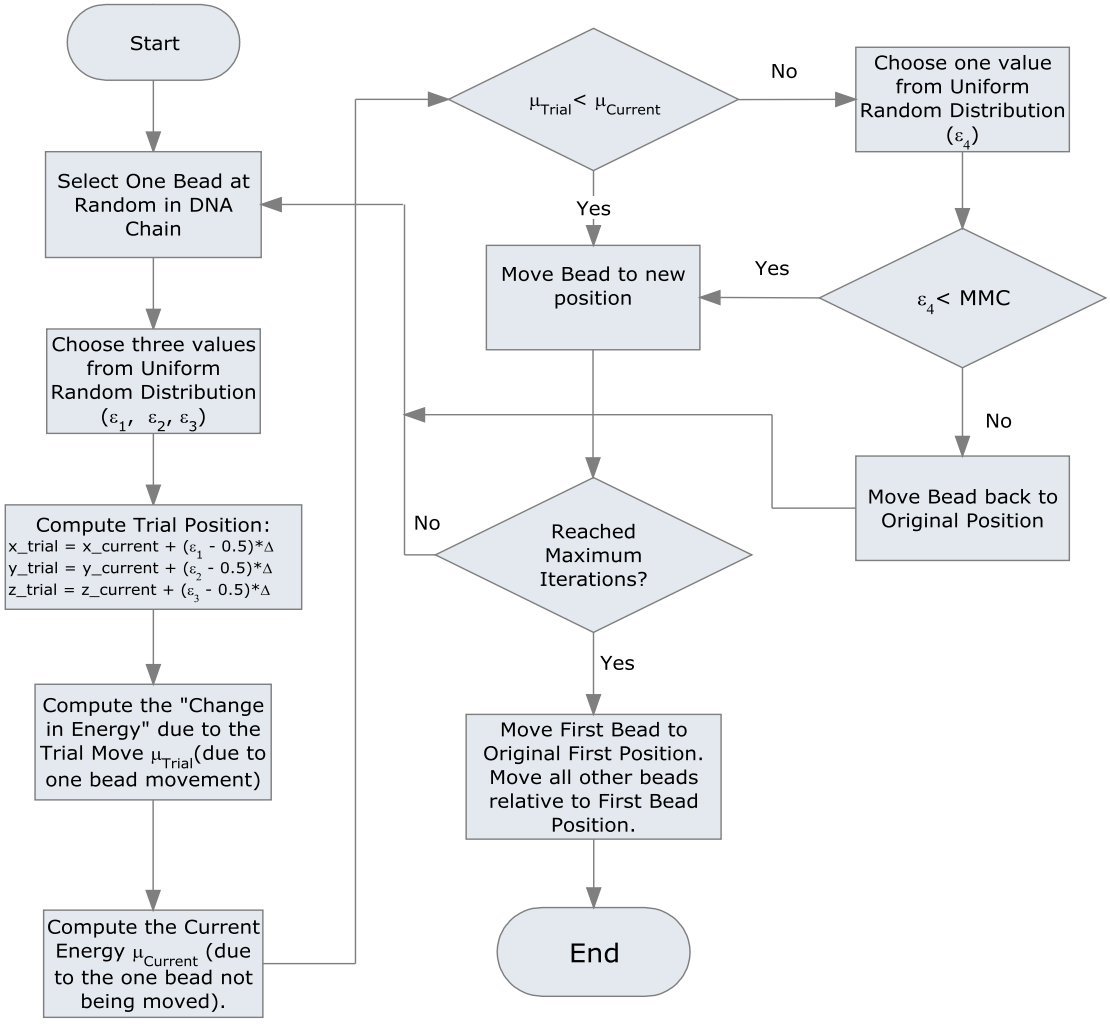

Figure 62: Metropolis Monte Carlo (MMC) simulation flow chart

As was described both in Chapters 4 and 5, in some instances, before a translocation time simulation was performed, the Metropolis Monte Carlo (MMC) simulation was carried out[118] for 50,000 trials so as to place the polymer in its minimum energy state. I describe here the MMC procedure, using the flow chart in Figure 62 as a guide for understanding.

First, one bead (or monomer) is selected at random from the polymer chain. Next, three values (ε_1, ε_2, and ε_3) are randomly selected from a uniform distribution between 0 and 1. Next, using the random values above, the x coordinate, y coordinate, and z coordinate of the randomly selected monomer are changed to:

$$\text{x\_trial} = \text{x\_current} + (\varepsilon_1 - 0.5)\Delta \tag{A-1}$$

$$\text{y\_trial} = \text{y\_current} + (\varepsilon_2 - 0.5)\Delta \tag{A-2}$$

$$\text{z\_trial} = \text{z\_current} + (\varepsilon_3 - 0.5)\Delta \tag{A-3}$$

where x_current, y_current, and z_current are the current x, y, and z coordinates of the monomer and Δ is a fixed parameter that scales how much the trial move will be. Through extensive trial testing I arrived at a value of $\Delta = 0.15$.

Next, the energy is computed for both the polymer in its original state, $\mu_{Current}$, and the polymer after the trial move, $\mu_{Trial.}$ If the new energy value is smaller than the current energy value ($\mu_{Trial.} < \mu_{Current}$), then the move is always accepted and the bead is moved to its new position. On the other hand, if the new energy is larger than the current energy ($\mu_{Trial.} > \mu_{Current}$) then the move is accepted with probability:

$$P(Accept) = e^{-\frac{(\mu_{Trial} - \mu_{Current})}{kT}} \tag{A-4}$$

This is done by first selecting another random value from a uniform distribution between 0 and 1, ε_4. Then, if ε_4 is smaller than the result computed from equation A-4, the move will be accepted. If not, the move will be rejected and the bead will be placed back to its original position.

During the procedure, the beads are free to move anywhere in the simulation volume. However, once the procedure is completed, the first bead must be placed inside the nanopore to begin the simulation. Hence, at the conclusion of the MMC procedure, the first monomer is moved to its new position inside the nanopore and all other monomers are moved relative to the first monomer position keeping the polymer in its minimum energy state.

Table 1 below provides the final bead-to-bead distance for MMC simulation using 10 beads with initial distance (5 Å) different than equilibrium value (4.3 Å) using Fraenkel spring model. As shown, the final bead-to-bead distance is very similar to the equilibrium value.

Table 1: Simulation data from MMC simulation using 10 bead polymer incorporating Fraenkel spring model.

Bead Positions	Initial Distance (Å)	Final Distance (Å)	Equilibrium Distance (Å)	Percent Difference (%)
1-2	5	4.23	4.3	1.72
2-3	5	4.39	4.3	2.11
3-4	5	4.25	4.3	1.26
4-5	5	4.30	4.3	0.09
5-6	5	4.31	4.3	0.28
6-7	5	4.25	4.3	1.18
7-8	5	4.24	4.3	1.30
8-9	5	4.27	4.3	0.75
9-10	5	4.33	4.3	0.61

Table 2 below tabulates the final bead-to-bead distance for MMC simulation using 10 beads with initial distance (3 Å) different than equilibrium value (4.48 Å) using FENE spring model. As shown, the final bead-to-bead distance is very similar to the equilibrium value with the exception of distance between beads 4 and 5. In addition, the percent differences are higher than those produced by the Fraenkel spring model. This is probably due to the fact that, as shown in Figure 61, the potential energy function is much more rigid for the Fraenkel model than the FENE model. And, as indicated in Figure 9(b), the accepted probability graph for the FENE model is much broader than the Fraenkel model indicating large displacement distances from the minimum (4.48 Å) will still result in small energy values.

Table 2: Simulation data from MMC simulation using 10 bead polymer incorporating FENE spring model.

Bead Positions	Initial Distance (Å)	Final Distance (Å)	Equilibrium Distance (Å)	Percent Difference (%)
1-2	3	4.54	4.48	1.24
2-3	3	4.39	4.48	2.03
3-4	3	4.64	4.48	3.57
4-5	3	5.29	4.48	18.07
5-6	3	4.54	4.48	1.40
6-7	3	4.39	4.48	2.12
7-8	3	4.21	4.48	6.10
8-9	3	4.35	4.48	2.85
9-10	3	4.53	4.48	1.06

A.3 Integration Time Step

As mentioned before the integration time step, Δt, used in my simulations was chosen to be 0.1 psec for the Velocity Verlet and Langevin Dynamics integrators and 0.05 psec for the Brownian Dynamics integrator. To arrive at these times step values, I first estimated the frequency of oscillation of each monomer for both the Fraenkel and the FENE-WCA models. By first noting the frequency of oscillation of a spring can be found using the formula:

$$f = \frac{1}{2\pi}\sqrt{\frac{k}{m}} \tag{A-5}$$

where f is the frequency in Hz, k is the spring constant, and m is the mass of each monomer. Using the parameters provided earlier for the Fraenkel model, and estimating that, using the Nyquist criterion which states the sampling time (or time step) should be twice the highest frequency of interest, I obtain a time step of approximately 0.2 psec.

Using the Nyquist criteria and Equation (A-5) for the FENE spring model, I obtained a time step of approximately 3.7 psec. This higher time step makes the FENE model more attractive than the Fraenkel. On the other hand, the spring constant for the WCA model also needs to be computed, which I estimated as the second derivative of Equation (2-3) and found to be:

$$f_{WCA} = \frac{24\varepsilon}{r^2}\left[26\left(\frac{\sigma}{r}\right)^2 - 7\left(\frac{\sigma}{r}\right)^6\right] \quad \text{(A-6)}$$

Using the polymer values for the WCA model provided earlier in Chapter 2, and setting r = 4.48 Å (which is the minimum distance between monomers) I obtained a time step of approximately 0.998 psec. If the Nyquist criterion is used for the combination of the FENE-WCA spring model, then the sample rate (or time step) must be at least twice the highest frequency of the two, hence the overall time step is estimated to be 0.998 psec.

Hence, it appears that the time steps used in these simulations (0.1 psec and 0.05 psec) are much smaller than the estimated time steps from the formulas above. However, it should be noted that not only is there a time step associated with the polymer-polymer interactions, but there also is a time step associated with the polymer-pore interactions as well. In fact, more often than not, when I tried to increase the time step above 0.1 psec, the polymer chains would break apart inside the nanopore and thus the simulation would fail. In addition, increasing the time step above 0.1 psec in simulations using the Velocity Verlet algorithm would not meet the conservation of energy requirement. Finally, as shown in the extensive testing that I performed, my simulation results match very well with the theoretical values for Rouse polymers.

When performing Brownian dynamics simulations using the TEA algorithm, I noticed a higher fail rate (i.e. polymer chains breaking apart) for polymer translocation through nanopores using a time step of 0.1 psec. When decreasing the time step to 0.05

psec, I obtained a higher success rate for translocation process. As a result, this is the integration time step used in my simulations. As shown in Table 3, I did a comparison for the diffusion coefficient of one monomer with a diameter of 4.3 Å using different time steps and obtained approximately the same value which all agreed very well with the theoretical value. Finally, just as in the Langevin dynamics integration algorithm, as shown in the extensive testing that I performed, the simulation results match very well with the theoretical values for both Rouse and Zimm polymers.

Table 3: Diffusion Coefficient vs. Time Step for one monomer with diameter 4.3 Å.

Time Step (psec)	Theoretical D (cm^2/sec)	Simulation D (cm^2/sec)	Percent Difference
0.1	1.015E-5	0.9675E-5	4.79
0.05	1.015E-5	0.9977E-5	1.72
0.01	1.015E-5	0.9879E-5	2.71

A.4 PNP Convergence

In order to ensure the PNP solutions converged to an accurate solution, the simulations were first performed for 300,000 trials using the Successive Over-Relaxation (SOR) method[123,124] initially, but then reduced to 200,000 trials because the solution had converged at that point. To obtain the final simulation result for the dielectric slabs given in Figures 14 - 17, I first performed simulations with a charged dielectric slab with no ions present, using an initial condition of 0 volts throughout the simulation volume. After this simulation was completed, I used these results (Figure 13) as the initial condition of my next simulation which I included the electrolyte solution. In this

simulation, I assumed an equal concentration of 1 M throughout the simulation volume. Although this was probably not a good initial guess, the solutions did converge to a final solution as shown in Figures 64 - 66.

Figure 63 provides a plot of the RMS error versus the SOR trial for the potential, and the ion concentration of both the positive valence and negative valence ions. As shown, the simulations are converging with the RMS error reaching a minimum value around 200,000 trials. Figure 64 shows the positive valence ionic concentration as a function of SOR iteration as a function of z, with both x and y = 50 Å (because of the dielectric slab being used, the solution is symmetric and the same for all x and y values) using a 50 Å slab. As shown, in Figure 64 (a) the ionic concentration at first oscillates to higher and lower values, but later converges to a final value at around 200,000 trials. Because this is a dielectric slab, the concentration is zero inside the slab (between z = 275 and z = 325). Similar results for the negative valence ion are provided in Figure 65.

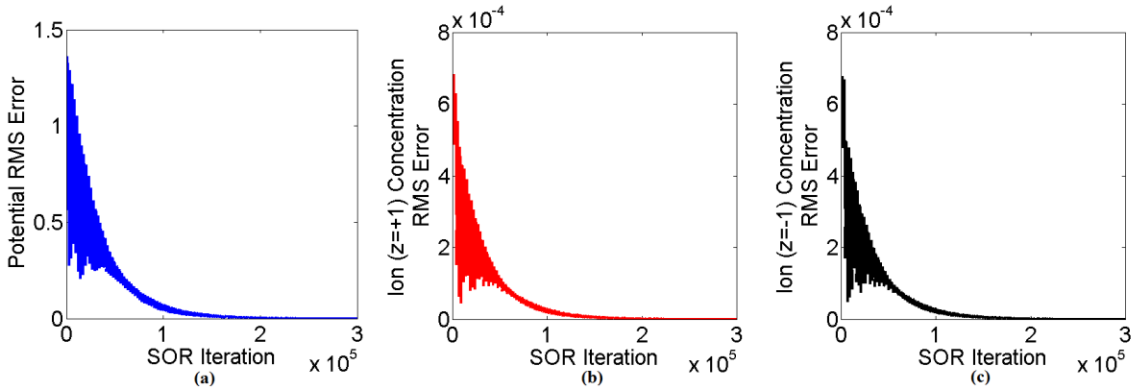

Figure 63: RMS Error versus SOR Iteration for 300,000 trials for (a) potential, (b) positive valence ion, and (c) negative valence ion.

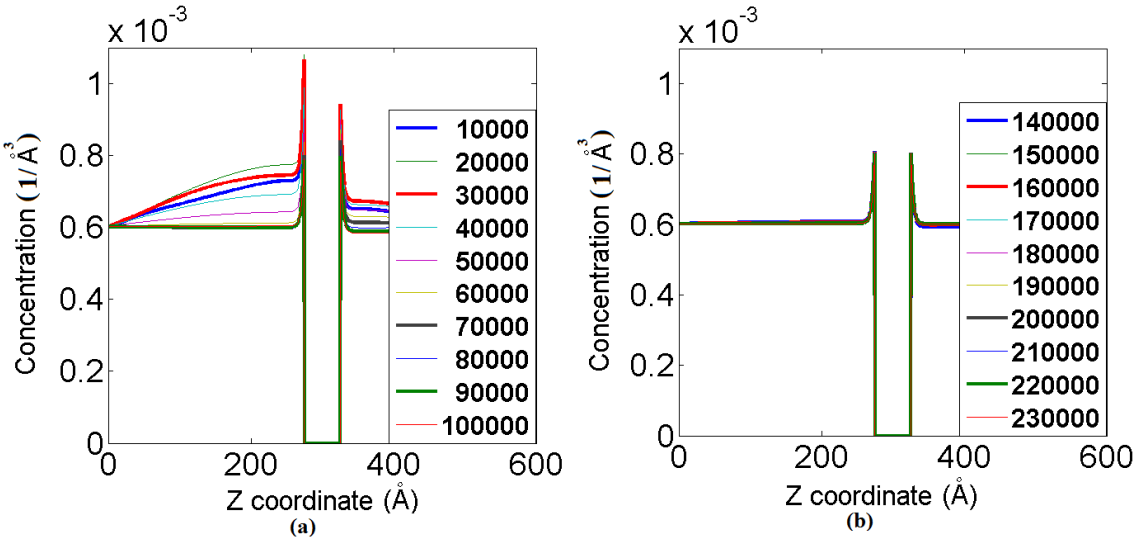

Figure 64: Ionic concentration of positive valence ion versus z for maximum SOR trials of: (a) 100,000 and (b) 230,000 trials using 50 Å dielectric slab with both x and y = 50 Å.

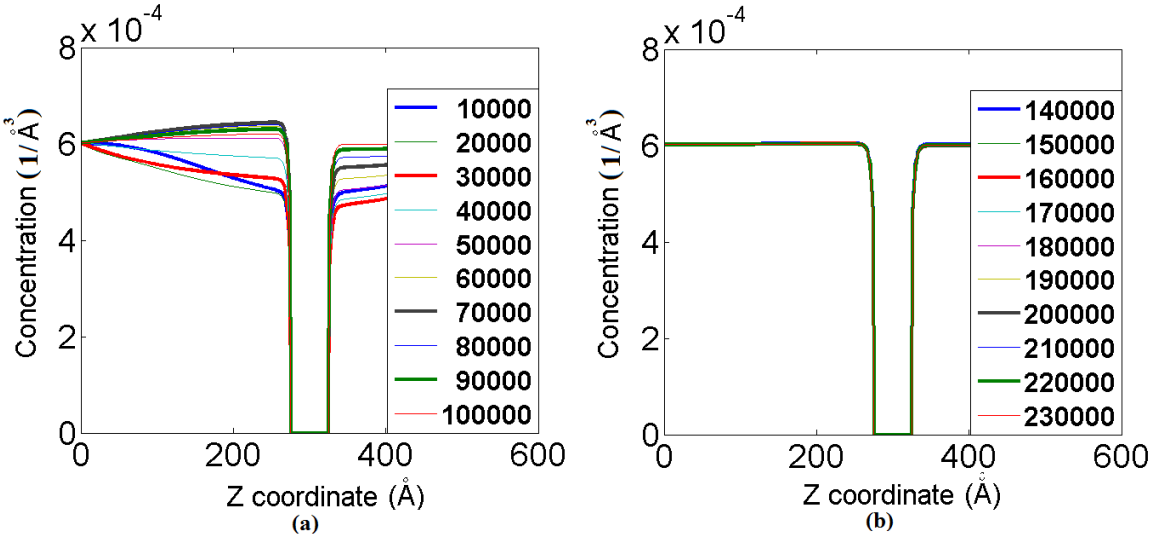

Figure 65: Ionic concentration of negative valence ion versus z for maximum SOR trials of: (a) 100,000 and (b) 230,000 trials using 50 Å dielectric slab with both x and y = 50 Å.

Figure 66 shows the calculated potential as a function of SOR iteration as a function of z, with both x and y = 50 Å. Just as in Figures 64 and 65, the potential at first oscillates to lower and higher values before reaching a steady-state value around 200,000 trials. The final slab simulations were then used as the initial conditions for the pore simulations given in Chapter 5, each using 200,000 SOR trials to compute the final solution.

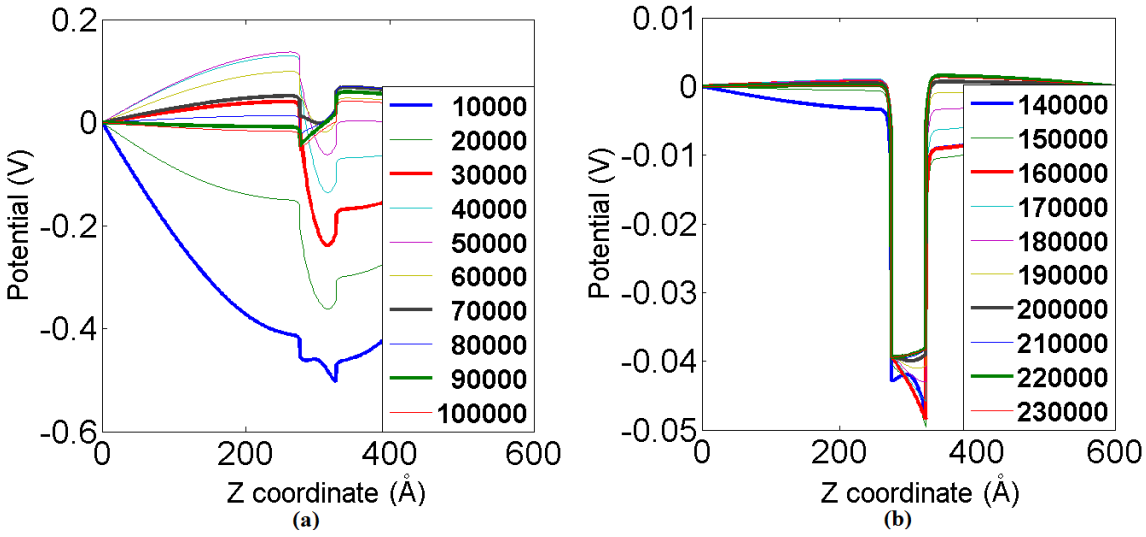

Figure 66: Potential versus z for maximum SOR trials of: (a) 100,000 and (b) 230,000 trials using 50 Å dielectric slab with both x and y = 50 Å.

A.5 Electric Field Calculations

As described earlier, the electric field is computed using the following difference formula:

$$\vec{E}_{x,IJK} = \frac{\phi_{I+1JK} - \phi_{I-1JK}}{2\Delta x} \tag{A-7}$$

This formula is valid for everywhere except where the Dirichlet boundary conditions are applied, which are at z = 0 and z = 600 Å. To compute the field at z = 0, a forward numerical difference formula is used given by Equation (A-8)[124], whereas to compute the field at z = 600 Å, a backward numerical difference formula is used given by Equation (A-9)[124].

$$\vec{E}_K = -\frac{-11\phi_K + 18\phi_{K+1} - 9\phi_{K+2} + 2\phi_{K+3}}{6\Delta x} \tag{A-8}$$

$$\vec{E}_K = -\frac{-2\phi_{K-3} + 9\phi_{K-2} - 18\phi_{K-1} + 11\phi_K}{6\Delta x} \tag{A-9}$$

A.6 Trilinear Interpolation Method

As described earlier, the potential and ionic concentrations are computed using the coupled PNP equations on a 1 Å x 1 Å x 1 Å grid in the simulation volume. From this potential, the electric field and resultant force can be obtained. Even though the potential is computed on a grid, the monomer is permitted to travel at any point in the simulation

volume. In order to compute the electric field on each monomer between grid points, first, the electric field is computed at the eight nearest grid points to the monomer using Equations (A-7) – (A-9) above. Then, a trilinear interpolation method, as discussed by Kang [126], is used to compute the electric field at the position of the monomer. The trilinear interpolation method, given the values of all eight vertices on a cube (Figure (67)), computes the value of a quantity *p* at a point x, y, and z, using equations (A-10 – A-21)[126]:

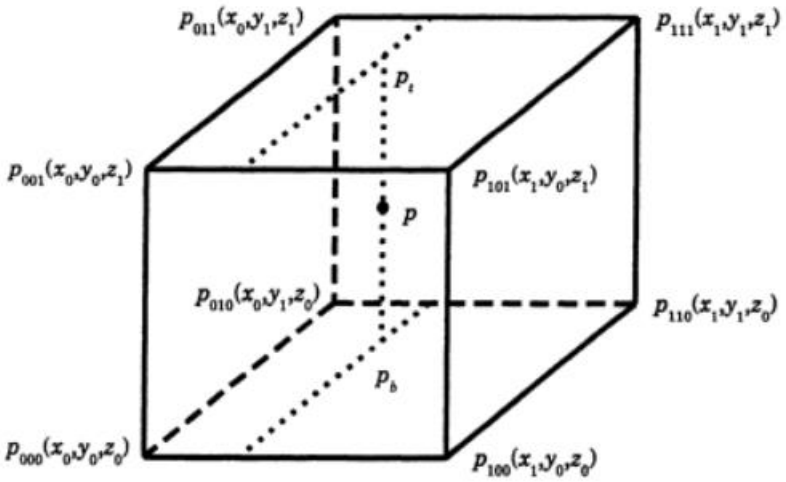

Figure 67: Trilinear interpolation method, as discussed by Kang [126], used to compute the electric field at the center of each monomer. The electric field is first found at all eight vertices on a cube that contains the monomer. Then, equations (A-10 – A-21) are used to find the electric field at the desired x, y, and z point.

$$p(x,y,z) = c_o + c_1\Delta x + c_2\Delta y + c_3\Delta z + c_4\Delta x\Delta y + c_5\Delta x\Delta z + c_6\Delta y\Delta z + c_7\Delta x\Delta y\Delta z \tag{A-10}$$

$$\Delta x = x - x_0 \tag{A-11}$$

$$\Delta y = y - y_0 \tag{A-12}$$

$$\Delta z = z - z_0 \tag{A-13}$$

$$c_0 = p_{000} \tag{A-14}$$

$$c_1 = \frac{p_{100} - p_{000}}{x_1 - x_0} \tag{A-15}$$

$$c_2 = \frac{p_{010} - p_{000}}{y_1 - y_0} \tag{A-16}$$

$$c_3 = \frac{p_{001} - p_{000}}{z_1 - z_0} \tag{A-17}$$

$$c_4 = \frac{p_{110} - p_{010} - p_{100} + p_{000}}{(x_1 - x_0)(y_1 - y_0)} \tag{A-18}$$

$$c_5 = \frac{p_{101} - p_{001} - p_{100} + p_{000}}{(x_1 - x_0)(z_1 - z_0)} \quad \text{(A-19)}$$

$$c_6 = \frac{p_{011} - p_{001} - p_{010} + p_{000}}{(y_1 - y_0)(z_1 - z_0)} \quad \text{(A-20)}$$

$$c_7 = \frac{p_{111} - p_{011} - p_{101} - p_{110} + p_{100} + p_{001} + p_{010} - p_{000}}{(x_1 - x_0)(y_1 - y_0)(z_1 - z_0)} \quad \text{(A-21)}$$

REFERENCES

[1] A. Milchev, Single-polymer dynamics under constraints: scaling theory and computer experiment, J. Phys. Condens. Matter. 23 (2011) 103101.

[2] J.J. Nakane, M. Akeson, A. Marziali, Nanopore sensors for nucleic acid analysis, J. Phys. Condens. Matter. 15 (2003) R1365–R1393.

[3] A. Meller, L. Nivon, E. Brandin, J. Golovchenko, D. Branton, Rapid nanopore discrimination between single polynucleotide molecules, Proc. Natl. Acad. Sci. U. S. A. 97 (2000) 1079–1084.

[4] M. Muthukumar, Mechanism of DNA Transport Through Pores, Annu. Rev. Biophys. Biomol. Struct. 36 (2007) 435–450.

[5] A. Meller, Dynamics of polynucleotide transport through nanometre-scale pores, J. Phys. Condens. Matter. 15 (2003) R581–R607.

[6] R.S.S. de Zoysa, D.A. Jayawardhana, Q. Zhao, D. Wang, D.W. Armstrong, X. Guan, Slowing DNA Translocation through Nanopores Using a Solution Containing Organic Salts, J. Phys. Chem. B. 113 (2009) 13332–13336.

[7] H. Chang, F. Kosari, G. Andreadakis, M.A. Alam, G. Vasmatzis, R. Bashir, DNA-Mediated Fluctuations in Ionic Current through Silicon Oxide Nanopore Channels, Nano Lett. 4 (2004) 1551–1556.

[8] S.M. Iqbal, D. Akin, R. Bashir, Solid-state nanopore channels with DNA selectivity, Nat. Nanotechnol. 2 (2007) 243–248.

[9] A.J. Storm, C. Storm, J. Chen, H. Zandbergen, J.-F. Joanny, C. Dekker, Fast DNA Translocation through a Solid-State Nanopore, Nano Lett. 5 (2005) 1193–1197.

[10] A.J. Storm, J.H. Chen, H.W. Zandbergen, C. Dekker, Translocation of double-strand DNA through a silicon oxide nanopore, Phys. Rev. E. 71 (2005) 051903.

[11] J. Li, M. Gershow, D. Stein, E. Brandin, J.A. Golovchenko, DNA molecules and configurations in a solid-state nanopore microscope, Nat Mater. 2 (2003) 611–615.

[12] D. Fologea, M. Gershow, B. Ledden, D.S. McNabb, J.A. Golovchenko, J. Li, Detecting Single Stranded DNA with a Solid State Nanopore, Nano Lett. 5 (2005) 1905–1909.

[13] D. Fologea, J. Uplinger, B. Thomas, D.S. McNabb, J. Li, Slowing DNA Translocation in a Solid-State Nanopore, Nano Lett. 5 (2005) 1734–1737.

[14] S.W. Kowalczyk, A.R. Hall, C. Dekker, Detection of Local Protein Structures along DNA Using Solid-State Nanopores, Nano Lett. 10 (2010) 324–328.

[15] S.W. Kowalczyk, M.W. Tuijtel, S.P. Donkers, C. Dekker, Unraveling Single-Stranded DNA in a Solid-State Nanopore, Nano Lett. (0).

[16] A.G. Ahmadi, Z. Peng, P.J. Hesketh, S. Nair, Wafer-scale process for fabricating arrays of nanopore devices, J. MicroNanolithography MEMS MOEMS. 9 (2010) 033011.

[17] D. Fologea, E. Brandin, J. Uplinger, D. Branton, J. Li, DNA conformation and base number simultaneously determined in a nanopore, ELECTROPHORESIS. 28 (2007) 3186–3192.

[18] M. Wanunu, J. Sutin, B. McNally, A. Chow, A. Meller, DNA Translocation Governed by Interactions with Solid-State Nanopores, Biophys. J. 95 (2008) 4716–4725.

[19] U.F. Keyser, B.N. Koeleman, S. van Dorp, D. Krapf, R.M.M. Smeets, S.G. Lemay, et al., Direct force measurements on DNA in a solid-state nanopore, Nat Phys. 2 (2006) 473–477.
[20] M. Wanunu, T. Dadosh, V. Ray, J. Jin, L. McReynolds, M. Drndić, Rapid electronic detection of probe-specific microRNAs using thin nanopore sensors, Nat. Nanotechnol. 5 (2010) 807–814.
[21] A.G. Ahmadi, S. Nair, Engineered Nanopores, in: P.J. Hesketh (Ed.), BioNanoFluidic MEMS, 2008: pp. 233–250.
[22] D. Branton, D.W. Deamer, A. Marziali, H. Bayley, S.A. Benner, T. Butler, et al., The potential and challenges of nanopore sequencing, Nat. Biotechnol. 26 (2008) 1146–1153.
[23] 2013 Release: NHGRI celebrates 10th anniversary of the Human Genome Project. www.genome.gov. National Human Genome Research Institute, 12 April 2013. Web. 19 August 2013.
[24] G. Kolata, The Human Genome Project, Then and Now. www.nytimes.com. The New York Times, 15 April 2013. Web. 19 August 2013.
[25] C. Dekker, Solid-state nanopores, Nat Nano. 2 (2007) 209–215.
[26] M. Wanunu, G.V. Soni, A. Meller, Single-Molecule Studies of Nucleic Acid Interactions Using Nanopores, in: P. Hinterdorfer, A.V. Oijen (Eds.), Handb. Single-Mol. Biophys., Springer, 2009: pp. 265–291.
[27] B.M. Venkatesan, R. Bashir, Nanopore sensors for nucleic acid analysis, Nat. Nanotechnol. 6 (2011) 615–624.
[28] D. Stoddart, A.J. Heron, E. Mikhailova, G. Maglia, H. Bayley, Single-nucleotide discrimination in immobilized DNA oligonucleotides with a biological nanopore, Proc. Natl. Acad. Sci. 106 (2009) 7702–7707.
[29] K. Healy, Nanopore-based single-molecule DNA analysis, Nanomed. 2 (2007) 459–481.
[30] M. Wanunu, Nanopores: A journey towards DNA sequencing, Phys. Life Rev. 9 (2012) 125–158.
[31] E.A. Manrao, I.M. Derrington, A.H. Laszlo, K.W. Langford, M.K. Hopper, N. Gillgren, et al., Reading DNA at single-nucleotide resolution with a mutant MspA nanopore and phi29 DNA polymerase, Nat. Biotechnol. 30 (2012) 349–353.
[32] M. Faller, The Structure of a Mycobacterial Outer-Membrane Channel, Science. 303 (2004) 1189–1192.
[33] N. Patterson, D.P. Adams, V.C. Hodges, M.J. Vasile, J.R. Michael, P.G. Kotula, Controlled fabrication of nanopores using a direct focused ion beam approach with back face particle detection, Nanotechnology. 19 (2008) 235304.
[34] S. Yue, C. Gu, Nanopores fabricated by focused ion beam milling technology, in: Nanotechnol. 2007 IEEE-NANO 2007 7th IEEE Conf., 2007: pp. 628–631.
[35] R. Kox, C. Chen, G. Maes, L. Lagae, G. Borghs, Shrinking solid-state nanopores using electron-beam-induced deposition, Nanotechnology. 20 (2009) 115302.
[36] A. Radenovic, E. Trepagnier, R. Csencsits, K.H. Downing, J. Liphardt, Fabrication of 10 nm diameter hydrocarbon nanopores, Appl. Phys. Lett. 93 (2008) 183101.
[37] D. Krapf, M.-Y. Wu, R.M.M. Smeets, H.W. Zandbergen, C. Dekker, S.G. Lemay, Fabrication and Characterization of Nanopore-Based Electrodes with Radii down to 2 nm, Nano Lett. 6 (2006) 105–109.

[38] A.P. Ivanov, E. Instuli, C. McGilvery, G. Baldwin, D.W. McComb, T. Albrecht, et al., DNA Tunneling Detector Embedded in a Nanopore, Nano Lett. (2011).
[39] S. Bhattacharya, S. Nair, A. Chatterjee, An Accurate DNA Sensing and Diagnosis Methodology Using Fabricated Silicon Nanopores, IEEE Trans. Circuits Syst. Regul. Pap. 53 (2006) 2377–2383.
[40] J.B. Heng, A. Aksimentiev, C. Ho, P. Marks, Y.V. Grinkova, S. Sligar, et al., Stretching DNA Using the Electric Field in a Synthetic Nanopore, Nano Lett. 5 (2005) 1883–1888.
[41] C. Ho, R. Qiao, J.B. Heng, A. Chatterjee, R.J. Timp, N.R. Aluru, et al., Electrolytic transport through a synthetic nanometer-diameter pore, Proc. Natl. Acad. Sci. U. S. A. 102 (2005) 10445–10450.
[42] A. Aksimentiev, J.B. Heng, G. Timp, K. Schulten, Microscopic Kinetics of DNA Translocation through Synthetic Nanopores, Biophys. J. 87 (2004) 2086–2097.
[43] G. Sigalov, J. Comer, G. Timp, A. Aksimentiev, Detection of DNA Sequences Using an Alternating Electric Field in a Nanopore Capacitor, Nano Lett. 8 (2008) 56–63.
[44] J. Heng, The Electromechanics of DNA in a Synthetic Nanopore, Biophys. J. 90 (2006) 1098–1106.
[45] J. Chuang, Y. Kantor, M. Kardar, Anomalous dynamics of translocation, Phys. Rev. E. 65 (2001) 011802.
[46] D. Panja, G.T. Barkema, R.C. Ball, Anomalous dynamics of unbiased polymer translocation through a narrow pore, J. Phys. Condens. Matter. 19 (2007) 432202.
[47] Y. Kantor, M. Kardar, Anomalous dynamics of forced translocation, Phys. Rev. E. 69 (2004) 021806.
[48] H. Vocks, D. Panja, G. Barkema, R. Ball, Pore-blockade times for field-driven polymer translocation, J. Phys.-Condens. MATTER. 20 (2008).
[49] V.V. Lehtola, R.P. Linna, K. Kaski, Dynamics of forced biopolymer translocation, EPL Eur. Lett. 85 (2009) 58006.
[50] V. Lehtola, R. Linna, K. Kaski, Critical evaluation of the computational methods used in the forced polymer translocation, Phys. Rev. E. 78 (2008).
[51] J. Dubbeldam, V. Rostiashvili, A. Milchev, T. Vilgis, Forced translocation of a polymer: dynamical scaling vs. MD-simulation, ArXiv11105763v1 Cond-Matsoft. (2011).
[52] K. Luo, T. Ala-Nissila, S.-C. Ying, R. Metzler, Driven polymer translocation through nanopores: Slow-vs.-fast dynamics, EPL Eur. Lett. 88 (2009) 68006.
[53] R. Metzler, K. Luo, Polymer translocation through nanopores: Parking lot problems, scaling laws and their breakdown, Eur. Phys. J. Spec. Top. 189 (2010) 119–134.
[54] C.M. Edmonds, Y.C. Hudiono, A.G. Ahmadi, P.J. Hesketh, S. Nair, Polymer translocation in solid-state nanopores: Dependence of scaling behavior on pore dimensions and applied voltage, J. Chem. Phys. 136 (2012) 065105–065105–10.
[55] A. Bhattacharya, W.H. Morrison, K. Luo, T. Ala-Nissila, S.-C. Ying, A. Milchev, et al., Scaling exponents of forced polymer translocation through a nanopore, Eur. Phys. J. E. 29 (2009) 423–429.
[56] A. Bhattacharya, K. Binder, Out-of-equilibrium characteristics of a forced translocating chain through a nanopore, Phys. Rev. E. 81 (2010).

[57] M. Fyta, S. Melchionna, S. Succi, E. Kaxiras, Hydrodynamic correlations in the translocation of a biopolymer through a nanopore: Theory and multiscale simulations, Phys. Rev. E. 78 (2008).
[58] A. Izmitli, D.C. Schwartz, M.D. Graham, J.J. de Pablo, The effect of hydrodynamic interactions on the dynamics of DNA translocation through pores., J. Chem. Phys. 128 (2008) 085102.
[59] V.V. Lehtola, R.P. Linna, K. Kaski, Unforced polymer translocation compared to the forced case, Phys. Rev. E. 81 (2010).
[60] F. Kapahnke, U. Schmidt, D.W. Heermann, M. Weiss, Polymer translocation through a nanopore: The effect of solvent conditions, J. Chem. Phys. 132 (2010) 164904.
[61] P.-H. Lee, V. Helms, T. Geyer, Coarse-grained Brownian dynamics simulations of protein translocation through nanopores, J. Chem. Phys. 137 (2012) 145105–145105–12.
[62] I. Huopaniemi, K. Luo, T. Ala-Nissila, S.-C. Ying, Langevin dynamics simulations of polymer translocation through nanopores, J. Chem. Phys. 125 (2006) 124901.
[63] K. Luo, T. Ala-Nissila, S.-C. Ying, A. Bhattacharya, Dynamics of DNA translocation through an attractive nanopore, Phys. Rev. E. 78 (2008) 061911.
[64] K. Luo, T. Ala-Nissila, S.-C. Ying, A. Bhattacharya, Influence of Polymer-Pore Interactions on Translocation, Phys. Rev. Lett. 99 (2007) 148102.
[65] K. Luo, S. Ollila, I. Huopaniemi, T. Ala-Nissila, P. Pomorski, M. Karttunen, et al., Dynamical scaling exponents for polymer translocation through a nanopore, Phys. Rev. E. 78 (2008).
[66] H.W. de Haan, G.W. Slater, Mapping the variation of the translocation α scaling exponent with nanopore width, Phys. Rev. E. 81 (2010).
[67] S. Guillouzic, G.W. Slater, Polymer translocation in the presence of excluded volume and explicit hydrodynamic interactions, Phys. Lett. 359 (2006) 261–264.
[68] M.G. Gauthier, G.W. Slater, Molecular Dynamics simulation of a polymer chain translocating through a nanoscopic pore, Eur. Phys. J. E. 25 (2008) 17–23.
[69] M.G. Gauthier, G.W. Slater, Nondriven polymer translocation through a nanopore: Computational evidence that the escape and relaxation processes are coupled, Phys. Rev. E. 79 (2009) 021802.
[70] J. Dubbeldam, A. Milchev, V. Rostiashvili, T. Vilgis, Polymer translocation through a nanopore: A showcase of anomalous diffusion, Phys. Rev. E. 76 (2007).
[71] D. Wei, W. Yang, X. Jin, Q. Liao, Unforced translocation of a polymer chain through a nanopore: The solvent effect, J. Chem. Phys. 126 (2007) 204901.
[72] W. Sung, P.J. Park, Polymer translocation through a pore in a membrane, Phys. Rev. Lett. 77 (1996) 783–786.
[73] M. Muthukumar, Polymer translocation through a hole, J. Chem. Phys. 111 (1999) 10371.
[74] M. Doi, S.F. Edwards, The Theory of Polymer Dynamics, Oxford University Press, USA, 1988.
[75] M.G. Gauthier, G.W. Slater, A Monte Carlo algorithm to study polymer translocation through nanopores. II. Scaling laws, J. Chem. Phys. 128 (2008) 205103.

[76] T. Ikonen, A. Bhattacharya, T. Ala-Nissila, W. Sung, Influence of non-universal effects on dynamical scaling in driven polymer translocation, J. Chem. Phys. 137 (2012) 085101.
[77] T. Sakaue, Nonequilibrium dynamics of polymer translocation and straightening, Phys. Rev. E. 76 (2007).
[78] T. Sakaue, Sucking genes into pores: Insight into driven translocation, Phys. Rev. E. 81 (2010).
[79] T. Saito, T. Sakaue, Dynamical diagram and scaling in polymer driven translocation, Eur. Phys. J. E. 34 (2011).
[80] T. Saito, T. Sakaue, Erratum to: Dynamical diagram and scaling in polymer driven translocation, Eur. Phys. J. E. 35 (2012).
[81] T. Sakaue, M. Tokuyama, I. Oppenheim, H. Nishiyama, Nonequilibrium Dynamics of a Manipulated Polymer: Stretching and Relaxation, in: AIP, 2008: pp. 508–511.
[82] T. Ikonen, A. Bhattacharya, T. Ala-Nissila, W. Sung, Unifying model of driven polymer translocation, Phys. Rev. E. 85 (2012) 051803.
[83] T. Ikonen, A. Bhattacharya, T. Ala-Nissila, W. Sung, Scaling theory of driven polymer translocation, arXiv:1211.7043. (2012).
[84] P. Rowghanian, A.Y. Grosberg, Force-Driven Polymer Translocation through a Nanopore: An Old Problem Revisited, J. Phys. Chem. B. 115 (2011) 14127–14135.
[85] P. Rowghanian, A.Y. Grosberg, Propagation of tension along a polymer chain, Phys. Rev. E. 86 (2012) 011803.
[86] K. Luo, I. Huopaniemi, T. Ala-Nissila, S.-C. Ying, Polymer translocation through a nanopore under an applied external field, J. Chem. Phys. 124 (2006) 114704–7.
[87] M.G. Gauthier, G.W. Slater, A Monte Carlo algorithm to study polymer translocation through nanopores. I. Theory and numerical approach, J. Chem. Phys. 128 (2008) 065103.
[88] D.E. Smith, T.T. Perkins, S. Chu, Dynamical scaling of DNA diffusion coefficients, Macromolecules. 29 (1996) 1372–1373.
[89] R.M. Robertson, S. Laib, D.E. Smith, Diffusion of isolated DNA molecules: Dependence on length and topology, Proc. Natl. Acad. Sci. 103 (2006) 7310 – 7314.
[90] A.E. Nkodo, J.M. Garnier, B. Tinland, H. Ren, C. Desruisseaux, L.C. McCormick, et al., Diffusion coefficient of DNA molecules during free solution electrophoresis, ELECTROPHORESIS. 22 (2001) 2424–2432.
[91] B. Cui, H. Diamant, B. Lin, Screened Hydrodynamic Interaction in a Narrow Channel, Phys. Rev. Lett. 89 (2002).
[92] R.G. Larson, The Structure and Rheology of Complex Fluids, Oxford University Press, USA, 1998.
[93] B. Tinland, A. Pluen, J. Sturm, G. Weill, Persistence Length of Single-Stranded DNA, Macromolecules. 30 (1997) 5763–5765.
[94] T.D. Pollard, W.C. Earnshaw, Cell Biology, Updated, Saunders, 2004.
[95] A.R. Mathieson, S. Matty, Influence of pH and ionic strength on size, shape, and electric charge of the deoxyribonucleic acid molecule, J. Polym. Sci. 23 (1957) 747–764.

[96] J. Mathé, H. Visram, V. Viasnoff, Y. Rabin, A. Meller, Nanopore Unzipping of Individual DNA Hairpin Molecules, Biophys. J. 87 (2004) 3205–3212.
[97] A.S. Panwar, M. Muthukumar, Enzyme-Modulated DNA Translocation through a Nanopore, J. Am. Chem. Soc. 131 (2009) 18563–18570.
[98] C.Y. Kong, M. Muthukumar, Modeling of polynucleotide translocation through protein pores and nanotubes, Electrophoresis. 23 (2002) 2697–2703.
[99] R.B. Bird, O. Hassager, R.C. Armstrong, C.F. Curtiss, Dynamics of Polymeric Liquids. VOLUME 2. (Kinetic Theory), John Wiley & Sons Inc, 1977.
[100] M.P. Allen, D.J. Tildesley, Computer Simulation of Liquids, Oxford University Press, USA, 1989.
[101] W.D. Cornell, P. Cieplak, C.I. Bayly, I.R. Gould, K.M. Merz, D.M. Ferguson, et al., A Second Generation Force Field for the Simulation of Proteins, Nucleic Acids, and Organic Molecules, J. Am. Chem. Soc. 117 (1995) 5179–5197.
[102] A.K. Rappe, C.J. Casewit, K.S. Colwell, W.A. Goddard, W.M. Skiff, UFF, a full periodic table force field for molecular mechanics and molecular dynamics simulations, J. Am. Chem. Soc. 114 (1992) 10024–10035.
[103] J.A. Wendel, W.A. Goddard III, The Hessian biased force field for silicon nitride ceramics: Predictions of thermodynamic and mechanical properties for α- and β-Si3N4., J Chem Phys. 97 (1992).
[104] D.L. Ermak, H. Buckholz, Numerical integration of the Langevin equation: Monte Carlo simulation, J. Comput. Phys. 35 (1980) 169–182.
[105] T. Geyer, U. Winter, An O(N2) approximation for hydrodynamic interactions in Brownian dynamics simulations, J. Chem. Phys. 130 (2009) 114905.
[106] T. Ando, T. Meguro, I. Yamato, Multiple Time Step Brownian Dynamics for Long Time Simulation of Biomolecules, Mol. Simul. 29 (2003) 471–478.
[107] B.R. Munson, D.F. Young, T.H. Okiishi, Fundamentals of Fluid Mechanics, 5th ed., Wiley, 2005.
[108] D.A. McQuarrie, Statistical Mechanics, 2nd ed., University Science Books, 2000.
[109] K. Luo, R. Metzler, The chain sucker: Translocation dynamics of a polymer chain into a long narrow channel driven by longitudinal flow, J. Chem. Phys. 134 (2011) 135102.
[110] D.L. Ermak, J.A. McCammon, Brownian dynamics with hydrodynamic interactions, J. Chem. Phys. 69 (1978) 1352.
[111] J. Rotne, S. Prager, Variational Treatment of Hydrodynamic Interaction in Polymers, J. Chem. Phys. 50 (1969) 4831–4837.
[112] R. Kubo, The fluctuation-dissipation theorem, Reports Prog. Phys. 29 (1966) 255–284.
[113] R.R. Schmidt, J.G.H. Cifre, J.G. de la Torre, Comparison of Brownian dynamics algorithms with hydrodynamic interaction, J. Chem. Phys. 135 (2011) 084116.
[114] M. Fixman, Construction of Langevin forces in the simulation of hydrodynamic interaction, Macromolecules. 19 (1986) 1204–1207.
[115] U. Winter, T. Geyer, Coarse grained simulations of a small peptide: Effects of finite damping and hydrodynamic interactions, J. Chem. Phys. 131 (2009) 104102–104102–7.
[116] T. Geyer, Many-particle Brownian and Langevin Dynamics Simulations with the Brownmove package, BMC Biophys. 4 (2011) 7.

[117] M. Długosz, P. Zieliński, J. Trylska, Brownian dynamics simulations on CPU and GPU with BD_BOX, J. Comput. Chem. 32 (2011) 2734–2744.
[118] D. Frenkel, B. Smit, Understanding Molecular Simulation, Second Edition: From Algorithms to Applications, 2nd ed., Academic Press, 2001.
[119] R.K. Pathria, Statistical Mechanics, Second Edition, 2nd ed., Butterworth-Heinemann, 1996.
[120] K.A. Dill, S. Bromberg, Molecular Driving Forces: Statistical Thermodynamics in Chemistry & Biology, 1st ed., Garland Science, 2002.
[121] M.G. Kurnikova, R.D. Coalson, P. Graf, A. Nitzan, A lattice relaxation algorithm for three-dimensional Poisson-Nernst-Planck theory with application to ion transport through the gramicidin A channel, Biophys. J. 76 (1999) 642–656.
[122] D. Johnston, Foundations of cellular neurophysiology, MIT Press, Cambridge, Mass., 1995.
[123] W.H. Press, B.P. Flannery, S.A. Teukolsky, W.T. Vetterling, Numerical Recipes in FORTRAN 77: The Art of Scientific Computing, 2nd ed., Cambridge University Press, 1992.
[124] J.D. Hoffman, Numerical Methods for Engineers and Scientists, Second Edition,, 2nd ed., CRC Press, 2001.
[125] J. Demmel, Solving the Discrete Poisson Equation using Jacobi, SOR and the FFT, CS267 Notes Lect. 24 Apr 13 1995. (1995).
[126] H.R. Kang, Color Technology for Electronic Imaging Devices (SPIE Press Monograph Vol. PM28), SPIE Publications, 1997.
[127] M. Muthukumar, C.Y. Kong, Simulation of polymer translocation through protein channels, Proc. Natl. Acad. Sci. 103 (2006) 5273.
[128] S. Kuyucak, O.S. Andersen, S.H. Chung, Models of permeation in ion channels, Reports Prog. Phys. 64 (2001) 1427.
[129] G. Moy, B. Corry, S. Kuyucak, S.H. Chung, Tests of continuum theories as models of ion channels. I. Poisson-Boltzmann theory versus Brownian dynamics, Biophys. J. 78 (2000) 2349–2363.
[130] B. Corry, S. Kuyucak, S.-H. Chung, Tests of Continuum Theories as Models of Ion Channels. II. Poisson-Nernst-Planck Theory versus Brownian Dynamics, Biophys. J. 78 (2000) 2364–2381.
[131] C.Y. Kong, M. Muthukumar, Simulations of Stochastic Sensing of Proteins, J. Am. Chem. Soc. 127 (2005) 18252–18261.
[132] J. Yota, Interlevel Dielectric Processes Using PECVD Silicon Nitride, Polyimide, and Polybenzoxazole for GaAs HBT Technology, J. Electrochem. Soc. 156 (2009) G173.
[133] W. Hayt, J. Buck, Engineering Electromagnetics, 7th ed., McGraw-Hill Science/Engineering/Math, 2005.
[134] S.S. Zumdahl, Chemistry Second Edition, D.C. Heath and Company, 1989.
[135] R. Schoch, J. Han, P. Renaud, Transport phenomena in nanofluidics, Rev. Mod. Phys. 80 (2008) 839–883.
[136] J.L.A. Dubbeldam, A. Milchev, V.G. Rostiashvili, T.A. Vilgis, Driven polymer translocation through a nanopore: A manifestation of anomalous diffusion, Eur. Lett. EPL. 79 (2007) 18002.

[137] L. Chen, A.T. Conlisk, Forces affecting double-stranded DNA translocation through synthetic nanopores, Biomed. Microdevices. 13 (2011) 403–414.
[138] C.T.A. Wong, M. Muthukumar, Polymer capture by electro-osmotic flow of oppositely charged nanopores, J. Chem. Phys. 126 (2007) 164903.
[139] G. Cumming, F. Fidler, D.L. Vaux, Error bars in experimental biology, J. Cell Biol. 177 (2007) 7–11.
[140] T. Schlick, Molecular Modeling and Simulation, 1st ed., Springer, 2002.
[141] P. Chen, J. Gu, E. Brandin, Y.-R. Kim, Q. Wang, D. Branton, Probing Single DNA Molecule Transport Using Fabricated Nanopores, Nano Lett. 4 (2004) 2293–2298.
[142] P. Chen, T. Mitsui, D.B. Farmer, J. Golovchenko, R.G. Gordon, D. Branton, Atomic Layer Deposition to Fine-Tune the Surface Properties and Diameters of Fabricated Nanopores, Nano Lett. 4 (2004) 1333–1337.
[143] M. Wanunu, A. Meller, Chemically Modified Solid-State Nanopores, Nano Lett. 7 (2007) 1580–1585.
[144] I.A. Jou, D.V. Melnikov, C.R. McKinney, M.E. Gracheva, DNA translocation through a nanopore in a single-layered doped semiconductor membrane, Phys. Rev. E. 86 (2012).
[145] D.V. Melnikov, J.-P. Leburton, M.E. Gracheva, Slowing down and stretching DNA with an electrically tunable nanopore in a p–n semiconductor membrane, Nanotechnology. 23 (2012) 255501.
[146] D.V. Melnikov, A. Nikolaev, J.P. Leburton, M.E. Gracheva, Polymer translocation through an electrically tunable nanopore in a multilayered semiconductor membrane., Methods Mol. Biol. Clifton NJ. 870 (2012) 187.
[147] M.E. Gracheva, J.P. Leburton, Electrolytic charge inversion at the liquid–solid interface in a nanopore in a doped semiconductor membrane, Nanotechnology. 18 (2007) 145704.
[148] A. Nikolaev, M.E. Gracheva, Simulation of ionic current through the nanopore in a double-layered semiconductor membrane, Nanotechnology. 22 (2011) 165202.
[149] B. Luan, H. Peng, S. Polonsky, S. Rossnagel, G. Stolovitzky, G. Martyna, Base-By-Base Ratcheting of Single Stranded DNA through a Solid-State Nanopore, Phys. Rev. Lett. 104 (2010).
[150] S. Polonsky, S. Rossnagel, G. Stolovitzky, Nanopore in metal-dielectric sandwich for DNA position control, Appl. Phys. Lett. 91 (2007) 153103–153103–3.
[151] M.E. Gracheva, D.V. Melnikov, J.-P. Leburton, Multilayered Semiconductor Membranes for Nanopore Ionic Conductance Modulation, ACS Nano. 2 (2008) 2349–2355.
[152] M.S. Kilic, M.Z. Bazant, A. Ajdari, Steric effects in the dynamics of electrolytes at large applied voltages. I. Double-layer charging, Phys. Rev. E. 75 (2007) 021502.
[153] M.S. Kilic, M.Z. Bazant, A. Ajdari, Steric effects in the dynamics of electrolytes at large applied voltages. II. Modified Poisson-Nernst-Planck equations, Phys. Rev. E. 75 (2007) 021503.
[154] T.-L. Horng, T.-C. Lin, C. Liu, B. Eisenberg, PNP Equations with Steric Effects: A Model of Ion Flow through Channels, J. Phys. Chem. B. 116 (2012) 11422–11441.
[155] D.T. Edmonds, Electricity and magnetism in biological systems, Oxford University Press, Oxford [England]; New York, 2001.

[156] R.G. Larson, The rheology of dilute solutions of flexible polymers: Progress and problems, J. Rheol. 49 (2005) 1–70.
[157] S.B. Smith, Y. Cui, C. Bustamante, Overstretching B-DNA: The Elastic Response of Individual Double-Stranded and Single-Stranded DNA Molecules, Sci. New Ser. 271 (1996) 795–799.
[158] S. Matysiak, A. Montesi, M. Pasquali, A.B. Kolomeisky, C. Clementi, Dynamics of Polymer Translocation through Nanopores: Theory Meets Experiment, Phys. Rev. Lett. 96 (2006) 118103.